UNIVERSITÀ DEGLI STUDI DI VERONA

DEPARTMENT OF COMPUTER SCIENCE
DOCTORAL PROGRAM IN COMPUTER SCIENCE

XXXVII CYCLE

Semi-Active Actuators for Gravity Compensation with Application to Exoskeletons

---

Author:
Francesco PASCUCCI

Supervisor:
Prof. Andrea CALANCA

PhD Program Coordinator:
Prof. Ferdinando CICALESE

Submitted in fulfillment of the requirements
for the degree of Doctor of Philosophy
in the Department of Computer Science

S.S.D. IBIO - 01/A

February 2025

UNIONE EUROPEA
Fondo Sociale Europeo
Ministero dell'Università e della Ricerca
PON RICERCA E INNOVAZIONE 2014 - 2020
REACT EU

La borsa di dottorato è stata cofinanziata con risorse del
Programma Operativo Nazionale Ricerca e Innovazione 2014-2020, risorse FSE REACT-EU
Azione IV.4 "Dottorati e contratti di ricerca su tematiche dell'innovazione"
e Azione IV.5 "Dottorati su tematiche Green"

Life's most persistent and urgent question is, "What are you doing for others?"

Martin Luther King Jr.

Abstract

Semi-Active Actuators for Gravity Compensation with Application to Exoskeletons

Gravity compensation is a well-established technique in robotic design to maintain balance throughout the range of motion while reducing actuator loads. Existing solutions can be classified into three categories: passive, active, and semi-active systems. Passive systems rely on mechanical components such as springs or counterweights to counteract gravitational forces, offering a simple and energy-efficient solution but lacking adaptability to dynamic loads. Active systems, on the other hand, use sensors and actuators to provide highly precise and versatile compensation at the cost of increased power consumption. A promising alternative is semi-active or semi-active systems, which combine both approaches to achieve high energy efficiency while ensuring high-performance gravity compensation. Surprisingly, semi-active solutions have received little attention from the research community. To bridge this gap, the research presented in this dissertation analyzes semi-active gravity compensation mechanisms aimed at reducing power consumption in robotic systems. Specifically, the study investigates applications in upper-limb exoskeletons to balance variable payloads and enhance usability in industrial and medical contexts.

The first part of this work evaluates the Agadexo Shoulder, a commercial semi-active upper-limb exoskeleton. This device integrates a semi-active gravity compensation system that combines elastic elements and motors to achieve an optimal torque curve and assistance level, supporting workers in their tasks. Experimental studies conducted in a simulated industrial environment demonstrated reductions in muscle activation of upper-body muscles. Additionally, subjective assessments reported decreased perceived effort and physical demand.

Building on these insights, the second part of the study introduces a novel semi-active actuation system: AGtuator, the Anti-Gravity actuator. Unlike traditional approaches, the AGtuator integrates actuation and gravity compensation into a single system. The active and passive elements work in series and are managed by a low-level torque control module. This allows the AGtuator not only to compensate for variable gravitational forces but also to generate customizable torque profiles. Experimental validation demonstrated that the AGtuator enables dynamic compensation of payload variations and the generation of customized torque profiles while maintaining low power consumption, addressing the primary limitations of existing systems.

To demonstrate its applicability, the AGtuator was used to develop a prototype upper-limb exoskeleton with shoulder and elbow joints. The results highlight the versatility of the AGtuator and, more broadly, semi-active gravity compensation systems, paving the way for more efficient, adaptable, and sustainable robotic solutions across a wide range of applications.

Contents

List of Figures

List of Tables

List of Abbreviations

AD	**A**nterior **D**eltoid
ADL	**A**ctivity of **D**aily **L**iving
AGtuator	**A**nti **G**ravity ag**tuator**
BB	**B**iceps **B**rachii
BR	**BR**achioradialis
CoP	**C**enter **o**f **P**ressure
CoR	**C**enter **o**f **R**otation
DoF	**D**egrees **o**f **F**reedom
EMG	**E**lectro **M**yo**G**raphy
ES	**E**rector **S**pinae
GC	**G**ravity **C**ompensation
GRF	**G**round **R**eaction **F**orces
HL	**H**ip **L**evel
IN	**IN**fraspinatus
LD	**L**atissimus **D**orsi
MGC	**M**echanical **G**ravity **C**ompensation
MISO	**M**ultiple **I**nput **S**ingle **O**utput
MSDs	**M**usculo**S**keletal **D**isorders
MVC	**M**aximum **V**oluntary **C**ontraction
PCA	**P**rincipal **C**omponent **A**nalysis
PD	**P**osterior **D**eltoid
PM	**P**ectoralis **M**ajor
RA	**R**ectus **A**bdominis
RoM	**R**ange **o**f **M**otion
RPE	**R**ating of **P**erceived **E**ffort
RMS	**R**oot **M**ean **S**quare
SD	**S**tandard **D**eviation
sEMG	**s**urface **E**lectro **M**yo**G**raphy
SGC	**S**tatic **G**ravity **C**ompensation
SL	**S**houlder **L**evel
UT	**U**pper **T**rapezius
WRMSDs	**W**ork- **R**elated **M**usculo**S**keletal **D**isorders

Chapter 1

Introduction

This work, titled *Semi-active Actuators for Gravity Compensation with Application to Exoskeletons*, arises from a deep personal desire: trying to do something for others.

In the field of robotics, gravity compensation is a crucial aspect. The compensation of forces due to external loads or the weight of the robot itself results in expensive, bulky, and heavy devices. A possible solution is represented by semi-active actuators, which indeed constitute the key aspect of this work. These systems, sometimes called with the generic word *hybrid*, combine an active actuation system (e.g., electric, hydraulic, or pneumatic) with a passive elastic element, aiming to enhance the system's overall efficiency. By reducing the required torque, smaller, more compact, and cost-effective actuators can be used.

Within robotics, a category that often works to counteract gravitational forces is exoskeletons, and for this reason, they have been chosen for an in-depth study on the use of semi-active actuators. An exoskeleton is a wearable robotic device designed to improve the quality of life for its users. Work-related musculoskeletal disorders (WRMSDs) are still today one of the primary health risks for workers worldwide and adopting exoskeletons is emerging as a preventive measure. Such devices can help workers alleviate the musculoskeletal system's workload, which is among the leading causes of physical discomfort related to work activities. The onset of these disorders can severely compromise an individual's well-being, negatively impacting their personal and family life. Moreover, exoskeletons can play a critical role in rehabilitation and personal assistance, supporting individuals with disabilities in regaining motor functions or achieving greater autonomy. Semi-active actuation systems for gravity compensation would allow a significant reduction in the cost of these devices, with the possibility of increasing their adoption. A product can have significant societal impacts only when accessible to users.

1.1 Contributions

The main contribution of this work is the conceptual development of a semi-active actuation system we called AGtuator, an Anti-Gravity actuator characterized by high energy efficiency and high versatility thanks to advanced control. The key feature of this system is its ability to adapt to variable loads, consuming energy only to reconfigure the gravity compensation system. AGtuator makes it possible to achieve a zero-stiffness system, meaning a balanced system free to move regardless of the external load. The proposed solution was implemented to demonstrate its effectiveness, and experiments confirmed its feasibility. Although there are numerous potential applications, we believe an excellent field of use is exoskeletons. This statement is supported by our analysis of the behavior of a commercially available industrial exoskeleton, which represents a second contribution. The third contribution is the design and development of an upper limb based on the AGtuator concept

with assistance to both the shoulder and the elbow. A recommended reading approach is outlined in the following section.

1.2 Structure of the Thesis

This work begins with two introductory chapters, Chapters 2 and 3, and can be divided into two parts.

The first part of the thesis, consisting of Chapters 3 and 4, focuses on studying an industrial upper-limb exoskeleton with a semi-active actuation system. The exoskeleton in question is Agadexo, commercialized by Agade S.r.l. [1], which at the time of writing, represents the most advanced system of its kind. This experience enabled familiarization with semi-active actuation systems to study their strengths and limitations. Furthermore, trying other exoskeletons allowed us to better identify the key aspects to focus on and confirmed the potential field of application for our work. Testing a semi-active exoskeleton confirmed that integrating motors into exoskeletons is feasible and promising. Agadexo proved to be effective in increasing support and preventing the onset of musculoskeletal disorders. Chapter 3 introduces exoskeletons, illustrating their main differences and use cases. Chapter 4 includes a comprehensive and in-depth study evaluating Agadexo's impact on simulated industrial tasks, the experimental design, and the results obtained.

The second part of the thesis, Chapters 2, 5, and 6, focuses on the study of gravity compensation and proposes a novel solution called AGtuator, standing for Anti-Gravity Actuator. Chapter 2 introduces the primary systems for gravity compensation in robotics, presenting various solutions in the literature. Chapter 5 introduces the AGtuator concept and a general control scheme is proposed. To showcase its high versatility and flexibility, possible scenarios and use cases are presented. This chapter concludes with implementing the AGtuator system in one of its use cases and its testing. Chapter 6 proposes a possible application of the AGtuator. First, we begin with studying a passive upper-limb exoskeleton, Paexo by Ottobock, and analyzing the limits of a hypothetic semi-active version that retains the mechanical structure. Then a semi-active exoskeleton with shoulder and elbow support based on the AGtuator concept is proposed. Chapter 6 also includes a study on optimizing the pulleys of a bungee cord to simulate a zero-free length elastic element.

1.2.1 Suggestions for the Readers

Before starting, some recommendations are provided to the readers. For those interested in the main contribution of the thesis and already familiar with the concept of gravity compensation in robotics, it is advisable to begin with the presentation of AGtuator in Chapter 5 and its application in Chapter 6.

Chapter 2

Gravity Compensation in Robotics

In industrial applications, robotic systems provide essential advantages such as precision, speed, and repeatability, making them indispensable in manufacturing and automation. However, these benefits have notable drawbacks, including high costs, safety concerns, and an inefficient payload-to-weight ratio. For instance, lifting a 50 kg payload may necessitate a 350 kg robotic system, highlighting the inefficiencies in weight distribution and energy consumption [2]. A key factor in improving robotic performance is the implementation of gravity compensation techniques, which reduce actuator effort and enhance overall system efficiency [3]. Gravity compensation plays a crucial role in mitigating the power required to counteract gravitational forces induced by a robot's own weight and any external loads. Without proper compensation, robotic actuators must exert significant force to maintain stability, leading to increased energy consumption, mechanical wear, and reduced operational lifespan [4]. In serial kinematic chain manipulators, the propagation of forces through multiple links further exacerbates the need for high-torque actuators to compensate for gravity-induced joint loads. This challenge makes efficient gravity compensation essential in robotic design, particularly in systems requiring high precision and energy efficiency.

Conventional gravity compensation systems have a major limitation: they can only balance a specific static external payload or, in some cases, a set of predefined loads [5]. This restricts the applicability to robotic systems, making them less efficient when handling dynamic payloads. However, gravity compensation systems, in addition to enabling the design of lighter and more cost-effective systems, enhance interaction and improve controllability [6] All these advantages confirm that developing advanced gravity compensation mechanisms is a key research focus.

2.1 Static Gravity Compensation

Static Gravity Compensation (SGC) is a widely used technique in robotic design to balance systems throughout their range of motion while reducing actuator loads. This can be achieved through two primary methods: adding a counterweight to align the system's center of mass with the pivot point or utilizing the energy stored in springs or rubber bands to counteract gravitational forces [7]. However, accurately matching the non-linear gravity-induced joint torques across varying angles remains challenging. Fully compensating for gravity often necessitates complex mechanical add-ons or results in an unavoidable increase in mass. To address these challenges, methods of partial gravity compensation have also been developed [8, 9].

2.1.1 Gravity Compensation by Counterweights

Counterweights have long played a significant role in mechanical systems, serving as a fundamental method for gravitational compensation [10]. This approach involves strategically placing additional weights to maintain a stationary center of mass, effectively balancing gravitational forces and reducing the load on actuators. Counterweights can be integrated into auxiliary linkages or mounted directly onto robotic links, offering flexibility in their implementation [11]. This method is particularly effective for planar and serial manipulators, where the forces are easier to manage linearly. However, when applied to spatial manipulators, counterweights pose significant challenges due to the increase in overall mass and the added complexity of the design. The most common passive strategy for gravity compensation involves aligning a link's center of mass with the joint axis by adding weight, which increases the mass, inertia, and volume of the system but can improve energy efficiency in quasi-static tasks by reducing the strain on the actuators [12]. Despite this, adding mass as a counterweight is typically undesirable because it increases the total size and weight of the robot, making it more difficult to move and energy-consuming during dynamic tasks. In many industrial robot designs, such as the KUKA R360 and PUMA 200, the masses of the motors are used for gravity correction, leveraging the motors' weight to reduce the reliance on external counterweights [13]. However, counterweights can still create issues in industrial applications due to limitations in the overall size of the manipulator and the potential for collisions with extended moving connections carrying the counterweights. This issue becomes particularly pronounced in environments where space is limited or the robotic arm has a high degree of freedom. Additionally, gravity compensation with counterweights is strongly position-dependent; the effectiveness of this solution varies significantly based on the orientation of the robotic system. As the robot moves, the counterweight system must be re-calibrated or adjusted to maintain balance, adding to the complexity of the design. Therefore, while counterweights can be a useful tool in balancing robotic systems, their design and implementation are far more intricate than they may initially seem, requiring careful consideration of the robot's range of motion, size constraints, and the specific tasks it is designed to perform.

2.1.2 Gravity Compensation by Springs

Spring-based methods for gravity compensation in robotic systems use elastic elements to reduce actuator torque while maintaining modularity. Springs can be integrated into robotic systems in multiple ways, including direct attachment to robotic links, incorporation into cable-and-pulley systems, or through auxiliary mechanisms such as cams and gear trains. A key advantage of these methods is their ability to significantly reduce actuator torque. For instance, systems employing non-circular pulleys have demonstrated reductions in actuator torque by as much as 50–80% through effective weight compensation [14]. These methods rely on two primary types of springs: zero-free length springs and non-zero-free length springs. Zero-free length springs exert forces directly proportional to displacement, making them ideal for precise gravity compensation. Zero-free length springs are designed to produce zero force at zero length, achieved through built-in tension. Although a physical coil spring cannot shrink indefinitely due to coil contact, the concept is realized by setting the equilibrium point at zero length. This property makes them suitable for direct connection to robotic links, ensuring full gravity compensation. In contrast, non-zero-free length springs provide only partial compensation but are

more commonly used for their practicality in various robotic applications. When springs are used in auxiliary mechanisms like cables, pulleys, or cams, zero-free length properties become less critical. While zero-free length springs provide the ideal theoretical solution, practical applications often rely on standard springs due to cost and manufacturing constraints. As a result, most robotic gravity compensation systems use non-zero-free length springs due to their availability and ease of implementation [15].

Unlike counterweights or other balancing methods, spring-based approaches do not introduce additional mass. Instead, they utilize elastic strain energy to counteract gravitational potential, offering an efficient passive compensation mechanism. However, achieving accurate compensation across varying joint angles and multiple degrees of freedom persists as a difficult problem. Gravity-induced joint torques are inherently nonlinear, and perfect compensation would require nonlinear springs, which are difficult to manufacture and integrate into compact robotic designs. Consequently, many implementations use standard linear springs while modifying the moment arm geometry to create an effective nonlinear moment [16, 8]. Despite their advantages, fully passive gravity compensation remains challenging. Ongoing research explores ways to enhance accuracy and compactness in integrating elastic elements for robotic gravity compensation.

2.2 Adaptive Gravity Compensation

The introduction of variable payloads posed new challenges for robotic systems and gravity compensation techniques. Conventional static balancers are effective for constant loads, but adapting to changes in payload traditionally required manual intervention or energy input. The solutions described above have only included passive compensation methods. There are fully passive solutions that allow adaptation to variable loads but with significant limitations, such as the need to stop the system in a specific position. The literature describes methods such as increasing or decreasing the initial tension of the springs [17], and adjusting the positions of specific pivot and attachment points [18]. However, using active elements, such as a motor at the joint, is undoubtedly the simplest, most precise, and most reactive solution to make the system more robust to payload variations and disturbances. Thus, solutions utilizing electric motors alongside elastic elements exist. The simplest solution involves placing a motor and an elastic element in parallel to reduce the torque requirements of the actuator [19]. More complex solutions that aim to combine active and passive elements are beginning to emerge.

2.2.1 Self Regulating Gravity Balancers

Self-regulated gravity balancers represent a significant advancement in mechanical balancing technology by enabling autonomous adjustments and reducing the need for manual recalibration. These passive systems automatically adapt to varying payloads, ensuring stable and predictable operation while minimizing human error. Their ability to maintain constant potential energy translates into significant energy savings, as less effort is required for movement and positioning.

One of the most notable innovations in this field is the single degree of freedom (DoF) self-regulated gravity balancer, which integrates traditional spring-based

mechanisms with adaptive spring adjustment features. A key design involves attaching a tensile spring to the gravity balancing mechanism, counteracting the payload's weight through strategically controlled attachment points. The system dynamically adjusts the spring's position via cables driven by a dedicated spring-adjustment mechanism, allowing automatic recalibration to maintain consistent potential energy without manual intervention. Another effective approach employs cam-follower mechanisms combined with rack-and-pinion systems. Specifically, engineered cam profiles adjust spring positions in response to payload variations, ensuring consistent gravitational compensation across a broad range of motion. This method not only enhances performance but also simplifies the balancer's overall design [20]. Similarly, slider-pulley-counterweight systems use auxiliary structures to automatically modify spring attachment points, effectively redistributing force to maintain balance without manual recalibration [21].

These innovations have broad applications across multiple industries. In robotics, self-regulated balancers enable robotic arms and manipulators to handle objects of varying weights with increased precision and reduced energy consumption [22]. In rehabilitation, they enhance assistive devices by offering consistent support, regardless of the patient's limb weight, facilitating smoother therapeutic exercises. Industrial machinery also benefits, as these balancers allow for efficient material handling without frequent recalibration, proving invaluable in environments where productivity and precision are paramount. Despite these advancements, passive mechanisms relying on counterweights and other structures remain in use, though they tend to be bulky, heavy, and complex [23]. More compact systems exist but are often limited to a narrow range of motion, making their practical application challenging [24].

2.2.2 Energy Free Systems

Zero-stiffness mechanisms achieve static balancing by distributing forces and moments so that their potential energy remains constant across a designated motion range. This unique characteristic ensures that no additional energy is required to move or hold a load in place. Static equilibrium is typically achieved through mechanisms designed with springs, counterweights, or specially configured linkages. Energy-free adjustments in zero-stiffness mechanisms are achieved through innovative methods that allow systems to adapt to varying payloads without consuming additional energy [25, 26]. These principles, shown in Figure 2.1 are central to enhancing the versatility and efficiency of such systems in real-world applications.

The first method, known as *Simultaneous Displacement*, adjusts the system's balancing parameters by modifying distances within the mechanism without altering the spring's length [27]. This approach ensures energy-neutral operation and is particularly useful in static settings such as ergonomic supports. For example, Herder et al. [28] demonstrated its effectiveness in balancing systems designed for patients with limited mobility. Another two significant innovations involve the use of multiple springs. The *Virtual Spring* concept employs two substitute springs connected through a pantograph [29]. This method enables the recalibration of the system without physically elongating the springs. The *Storage Spring* method introduces an auxiliary spring that temporarily stores the energy required to adjust the primary mechanism [30]. This strategy is advantageous in systems requiring frequent adjustments, such as robotic arms handling variable weights. Herder et al. (2009) further

refined this method, highlighting its potential for industrial robotics. Finally, *Stiffness Adjustment* allows the tuning of a system by altering the number of active coils in the spring [31].

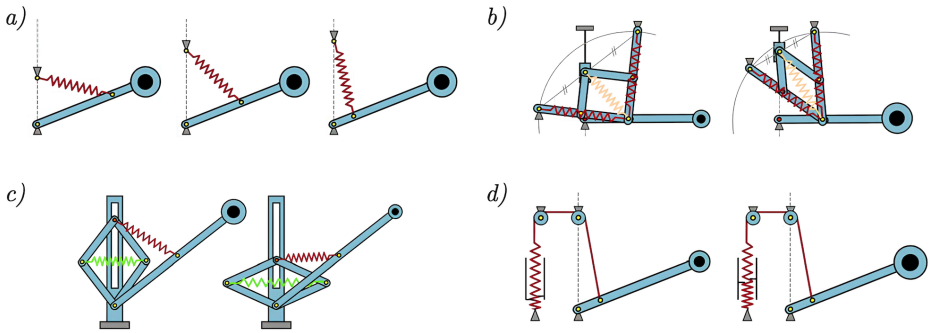

FIGURE 2.1: Examples of Energy-Free solutions, courtesy of [28]. In detail: a) Simultaneous Displacement; b) Virtual Spring; c) Storage Spring; d) Stiffness Adjustment

However, these solutions have the disadvantage of stopping the system in a specific position and requiring manual reconfiguration when the payload changes [32]. Moreover, all the principles can be adjusted in an energy-neutral way only in this specific position. This represents a fundamental limitation, as it prevents the system from generating energy in other configurations, where adjustments can still be made but not in an energy-neutral manner [28].

2.2.3 Gravity compensation by using auxiliary actuators

The final category of gravity compensation methods involves auxiliary actuators, which utilize active mechanisms such as pneumatic, hydraulic, or motor-driven systems to dynamically counteract gravitational effects. They are called auxiliaries because they are additional to those already present in the system. Although it may seem simpler to use the actuators already present in the system to compensate for payload variations, having a dedicated auxiliary actuator preserves the system's efficiency. An example can be found in rehabilitative exoskeletons, in which a motor-driven system with Bowden cable actuation, designed to compensate for the weight of patients' arms and control the exoskeleton's position, enhances mobility and reduces fatigue [33].

The key advantage of auxiliary actuators is their ability to adjust to varying payloads and positions, making them particularly effective for applications requiring precise and dynamic compensation. In spatial parallel mechanisms, for example, balancing gravitational forces presents a major challenge, as conventional compensation strategies either increase the system's overall mass or require intricate designs. A practical alternative involves integrating an auxiliary mechanism that employs pneumatic or hydraulic actuators to apply a balancing force, effectively reducing these limitations [34]. Beyond conventional actuators, innovative approaches have been explored to achieve gravity compensation. For instance, using cylindrical Halbach arrays enables magnetic levitation-based compensation, minimizing friction and wear while maintaining system efficiency [35].

However, while auxiliary actuators offer significant advantages, their implementation requires careful consideration of factors such as control complexity, system integration, and potential increases in weight and cost. Advanced control algorithms

are essential to synchronize auxiliary actuators with the primary system, ensuring seamless operation and preventing issues such as oscillations or instability [36]. Overall, auxiliary actuators provide a versatile solution for gravity compensation across various applications, continuing to evolve through advancements in control algorithms and engineering design.

Chapter 3

Exoskeleton State of the Art

Exoskeletons and orthoses are wearable devices that can be used to augment the strength and mobility of the user. They consist of either rigid or soft structures that are attached to the body and, in some cases, powered by actuators. Exoskeletons have a wide range of potential applications, including industrial and military uses, as well as rehabilitation and assistive technology for individuals with mobility impairments. In general, the term "exoskeleton" refers to a device that improves the performance of an able-bodied wearer, whereas the term "orthosis" refers to a device that aids a person with a limb pathology [37]. Although the proposed work is focused on orthosis for upper limb, the word *exoskeleton* will be mainly used as it is more widespread in scientific literature. The word “exoskeleton” comes from Greek $\varepsilon\xi\omega$, “outer” and $\sigma\kappa\varepsilon\lambda\varepsilon\tau o\varsigma$, “skeleton”. Exoskeletons are not a new concept; the first prototypes trace back to the 1960s in military applications [38]. While their prevalence in the medical field remains prominent, particularly in rehabilitation therapies, exoskeletons have gained traction in the industrial domain due to material advancements and improved control algorithms [39].

3.1 Upper Limb Exoskeletons

Exoskeletons can be classified based on their field of application (military, medical, industrial, sports), type of actuation (active, passive) or supported body segment (upper limb, trunk, hip, lower limb, full body, etc.). The first two classifications will be deepened in the next chapters. As for the supported body segments, this work focuses only on the upper limb, as mentioned before and does not include other types of exoskeletons.

Exoskeletons can be broadly classified into two categories: rigid and soft. Rigid exoskeletons are made up of hard materials such as metal or plastic and are designed to provide support and structure to the wearer’s body. These exoskeletons typically have a series of jointed segments that allow for a range of motion and can be controlled by the wearer to perform various tasks. Rigid exoskeletons can also be divided into end-effector robots and exoskeleton robots. The first ones can be classed as non-anthropomorphic and they are based on an industrial robot arms, with the human upper limb (hand or forearm) attached to the robot at one point [40]. Typical end-effector-based systems include serial manipulators (e.g., MIT Manus [41] and ACRE [42]) and parallel (e.g., CRAMER [43] and InMotion ARM (Figure 3.1)).

Instead, an exoskeleton-like device has a framework similar to the human arm (anthropomorphic kinematic structure) and it is attached to the side of the human arm at various points. The axes of the exoskeleton robot’s joints corresponds to the axes of the human upper limb joints. The physical interface at several points makes

FIGURE 3.1: inMotion ARM, an end-effector exoskeleton [44]

determining posture during movement much easier than non-anthropomorphic devices. However, robotic joints must be precisely aligned with the user's joint axes, requiring misalignment-compensation strategies to compensate for axis mismatches. The proposed work focused on rigid exoskeletons and the design procedure will be discussed in detail later, including examples of products in commerce and found in literature.

Soft exoskeletons, on the other hand, are designed to be lightweight and comfortable to wear. A growing number of academic and industrial research organizations are developing wearable robots composed of textiles and elastomers rather than rigid linkages. J.L. Pons [45] elegantly pointed out in a recent insight on the evolution of exoskeletons technology how wearable robots are changing toward less restrictive and more bio-mimetic structures, favoring compliant materials that better fit to the anatomical complexity of the human body. This enables the devices to be portable and to help motions without interfering with human biomechanics. This new class of devices has been referred to as "Exomuscles", "Soft Exoskeletons", "ExoSuits" [46], or, most appropriately, "Robotic Suits" [47]. Robotic Suits are a type of wearable robot that are designed to assist with physical tasks by providing additional support to the wearer's muscles and joints. Unlike traditional exoskeletons, which are typically made from rigid materials such as metal or plastic, soft exoskeletons are made from flexible materials that can conform to the shape of the wearer's body. This allows for a greater range of movement and a more comfortable fit. Soft exoskeletons can be used in a variety of applications, including rehabilitation, industrial work, and military operations. For example, Park et al. [48] design a passive suit for the assistance of the shoulder elevation, shown in Figure 3.2. Because of the lack of rigid linkages and the use of soft materials as an interface with the subject's limbs, robotic suits are inherently compliant [46]. Using such materials has various advantages: they supports the wearer's movements without over-constricting the joints, they preservie mobility and flexibility; precise joint alignment is not required, they reduce the time required to wear the device; the comfort of wear and ease of donning and doffing is improved, they enhance usability; the overall weight of the device is reduced, as well as the encumbrance, enhancing portability; and the cost is reduced [49]. Despite the various benefits outlined, robotic suits pose several obstacles that require additional research. Characteristic of soft robotic suits is that they rely on the structural integrity of the human body to transfer reaction forces between body segments, rather than having their own load-bearing frame. They function primarily as an external muscle rather than an external skeleton [50]. This means that

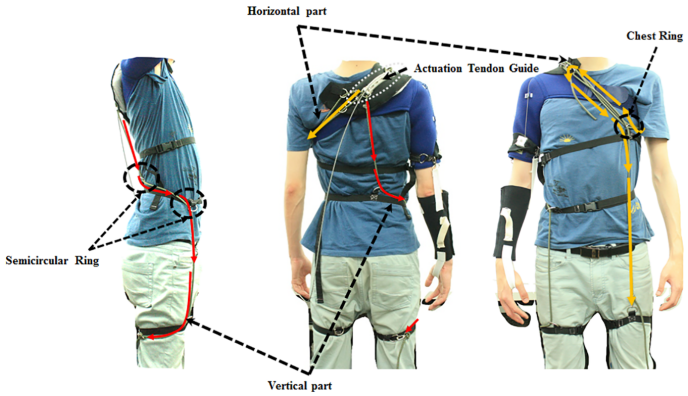

FIGURE 3.2: An ExoSuit for Shoulder Elevation by Park et al. [48]

the actuation is based on the user's skeletal structure, preventing the application of extreme torques that could harm the wearer. Furthermore, their inherent compliance sacrifices movement accuracy and degree of aid, making control incredibly hard [51].

3.1.1 Overview of the Upper-Limb

The goal of an exoskeleton is to support the kinematics and dynamics of the human musculoskeletal structure in order to sustain its mobility. Due to the complexity of the human upper limb's anatomical structure, there is no unanimous kinematic model available in the biomechanics literature that could help us design exoskeletons [52]. Furthermore, the design parameters of the exoskeleton are significantly dependent on the intended application and the subject. As a result, it is necessary to analyze human upper-limb anatomy to design the exoskeleton. The upper limb of a person has 7 degrees of mobility in total, and it is made up of a complicated skeletal structure that comprises the shoulder complex, the elbow complex, the wrist joint, and the fingers. Only the shoulder and elbow joints are described here since almost all upper-limb exoskeletons for physical assistance involve only these two articulations.

Essentially, the shoulder complex can be represented as a ball-and-socket joint. It is made up of the humerus's proximal end, the humeral head, and the scapula's feminine end, the glenoid cavity. Specifically, the shoulder is made up of four articulations: glenohumeral, acromioclavicular, sternoclavicular, and scapulothoracic). They connect three bones: the clavicle (or collarbone), the scapula (or shoulder blade), and the humerus (or upper-arm bone) [53]. The shoulder has a total of 5 degrees of freedom (Figure 3.3), 3 due to the Glenohumeral joint and 2 due to the Sternoclavicular joint [54]. The glenohumeral joint, often known as a ball socket joint or shoulder joint, is composed by the articulation of the humeral head and the glenoid cavity. This joint provides the primary motions of the shoulder complex, which are shoulder flexion/extension, shoulder abduction/adduction, and internal/external rotation. The glenohumeral joint, on the other hand, has an instantaneous center of rotation (COR) that changes with the movement of the human upper limbs. As a result, it is critical to account for the effect of the dynamic center of rotation when modeling the exoskeleton shoulder mechanism. The acromioclavicular joint is formed by the clavicle's lateral end and the scapula's acromion. The sternoclavicular joint, that connects the shoulder complex to the axial skeleton, is a compound joint that is divided into two compartments by articular disks. It is made up of clavicle, sternum,

and cartilage from the first rib. It is responsible for the shoulder translational movements. The scapulothoracic joint is generated by the scapula's female surface and the thorax's male surface. it is not quite correct to consider this a joint since it is a bone-muscle-bone articulation that is not synovial [55].

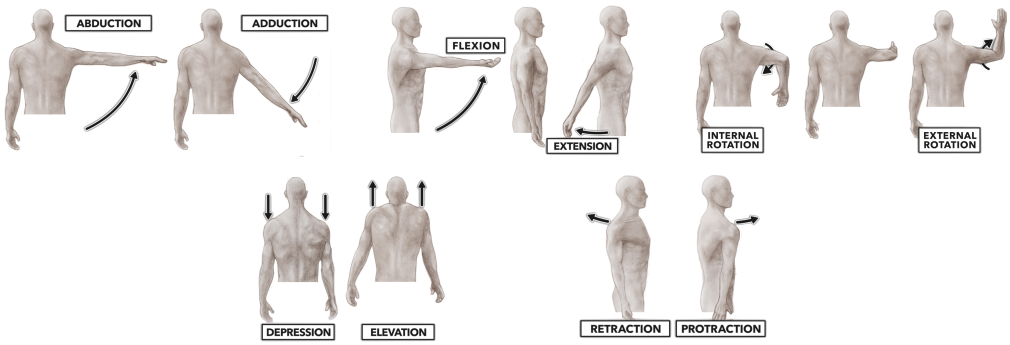

FIGURE 3.3: Shoulder Degrees of Freedom: flexion/extension, shoulder abduction/adduction, internal/external rotation, depression/elevation, and retraction/protraction [56]

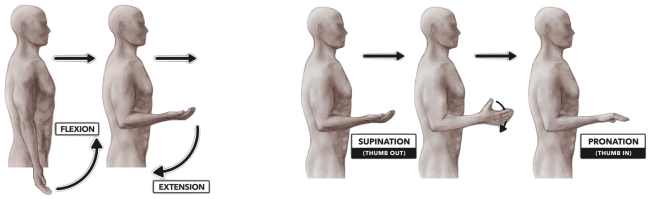

FIGURE 3.4: Elbow Degrees of Freedom: flexion/extension and supination/pronation [57]

The elbow joint is a synovial compound joint that includes the humeroradial, between the capitulum and radial head, and humeroulnar joints, between the trochlea and the ulnar trochlear notch. The humeroradial joint is also known as a ball socket joint because it is formed by the humerus (in the upper arm) and the radial (in the forearm). However, its strong resemblance to the humeroulnar joint and the proximal radiaulnar articulation limits joint movements from 3 to 2 degrees of freedom. The elbow joint complex provides for two degrees of freedom (DOF), as shown in Figure 3.4: flexion/extension, and supination/pronation. Most of the exoskeletons available in the literature simply mimic the elbow joint for 1-DOF flexion/extension.

In conclusion, the wrist joint connects the forearm to the hand. It has a total of 2 degrees of freedom which are wrist flexion/extension and radial/ulnar deviation [58].

3.2 Classification by Applications

Exoskeletons have been developed for three main scenarios: assisting elderly patients or subjects with disabilities with Activities of Daily Living (ADL) (assistive scenario), motor rehabilitation of impaired limbs (rehabilitation scenario) and motor augmentation of healthy subjects in contexts such as factory work, military applications and sport (augmentation scenario).

3.2.1 Assistive Scenario

With advances in technology and medicine in the twenty-first century, the global share of the old population began to rise fast. According to United Nations (UN) data, the proportion of older persons is expected to reach 2 billion by 2050 [59]. It is predicted that developing countries would house more elderly persons than developed countries [60]. Because the process of aging produces degeneration in skeletal and muscle structures, older people begin to experience decrease in muscle strength and volume, making them more susceptible to numerous age-related disorders. According to the findings of studies, upper-limb motions in the elderly are also altered by the aging process. The loss of muscle power in the upper limbs reduces mobility and inhibits daily tasks. Around 15% of older persons over the age of 65 require assistance with routine everyday tasks [61]. Wearable robots are intended to support ADL movements such as drinking, eating, reaching, and personal hygiene in the assistance scenario [62]. Upper limb inefficiency have a significant influence on the subject's quality of life because they limit the subject's ability to conduct basic activities independently. The use of assistive devices may help the user regain some of his or her independence and facilitate participation, which is important from a psychological and social standpoint. Figure 3.5 include MyoPro by Myomo, one of the devices that can be utilized by the elderly to do ADL. This product is commercially available. Exoskeletons can also be used to help people with neurological conditions, such as stroke or multiple sclerosis. Neuromuscular (stroke, spinal cord injury, muscular dystrophy, etc.) and neurodegenerative (multiple sclerosis, amyotrophic lateral sclerosis, etc.) illnesses can cause severe motor dysfunction due to weakness and loss of muscle control, making it difficult for individuals to perform everyday activities like walking or climbing stairs.

FIGURE 3.5: MyoPro by Myomo Exoskeletons for ADL [63]

3.2.2 Rehabilitation Scenario

In the field of rehabilitation, exoskeletons can be used to help individuals who have lost mobility due to physical disabilities or injuries, such as people who have had a stroke or individuals who have suffered a spinal cord injury. The stroke sufferer loses physical strength on one side of the body, known as paralysis or hemiplegia. This has a significant impact on the patient's ability to do everyday life work and activities. Following a stroke, patients are urged to attend therapy sessions in order to stimulate neural plasticity and regain functional abilities. Robots can also assist the clinician in performing rehabilitative exercises in the rehabilitation scenario. The advantage they have over traditional therapy is the increased number of repetitions that can be provided in a session, the ability to objectively quantify the subject's performance, the reduction of the therapist's physical burden, and the ability to monitor

the patient's participation in the training. This allows for an increase in dose, personalization of training intensity, and stimulation of subject participation, all of which are important elements in motor re-learning [64]. This can only reduce the time and cost of rehabilitation, making it more accessible and affordable for patients. Robotic devices can help patients throughout the recovery phase by restoring some of the function that was lost owing to the injury. Rehabilitation can have profound benefits for their overall health and well-being, including improved cardiovascular function, muscle strength, and mental health. Despite the clear benefits of exoskeletons in rehabilitation, there are also some challenges and limitations to their use. Exoskeletons can be expensive and bulky, making them difficult to use in some settings. They also require specialized training and support, which may not be readily available in all rehabilitation centers. Additionally, there are concerns about the safety and reliability of exoskeletons, as they are still a relatively new technology. Some examples are UL-EXO7 [65] and CADEN [66] (Figure 3.6).

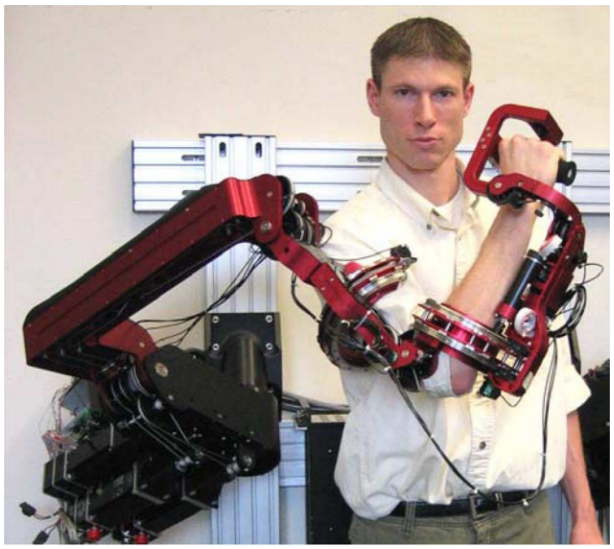

FIGURE 3.6: The CADEN-7 Exoskeleton for Rehabilitaion [66]

3.2.3 Augmentation Scenario

Originally exoskeletons were designed to augment the capabilities of the human body in military fields. This technology that has been around for decades, but has only recently started to be used industrial applications. Because of automated processes and the use of robots, the work load for employees is decreasing in many industrial working environments. Certain tasks and activities, however, will continue to be performed manually by a variety of industrial professionals. In particular, car manufacturers have pioneered research into the use of robots at workplaces, motivated by the great potential to improve the ergonomics of workstations in their manufacturing lines. Despite the widespread use of robots in most welding, painting, and assembling processes, final assembly lines still necessitate some manual operations, such as the assembly of the automobile interior, underbody, doors, windows, or trimmings, and door sealing. These are done quickly (work cycles of a few minutes for tiny cars), and in some cases involve uncomfortable postures while conducting high-precision motions. Although the causes of musculoskeletal disorders are multifactorial (e.g., age, genetics, psychological factors), one of the main contributing factors is musculoskeletal system biomechanical overload, which can

be facilitated by lifting heavy loads on a regular basis or performing monotonous repetitive work [67]. Many employees report significant physical strain from overhead work, as well as musculoskeletal disorders as a result. The repercussions of these illnesses extend far beyond regular working life and can significantly limit people affected's quality of life. The interest of companies lies on the fact thatwork-related musculoskeletal disorders (MSDs) are associated with high costs to employers, either in terms of direct compensation costs or indirect costs (e.g., lost wages, lost production, cost of recruiting and training replacement workers, and healthcare costs for rehabilitating the affected workers). Indeed, companies have expressed interest in exoskeletons as possible solutions to reduce exposure of their workers to physical risk factors that can cause MSDs. Paexo, Levitate, Mate and ShoulderX are commercially available products (Figure 3.7). One of the key challenges in the development of exoskeletons for industrial applications is ensuring that they are safe and easy to use. In order to be effective, exoskeletons must be designed to work seamlessly with all the natural movements of the human body. This requires careful attention to ergonomics and human factors, as well as rigorous testing to ensure that the exoskeleton does not cause any harm to the user.

FIGURE 3.7: Exoskeletons for Augmentation Scenario: Paexo [68], Levitate [69], Mate [70] and ShoulderX [71]

3.3 Classification by Actuation

Actuation is the process of generating force and torques which lead to movement. Exoskeletons are typically categorized as active, passive, or semi-active based on their actuation method [72]. The choice of actuators in the exoskeleton design depends on the intended application and it is a critical design step because it tends to increase the structure's weight. As a result, it is important to choose an actuator with a high power-to-weight ratio.

3.3.1 Active Exoskeletons

Active exoskeletons use powered actuators to move the joints and limbs of the exoskeleton. To drive the exoskeleton, appropriate speed and torque capabilities are required and different solutions can be adopted. Electric motors, hydraulic and pneumatic actuators are the three primary ways to actuate an exoskeleton. Electric actuators are widely used because of their ability to provide greater controllability through advanced motion control [40,46,130,131]. Hydraulic actuators, on the other hand, run on hydraulic pressure. They can generate more torque than electric and pneumatic actuators [73]. The disadvantage is that the system is relatively complex due to the need to keep pressurized oil under pressure to prevent leakage. Additionally, more space is required to accommodate oil pipes and conduits. Because

commercially available hydraulic systems are also heavy, rehabilitation robotics requires specially designed hydraulic systems. The latter actuator is the pneumatic actuator, powered by compressed air. They have a lower impedance than electric actuators, and they require little maintenance and can be stopped while under load without endangering patient safety. However, because a pneumatic system requires pneumatic pressure, exoskeleton robots with pneumatic actuators are mostly stationary platforms, limiting their service area. As a result, the number of exoskeletons that utilize pneumatic actuation is quite limited. Electric, hydraulic and pneumatic actuators can achieve motion in two main ways: direct actuation on joints and cable-driven actuation. Direct actuation on joints involves the use of motors directly attached to the joints of the exoskeleton. An example is the ARMin III [74]. Cable-driven actuation, on the other hand, involves the use of cables and pulleys to transmit force and movement from the actuators to the joints of the exoskeleton. Some powered exoskeletons use this mechanisms to boost power-to-weight ratio by allowing actuators to be located further away from the user's joints. Some examples of cable-driven exoskeletons are L-EXOS [40], IntelliArm [75] and ALEx [76] (Figure 3.8). This type of actuation can make exoskeletons lighter. However, it can be more complex to design and control human-robot interaction forces than direct actuation on joints because of elastic and friction dynamics within the cable-pulley systems.

FIGURE 3.8: ALEx, a Cable-Driven Exoskeleton [76]

The goal of an active exoskeleton is to provide the necessary assistance as freely and naturally as possible to perform the desired task. In this regards, transparency refers to the ability of the exoskeleton to operate smoothly and seamlessly with the user, providing support and assistance without hindering or obstructing their movements or actions. Transparency can be obtnaied either by mechanics or control. The device need to "feel transparent" but also generate significant interaction forces. These two requirements result in opposing actuation requirements: large forces are often accomplished through the use of high-ratio transmission gears, which may impair force control performance and transparency. Active exoskeletons are relatively heavy, huge, expensive, and complex due to the need for motors, control electronics and power supplies (such as batteries). Because of these characteristics, active exoskeletons are less wearable and portable, limiting their use to clinical and laboratory environments.

3.3.2 Passive Exoskeletons

To implement passive gravity balancing with springs in an exoskeleton, engineers must carefully design and calibrate the springs and other mechanical components [77]. Passive exoskeletons use springs or elastic bands to store and release energy at different stages of human movement [78]. This typically involves selecting the appropriate spring stifness and pre-loads to ensure that the exoskeleton remains balanced and stable, while still allowing the user to move freely. In the industrial

context passive exoskeletons are currently more mature than the active one since their operation does not require the use of actuators, batteries, wiring, and electronics. However, active exoskeletons can be much more versatile than passive devices in diverse operating settings [79]. Passive exoskeletons also have the advantage of being simpler to maintain, lighter, and easier to use. Furthermore, they are less expensive because they do not incorporate costly actuators and sensors.

3.3.3 Semi-Active Exoskeletons

To achieve a trade-off between the greater adaptability of active systems and the greater usability of passive devices it is possible to combine the two categories. Semi-passive exoskeletons use spring elements to balance gravity, allowing for the use of low-power servo motors in parallel to passive elements. In this way it is possible to lower costs and also adapt the behavior of the device based on the user's needs, for example, by adjusting the level of assistance or engaging/disengaging the actuation mechanisms.

3.3.4 Actuation in Industrial Exoskeletons

In the industrial context, most commercially available exoskeletons are passive [80]. They are easier to maintain and use, cost-effective, and generally lighter than active ones [81]. They support legs, back, or shoulders, and in rare cases, the entire arm [82]. Examples of passive upper-limb exoskeletons include Airframe Flex (Levitate Technologies, USA), CDYS (Crimson Dynamics, China), Ekso EVO (EksoBionics, USA), MATE (Comau, Italy), Ottobock Shoulder (Ottobock, Germany), ShoulderX (SuitX, USA), and Skelex (Skelex, The Netherlands). Numerous other instances could be cited, given the notable increase in the development of passive industrial exoskeletons over the past five years [83]. In comparison, active exoskeletons offer greater assistive torques and more versatile assistance, allowing them to adapt autonomously to different loads and tasks. Indeed, a review from 2015 indicated that powered exoskeletons tend to be more effective than passive ones in industrial scenarios [84]. However, this comes with a trade-off, as these devices are typically more cumbersome than their passive counterparts. This could hinder their practical implementation in industrial environments [85]. Commercially available active exoskeletons for shoulder support include ExoActive (Festool, Germany) (or S700 Exoskeleton by ExoIQ, Germany), Exoshoulder (Cyber Human Systems, Spain), and Muscle Upper (Innophys, Japan). In recent years, a third category, semi-active (or hybrid) exoskeletons, has emerged. Such exoskeletons combine attributes of both active and passive devices by integrating low-power actuation units with spring-based mechanisms [86]. The hybrid approach is the most promising for enabling the development of wearable, affordable, and compact exoskeletons, thanks to small batteries and compact actuation [87], maintaining the crucial ability of active exoskeletons to regulate and adapt the assistance provided, a significant drawback of passive exoskeletons. Today, semi-active exoskeletons constitute 6% of the total scientific publications [88]. As a point of comparison, passive exoskeletons make up around 60%, ten times more than semi-active ones. Based on the authors' knowledge, the only occupational semi-active exoskeleton for shoulder support available on the market is Agadexo Shoulder (Agade, Italy). However, literature presents another semi-active device for industrial use known as H-Pulse [89]. Additionally,

other commercially available exoskeletons fall into this category. Unlike those previously mentioned, these provide lower-back and lumbar support, and some examples are Cray X and Apogee (German Bionic, Germany), Exoback (RB3D, France), Japet.W (Japet, France), Lumbus II (J-PAS, Japan), and XoTrunk (Proteso, Italy).

3.4 Gravity Compensation in Exoskeletons

Mechanical Gravity Compensation (MGC) technology is particularly useful in exoskeletons designed for medical or rehabilitation purposes, where users may have reduced strength or mobility. It can also be beneficial in industrial settings, where exoskeletons are used to assist with heavy lifting and other strenuous tasks. Mechanical Gravity Compensation allows a robotic system to function with relatively small actuators that generate less torque. This is a crucial factor to enable the development of lightweight and wearable exoskeletons. Overall, MGC helps to improve the usability and effectiveness of exoskeletons in a wide range of applications. Unlike passive exoskeletons, semi-active exoskeletons can adapt in the presence of external loads and increase or decrease the level of assistance provided. To synergistically integrate MGC and active actuation power, semi-active exoskeletons require load estimation algorithms able to infer the load carried by the user. In most of the scenarios, this is still an open problem because information from voluntary muscle activation is required. Methods to attempt to solve this problem include the use of a musculoskeletal model and analysis of muscle signals measured with electromyography (EMG) devices [90].

Despite the many benefits of passive gravity compensation, there are also some challenges and limitations to its use. Some of the major challenges to this approach involve the need to accurately calculate gravitational forces to design the MGC system. This requires considering the weight of the exoskeleton itself, the weight of the person wearing it, and any additional equipment or payloads that may be carried. Including several DOFs greatly complicates this process. Besides ensuring proper kinematic compatibility between the exoskeleton and the user, it is extremely difficult to design a passive balancing system that is effective in all the configurations that can be reached with several DOFs. Moreover, even the most precise calculations encounter the problem of the interface between the exoskeleton and the person wearing it. This is due to the relative movements between the human-exoskeleton interface, designed to allow relative movements to avoid pain and discomfort. However, unlike passive exoskeletons, semi-passive systems can overcome approximations of the gravitational model by adjusting residual gravity forces with the usage of the actuator.

3.5 Benefits Related to Assistive Exoskeletons

Despite advancements in industrial automation and the increasing integration of robots, Work-Related Musculoskeletal Disorders (WRMSDs) remain a prevalent issue across various production environments. Back pain and arm and shoulder muscle pain affect 43% and 42% of European workers, respectively [91]. The primary causes of WRMSDs include age, genetics, and psychological factors, but a major contributor is biomechanical overload of the musculoskeletal system [92]. Overload is not limited to lifting heavy weights; repetitive movements are a significant cause of musculoskeletal disorders, accounting for 61% of cases [93]. Additionally, uncomfortable postures, such as overhead work, contribute to shoulder girdle muscle

pain [94]. Given the extensive range of motion of the shoulder joint, it is particularly vulnerable to both acute injuries and chronic overuse [95]. These health issues impose significant financial burdens on companies, reducing productivity and increasing costs associated with employee replacement and training [96]. However, automation alone cannot eliminate the problem, as manual labor remains essential for complex tasks requiring decision-making, dexterity, and adaptability [97]. In this context, exoskeletons present a promising solution for reducing excessive strain on human joints [98]. These wearable devices provide support, assistance, and protection to workers performing physically demanding tasks [99], thereby reducing injury risks and enhancing overall productivity.

The increasing availability of exoskeletons in the market is reflected in the growing body of scientific literature evaluating their effectiveness. Over the past five years, research on industrial exoskeleton performance has significantly expanded [100]. Studies assessing the impact of exoskeletons on the shoulder region have reported positive outcomes, including reduced muscle activity during shoulder flexion and abduction and decreased cardiovascular and metabolic strain [101]. Furthermore, exoskeletons have been found to lower perceived effort for both static and dynamic tasks, as well as for short and prolonged exercises [102]. Despite extensive research on the biomechanical and physiological effects of exoskeletons [103], a definitive evaluation of their overall implications remains elusive [104]. Many studies currently focus on establishing a standardized framework for assessing exoskeleton performance, including defining task types, measurement parameters, and experiment durations [105]. However, a key challenge in comparing exoskeletons is their task-specific design. For instance, most exoskeletons developed for material handling offer back support, whereas upper-limb exoskeletons are predominantly evaluated in overhead assembly and manufacturing settings [106]. While passive exoskeletons, commonly discussed in the literature, have shown promising performance, their effectiveness is largely restricted to the specific tasks for which they were designed. Research on industrial exoskeletons has demonstrated that upper-limb exoskeletons can objectively and subjectively reduce muscular and joint stress. Laboratory studies indicate that exoskeletons significantly decrease muscle activity in the anterior, middle, and posterior deltoid, as well as the trapezius, for tasks performed above shoulder level [107, 108]. Reduced activity in shoulder girdle muscles correlates with decreased shoulder compression forces, benefiting glenohumeral joint health [107]. Additionally, some studies have reported lower heart rates among participants using exoskeletons [109, 110, 111].

However, significant discrepancies exist between laboratory and field studies on exoskeleton effectiveness. One possible explanation is that real-world tasks involve not only overhead work but also secondary activities, which can influence the overall effectiveness of exoskeletons. While human movement is typically efficient, wearing an exoskeleton may introduce inefficiencies, leading to increased fatigue. Concerns regarding their use include discomfort, excessive muscle activity due to load redistribution, and potential muscle deconditioning. Many studies rely on small sample sizes and primarily focus on muscle activity, often neglecting biomechanical parameters and user comfort [112]. In some cases, long-term usability issues have been identified. For example, one study reported a decline in exoskeleton usage intention over a four-week period, potentially due to discomfort, heat accumulation, insufficient support perception, workplace incompatibility, or other personal factors [113].

Clear evidence of exoskeleton benefits is essential for large-scale industrial adoption. While laboratory research is well-documented in academic literature, its findings may not always translate to real-world conditions. A further obstacle to widespread adoption is the lack of standardization. As a relatively new technology, exoskeletons lack universally accepted design specifications, making it challenging for companies to identify suitable solutions and for manufacturers to ensure compatibility across different industrial applications. Additionally, cost remains a significant barrier, particularly for active exoskeletons, which require complex engineering and development, leading to high prices that limit their accessibility in industrial settings.

Despite these challenges, the use of exoskeletons in industrial applications is rapidly expanding. As technological advancements continue, it is expected that more companies will integrate exoskeletons to enhance workplace efficiency and safety. Addressing issues such as standardization, cost, and real-world applicability will be essential for maximizing the potential of exoskeletons in reducing WRMSDs and improving worker well-being.

Chapter 4

Evaluation of a Semi-Active Upper-Limb Exoskeleton

This chapter assesses the effectiveness of a semi-active upper-limb exoskeleton, tailored explicitly for workers in manual material handling tasks, supporting their upper limbs.. This study aims to simulate an industrial environment and measure the effect of the exoskeleton through electromyography (EMG) and postural analysis, along with subjective evaluations using validated assessments. Overhead tasks are not included in the study, as an active (or semi-active) exoskeleton would yield results similar to those already obtained with passive exoskeletons. Owing to their adaptability, semi-active exoskeletons can indeed fit a diverse array of tasks. For the use of a semi-active exoskeleton and the selection of tasks, the study aims to serve as an extension of existing literature.

4.1 Material and Methods

4.1.1 Participants recruitment

Fourteen healthy young men [age 27.1 ± 2.7 years (means ± SD), body mass 72.9 ± 6.6 kg, height 174.2 ± 4.2 cm] with no known neurological or motor disorders and no previous experience with Agadexo or other exoskeletons were recruited as participants for this study. Each participant voluntarily participated in the experiment and provided written consent exclusively for the publication of their data concerning this study. Among the participants, eleven participants were right-side, and three were left-side dominant. Ethical approval for the study was obtained from the Institutional Review Board at the Department of Neurosciences, Biomedicine, and Movement Sciences of the University of Verona (n.16/2023).

4.1.2 Apparatus

EMG signals were recorded using a wireless low-power signal conditioning electronics device (Zero Wire Aurion, Milan, Italy). A pair of EMG electrodes were attached over ten muscles on the dominant side of the body: Upper Trapezius (UT), Anterior Deltoid (AD), Posterior Deltoid (PD), Infraspinatus (IN), Latissimus Dorsi (LD), Erector Spinae near the L1 vertebra (ES), Rectus Abdominis (RA), Pectoralis Major (PM), Biceps Brachii (BB), and Brachioradialis (BR) (Figure 4.1). Muscle activity was measured only on the dominant side due to the system's limited number of channels. Adhesive electrodes were attached after cleaning the skin surface with denatured alcohol to enhance signal quality. Electrode placement followed the recommendation by the SENIAM project [114]. To record the three components of ground reaction forces and Center of Pressure (CoP) migration, a floor-embedded

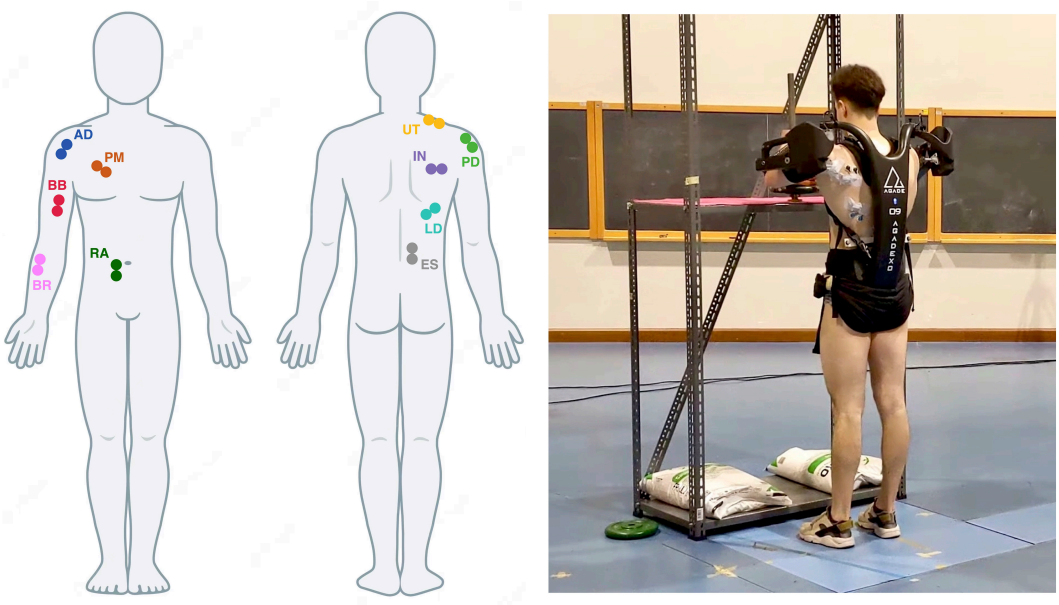

FIGURE 4.1: On the left: EMG sensor locations on the dominant side of the body. The selected muscles are Upper Trapezius (UT), Anterior Deltoid (AD), Posterior Deltoid (PD), Infraspinatus (IN), Latissimus Dorsi (LD), Erector Spinae near the L1 vertebra (ES), Rectus Abdominis (RA), Pectoralis Major (PM), Biceps Brachii (BB), and Brachioradialis (BR) On the right: a study participant, wearing the exoskeleton and equipped with EMG sensors, stands in front of a shelf.

force plate (model OR-5, AMTI, USA: 900x900 *mm*) was employed. The acquisition of data from EMG sensors and the force plate occurred at a sampling frequency of 1000 *Hz*.

To replicate a logistics and manufacturing work environment, two shelves were set up facing each other at approximately four meters. One of the shelves was placed in correspondence with the force plate. Each one had a shelf board measuring 600x1200 *mm*, and its height from the ground was adjusted based on the participant's height and the specific task (Figure 4.1). The study employed a box with handles and a weighted bar to simulate lifting and handling heavy objects. The box measured 450x350x200 *mm*. Two handles were placed vertically on each side, allowing a comfortable grip. The total weight of the box was 5.5 *kg*, and it could accommodate weightlifting plates to increase its weight. The weighted bar, a 500 *mm* tall aluminum tube with a 15 *mm* diameter, had a rigid base at one end. The bar's weight was half a kilogram and could be augmented with plates. The bar was meant to be gripped on its upper portion with both hands, one below the other, with the dominant hand positioned below the other.

4.1.3 Exoskeleton Used in the Study

The exoskeleton utilized for these tests is Agadexo Shoulder, from AGADE srl. This device is a semi-active upper-limb exoskeleton designed to reduce muscular effort in the shoulders during dynamic manual material handling tasks commonly encountered in manufacturing, logistics, and retail industries. This exoskeleton specifically assists shoulder elevation and abduction, supporting the glenohumeral joint in lifting and outward arm movements against gravity. This exoskeleton integrates a patented semi-active motion technology that minimizes power consumption by

using an electric motor and force and motion sensor in combination with a spring [115]. In this semi-active exoskeleton, the elastic element and the motor do not work in parallel but rather in series. The motor, through a linear actuator, moves one of the attachment points of the spring, thus controlling its length and, consequently, the intensity of the elastic torque provided. In this way, the device can provide assistive torques with the same versatility as an active exoskeleton while maintaining a compact weight and size. The device employs two wireless forearm bracelets to detect grasping external payloads during pick-and-place activities and provide assistance accordingly. In the transparent mode, when no payload is carried, the exoskeleton minimizes interaction forces with the user, closely following their movements. In the assistive mode, when the user lifts and carries payloads, the exoskeleton delivers a maximum torque of 30 Nm to counteract gravity and reduce strain on the shoulders. Within this mode, users can select from three levels of assistance: minimum, medium, and maximum. The exoskeleton is adjustable in length and was fitted for each participant according to the company's provided guidelines.

4.1.4 Procedure

Participants began their session following a 30-minute familiarization with the exoskeleton, as suggested by the company. During this time, participants became acquainted with the exoskeleton and the objects used in the research. The study comprised four distinct tasks, illustrated in Figure 4.2: the first three involved using the weighted bar, while the fourth task employed the box. For the choice of tasks, we relied on the company to test the exoskeleton under conditions similar to real-world use. The following is a detailed description of the exercises conducted in the study:

1. **Static Lifting** - Task 1 involved lifting the weighted bar while keeping a stationary posture. The shelf board on which the bar was positioned was aligned with the participant's hip height. Participants were instructed to lift the bar until their arms were parallel to the ground. After a one-second hold, the participant placed the bar back on the shelf;

2. **Load Carrying SL** - Task 2 required participants to displace the weighted bar between the two shelves at a four-meter distance. The shelf boards were set at chest level height, enabling participants to grasp the bar and forming with their upper arms a 90-degree angle between their upper arms and torso. Participants were instructed to maintain this angle throughout the task. The name of this task includes the acronym SL (Shoulder Level) to distinguish it from the following task;

3. **Load Carrying HL** - Task 3 resembled the previous one, but with a change in the height of the two shelves and the position of the weighted bar during transportation. Participants were instructed to lift and move the bar while keeping their forearms parallel to the ground. The name of this task includes the acronym HL (Hip Level) to differentiate it from the preceding task;

4. **Box Handling** - Task 4 exclusively employed the box. Participants were instructed to grab the box from the first shelf and displace it on the second shelf. During the displacement, the box was kept close to the body. The setup was structured so the participants could position the box on the second shelf, creating a 90-degree angle between their extended arms and torso.

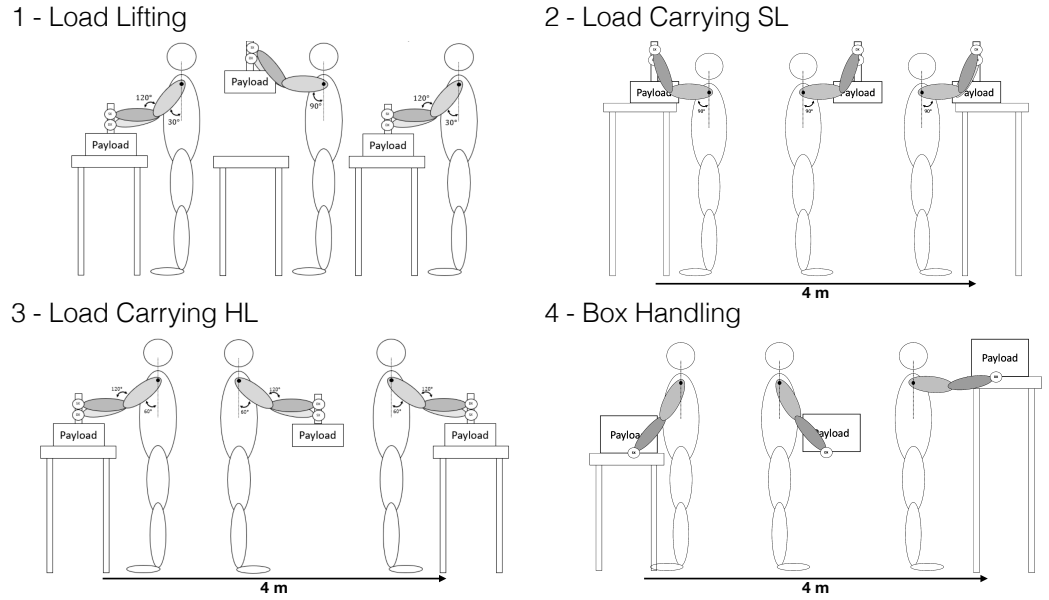

FIGURE 4.2: Illustration of the four tasks with their respective names and positions to maintain. The arrows in Tasks 2-4 indicate that participants must move between the two shelving units carrying the weight. Task 4 is the only one that involves using the box.

All tasks were conducted both with and without the exoskeleton. Additionally, 8 *kg* and 13 *kg* weights were utilized for each task. To maintain a reasonable duration for the experiment, each task was performed six times under each condition. After each set of six trials, participants rated their perceived effort using the Borg scale, ranging from 6 to 20 [116]. Then, a 2-minute break was taken. The sequence of task conditions (four) and the weights (two) were randomized across participants. However, it was decided to conduct two distinct blocks of trials, performing all tasks consecutively with and without the exoskeleton. Half of the participants began by completing all the trials with the exoskeleton, while the other half did the same without it. To study how different assistance levels affect the use, Tasks 1 and Task 2 (Static Lifting and Load Carrying SL) were performed with both medium and maximum assistance levels. Conversely, Tasks 3 and Task 4, namely Load Carrying HL and Box Handling, exclusively employed the maximum assistance level. This decision aimed to mitigate the duration of the test. Participants were unaware of the assistance level used during Tasks 1 and Task 2. In summary, Task 1 and Task 2 consisted of two weights and two levels of assistance of the exoskeleton, while Task 3 and Task 4 used two weights and only one level of assistance. With six repetitions per condition, the total number of trials was 120. These abbreviations will be used in the following text: NoExo for trials without the exoskeleton, ExoMed for trials with the exoskeleton and medium assistance, and ExoMax for trials with the exoskeleton and maximum assistance.

Upon completing all four tasks, participants completed the NASA Task Load Index (NASA-TLX) assessment [117]. Results were exclusive to trials without the exoskeleton and with maximum assistance. This is because these experimental conditions consisted of the same number of trials, while the tasks with medium assistance were fewer. Therefore, to maintain the integrity of the NASA-TLX results, it

was decided to group the trials at a medium assistance level and conduct them separately from the ExoMax trials. Additional trials were performed before concluding the experimental session to standardize the collected data. These trials involved two repetitions of each task, using a weight equal to 25% of the individual's body mass, and were solely performed without wearing the exoskeleton. Only trials with the highest EMG values were used for data analysis for each task. This standardization approach was employed due to the unfeasibility of a Maximum Voluntary Contraction (MVC) for all ten measured muscles. After completing the tests and removing all sensors from the participants' bodies, a questionnaire tailored to this study, consisting of 15 inquiries, with responses ranging from 0 to 10, was administered to all participants. The overall duration of the testing session was approximately three hours, accounting for familiarization, participant preparation, trial execution, and questionnaire completion. Based on participants' qualitative feedback, muscular fatigue was not perceived as an issue during the tasks.

4.1.5 Data Analysis

Data were processed offline in MATLAB software (R2022b, version 9.13.0). The EMG signals were subjected to rectification and filtering through a sixth-order, zero-phase digital Butterworth filter with a 5-50 Hz bandpass. Force plate signals were filtered with a 5 Hz low-pass, fourth-order, zero-phase digital Butterworth filter.

To facilitate the comparison of the same task between different experimental conditions and participants, time windows of interest were isolated to calculate the Root Mean Square (RMS) of the EMG signal for each muscle. These time segments corresponded to the lifting and one-second holding for Task 1 (Static Loading), the walking phase before placing the weighted bar on the shelf for Tasks 2 and 3 (Load Carrying SL and Load Carrying HL), and the positioning of the box once in front of the shelf for the Task 4 (Box Handling), excluding the walking phase. The decision to exclude in Task 4 the movement between the two shelves was made to highlight the lifting and positioning of the box. To quantify the level of muscle activation, the RMS of the signal was calculated, as done in other similar studies [118]. Before computing this value, the signals from each muscle were normalized by the maximum value of the EMG signal obtained during the normalization trials. Subsequently, the percentage variation with respect to trials without the exoskeleton was calculated using the following formula:

$$\Delta EMG[\%] = \left(\frac{EMG_{RMS}^{NoExo} - EMG_{RMS}^{Exo}}{EMG_{RMS}^{NoExo}} \cdot 100 \right) \tag{4.1}$$

where EMG_{RMS}^{NoExo} is the RMS of the normalized EMG signal computed for trials without the exoskeleton and EMG_{RMS}^{Exo} is the RMS of the normalized EMG signal computed in trials with the exoskeleton, with either the maximum and the intermediate level of assistance, where present.

Besides possible variations in muscle activity, it is crucial to contemplate additional associated factors linked to the presence of the exoskeleton, which could lead to unexpected long-term repercussions. Foremost among these is assessing whether the exoskeleton impacts balance and postural stability. To achieve this, a highly effective approach involves the examination of Center of Pressure (CoP) and Ground Reaction Forces (GRF), quantified using the force plate. The primary parameters for evaluating balance encompass CoP migration along the sagittal and coronal planes,

CoP velocity, and the area enclosing 95% of CoP migration within the smallest ellipse, determined through Principal Component Analysis (PCA) [119]. Among the tasks proposed in the study, only one is carried out entirely on the force plate: Static Lifting (Task 1). Therefore, the results are relevant solely to this exercise.

4.1.6 Statistical Analysis

A repeated measures Two-Way ANOVA was employed to analyze the RMS value of the EMG and force plate signals. The factors included load *Weight* (with two levels: 8 *kg* and 13 *kg*), and *Assistance* (with three levels, specifically NoExo, ExoMax, and ExoMed in Task 1 and Task 2 and two levels, NoExo and ExoMax, in Task 3 and Task 4). Pairwise contrasts with Bonferroni corrections were conducted to examine significant interactions. The NASA-TLX output and BORG Ratings are categorical and non-normally distributed; therefore, a Wilcoxon signed-rank test was used for paired comparisons. For all statistical analyses, the critical p-value was set at 0.05. The complete results of the statistical analysis are reported in Appendix A.

4.2 Results

4.2.1 Muscular Activity

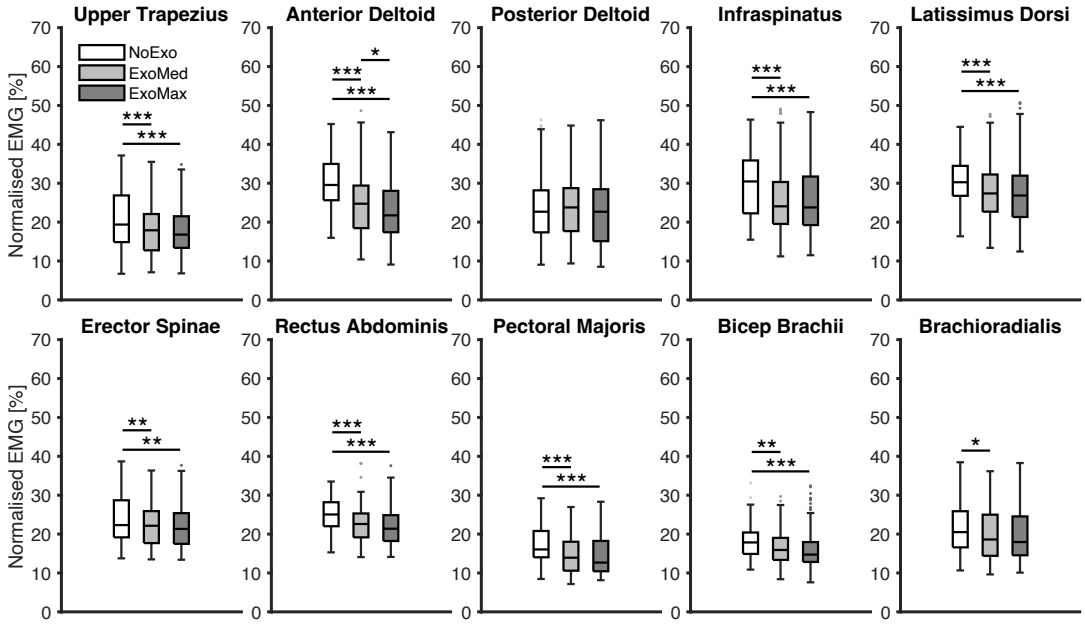

FIGURE 4.3: EMG results for *Assistance* Factor in Task 1 - Static Lifting. Using the exoskeleton significantly decreases the average activity levels in nearly all muscle groups. During the only task that didn't involve a movement between the two shelves, only slight variations were observed between the two different levels of assistance provided by the exoskeleton. $*$ indicates p-values ≤ 0.05, $**$ indicates p-values ≤ 0.01, and $***$ indicates p-values ≤ 0.001

Using the exoskeleton consistently resulted in decreased average muscle activity. Muscles such as the Upper Trapezius, Anterior Deltoid, and Rectus Abdominis generally showed notable reductions in all tasks. These results highlight the adaptability of the exoskeleton to various tasks, illustrating the potential of hybrid systems for dynamic applications. However, the Posterior Deltoid and Brachioradialis

were less affected. The overall reduction in muscle activity was more pronounced in conditions involving higher levels of assistance. Differences between medium and maximum assistance levels were less common.

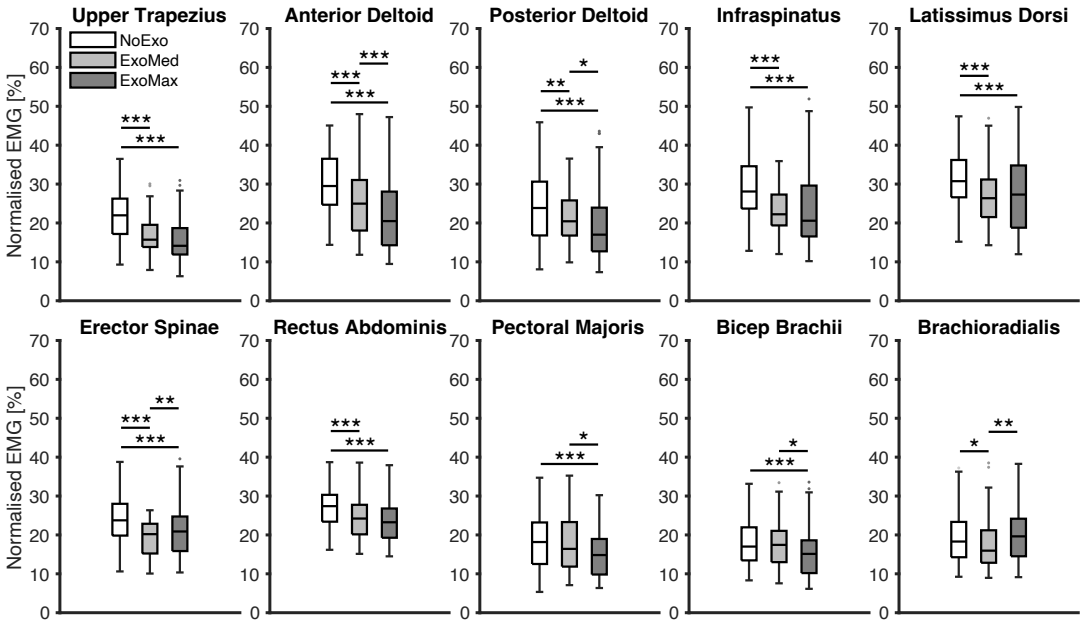

FIGURE 4.4: EMG results for *Assistance* Factor in Task 2 - Load Carrying SL. This particular task proved to be the most demanding of all, as every muscle group considered in the study exhibited a notable reduction in average activity when the exoskeleton was worn. Additionally, a significant difference between the levels of assistance provided by the exoskeleton was observed, highlighting the impact of varying assistance on muscle activity. $*$ indicates p-values ≤ 0.05, $**$ indicates p-values ≤ 0.01, and $***$ indicates p-values ≤ 0.001

In detail, the box plot for Static Lifting (Task 1) depicts significant differences when using the exoskeleton, almost always regardless of the level of assistance used (Figure 4.3). Great differences were observed for all the muscles except for the Posterior Deltoid (UT - $F(2,26)=15.15$, $p<.001$, $\eta^2=.05$; AD - $F(2,26)=52.07$, $p<.001$, $\eta^2=.13$; IN - $F(2,26)=23.03$, $p<.001$, $\eta^2=.06$; LD - $F(2,26)=16.18$, $p<.001$, $\eta^2=.04$; ES - $F(2,26)=7.27$, $p<.001$, $\eta^2=.02$; RA - $F(2,26)=23.59$, $p<.001$, $\eta^2=.07$; PM - $F(2,26)=15.59$, $p<.001$, $\eta^2=.06$; BB - $F(2,26)=11.05$, $p<.001$, $\eta^2=.03$; BR - $F(2,26)=3.94$, $p<.001$, $\eta^2=.01$).

In Task 2, Load Carrying SL, all muscles exhibit significant variations between the NoExo trials and the two levels of assistance, with the sole exception being the Brachioradialis muscle, which did not show differences between NoExo and ExoMax (Figure 4.4) (UT - $F(2,26)=84.95$, $p<.001$, $\eta^2=.25$; AD - $F(2,26)=50.45$, $p<.001$, $\eta^2=.15$; PD - $F(2,26)=19.36$, $p<.001$, $\eta^2=.08$; IN - $F(2,26)=33.97$, $p<.001$, $\eta^2=.11$; LD - $F(2,26)=12.3$, $p<.001$, $\eta^2=.04$; ES - $F(2,26)=21.6$, $p<.001$, $\eta^2=.08$; RA - $F(2,26)=23.81$, $p<.001$, $\eta^2=.09$; PM - $F(2,26)=9.69$, $p<.001$, $\eta^2=.05$; BB - $F(2,26)=10.68$, $p<.001$, $\eta^2=.05$; BR - $F(2,26)=6.74$, $p=.002$, $\eta^2=.03$).

In Tasks 1 and 2, where two levels of assistance were employed, variations between NoExo and ExoMax was observed almost exclusively in Task 2. Among these, Erector Spinae and Brachioradialis showed an anomalous trend compared to the others, with their activation being higher in the case of maximum assistance compared to the medium level.

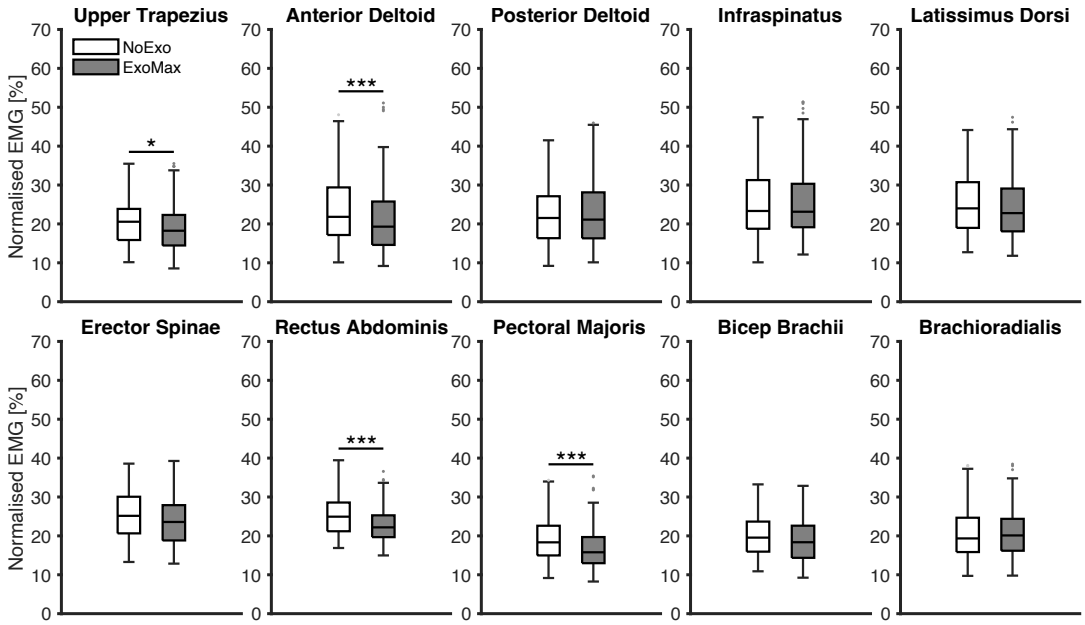

FIGURE 4.5: EMG results for *Assistance* Factor in Task 3 - Load Carrying HL. When the exoskeleton was utilized in a sub-optimal configuration, it reduced average activity in only four specific muscles. This limited impact suggests that the configuration was not effective in uniformly decreasing muscle activity across all muscle groups, highlighting the importance of optimal settings for achieving comprehensive muscle relief. $*$ indicates p-values ≤ 0.05, $**$ indicates p-values ≤ 0.01, and $***$ indicates p-values ≤ 0.001

In Task 3 (Load Carrying HL), which exclusively used the maximum assistance level, significant reduction of EMG activity when using the exoskeleton were observed (Figure 4.5). , specifically on Upper Trapezius, Anterior Deltoid, Rectus Abdominis, and Pectoralis Major (UT - F(2,26)=5.67, p=.018, η^2=.1; AD - F(2,26)=12.16, p<.001, η^2=.03; RA - F(2,26)=16.97, p<.001, η^2=.05; PM - F(2,26)=17.81, p<.001, η^2=.04). The list could also include Biceps Brachii with a p-value of 0.0503 (F(2,26)=3.86, η^2=.01).

Even in Task 4 (Box Handling), and as in all previous ones, the Brachioradialis muscle shows no differences between the ExoMax and NoExo conditions (Figure 4.6). The statistical analysis significant differences for 7 muscles out of 10 (UT - F(2,26)=70.43, p<.001, η^2=.15; AD - F(2,26)=102.56, p<.001, η^2=.2; PD - F(2,26)=21.79, p<.001, η^2=.06; LD - F(2,26)=36.68, p<.001, η^2=.08; ES - F(2,26)=25.4, p<.001, η^2=.05; RA - F(2,26)=13.6, p<.001, η^2=.04; BB - F(2,26)=4.24, p=.04, η^2=.01).

No particular change emerged by examining the interaction between the two factors *Assistance* and *Weight*, with the trend remaining nearly the same for both the 8 and 13 *kg* conditions. Only the Pectoralis Major in both Load Carrying tasks (Task 2: F(2,26)=3.86, p=.022, η^2=.02; Task 3: F(2,26)=8.41, p=.004, η^2=.02) and the Latissimus Dorsi in Box Handling (Task 4: F(2,26)=4.45, p=.036, η^2=.01) showed a significant difference in this interaction.

4.2.2 Balance and Postural Stability

Among the parameters computed from force plate data, only three displayed significance in the *Assistance* factor: Center of Pressure velocity (F(2,26)=3.86, p =.022, η^2=.01), the maximum force exerted in the direction perpendicular to the ground

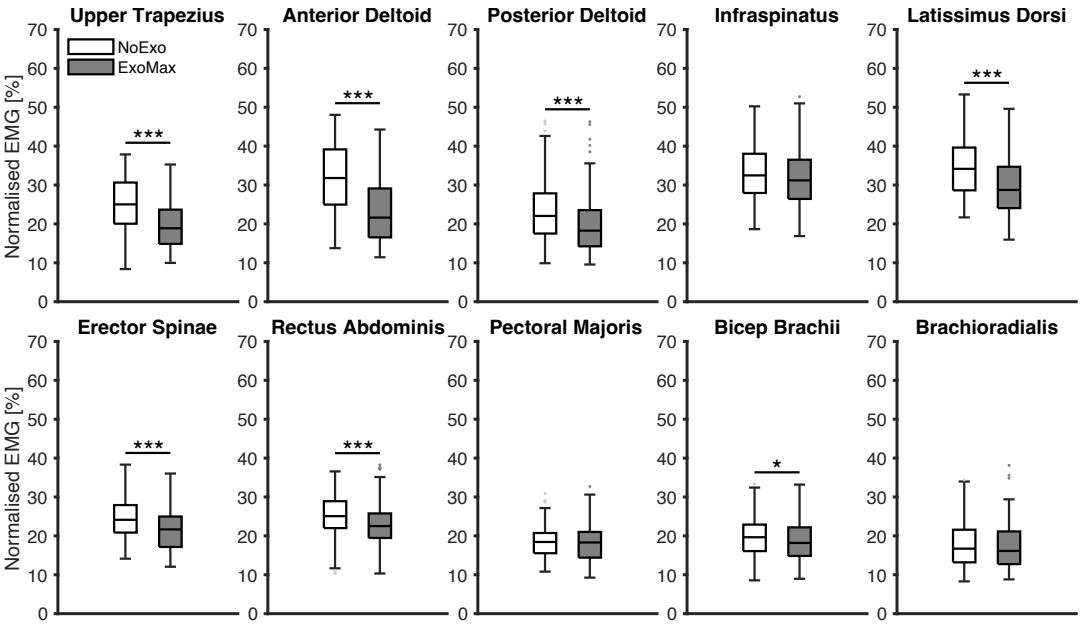

FIGURE 4.6: EMG results for *Assistance* Factor in Task 4 - Box Handling. The task involving the box showed a noticeable decrease in activity across most muscles, indicating the exoskeleton's effectiveness in reducing muscle strain during material handling. $*$ indicates p-values ≤ 0.05, $**$ indicates p-values ≤ 0.01, and $***$ indicates p-values ≤ 0.001

(F(2,26)=6.12, p =.002, η^2=.004), and the average time for lifting the weighted bar (F(2,26)=5.32, p=0.005, η^2=.03). Among these, the first two also have significant interaction between the *Assistance* x *Weight* Factors (F(2,26)=5.8, p=.003, η^2=.02 and F(2,26)=3.69, p=.026, η^2=.002). These outcomes are present only when the weight of 13 *kg* was used (Figure 4.7). Lastly, the area of the ellipse calculated through PCA and migration in Antero-Posterior and Medio-Lateral directions remained unchanged regardless of the exoskeleton's presence or the different levels of assistance.

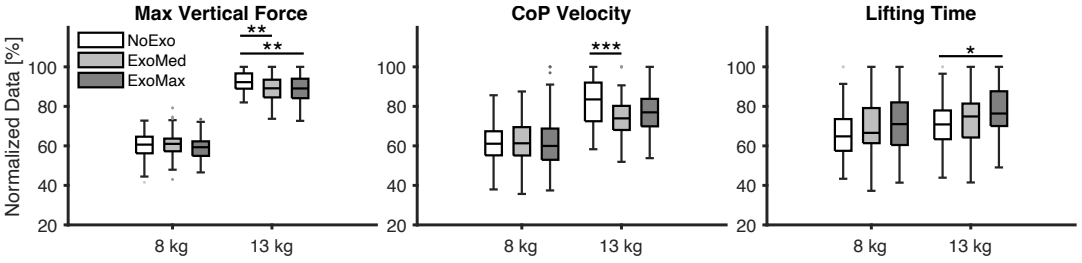

FIGURE 4.7: Force Plate results *Assistance* x *Weight* Factors. The results suggest that using the exoskeleton helps participants perform movements more smoothly, which in turn reduces the stress and strain on their joints and muscles. $*$ indicates p-values ≤ 0.05, $**$ indicates p-values ≤ 0.01, and $***$ indicates p-values ≤ 0.001

4.2.3 Subjective Feedbacks and End-of-session Questionnaire

The subjective results from the Borg scale and NASA-TLX indicate that participants perceived a reduction in effort while using the exoskeleton without increasing cognitive load. In the NASA-TLX, significant differences were found only in Physical

Demand (p=.004= and Effort (p=.006) items (Figure 4.8), corresponding to a 34.0% and a 44.9% reduction, respectively. All other items showed no significant differences. It is important to remember that these results pertain only to the trials without the exoskeleton and those with maximum assistance, called ExoMax, considering all four tasks collectively.

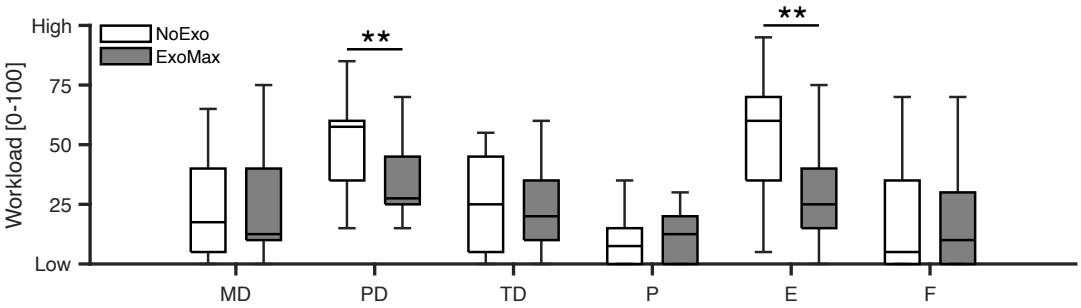

FIGURE 4.8: Results for NASA-TLX categories: Mental Demand (MD), Physical Demand (PD), Temporal Demand (TD), Performance (P), Effort (E), and Frustration (F). In Performance (P), 0 stands for "Good" and 100 for "Poor." Using the exoskeleton resulted in an overall reduction in Effort (-44.9%) and Physical Demand (-34.0%) across all tasks without deteriorating Performance or requiring additional Mental Demand. The exoskeleton proved to be effective and easy to use. $*$ indicates p-values ≤ 0.05, $**$ indicates p-values ≤ 0.01, and $***$ indicates p-values ≤ 0.001

The median values reported by participants on the Borg scale were lower when the exoskeleton was used. Considering both the *Assistance* and *Weight* factors, the results were similar for Tasks 1 and 2: a significant difference between using maximum assistance and not using the exoskeleton was present for both 8 and 13 kilograms (Figure 4.9). Focusing solely on the *Assistance* factor, participants reported significant differences in perceived effort between NoExo and ExoMax across all four tasks (Task 1: p$<$.001; Task 2: p$<$.001; Task 3: p=.003; Task 4: p=.002). In the tasks where medium assistance was also provided, namely Tasks 1 and 2, no differences were found between the two levels of assistance.

Lastly, inquiries with responses ranging from 0 to 10 explored various aspects of the exoskeleton and its usage. Overall, the questionnaire's outcome was positive, with inquiries like "I would use this exoskeleton if I had to redo these tasks" receiving a rating of 8 ± 2 (mean ± SD) and "I believe exoskeletons are an important technological innovation" with a rating of 9.2 ± 0.9. Only two of them received a low score (less than six): "I feel unrestricted in my movements when wearing the exoskeleton" with a score of 5.7 ± 1.7, and "The exoskeleton allows me to move as I would like" with a score of 5.5 ± 2.5. All inquiries won't be detailed here; they will be used in the Discussion to provide integration and explanation of the obtained results.

4.3 Discussion

The present study aims to investigate the effect of an occupational semi-active exoskeleton in an industrial context. Three different areas of exoskeleton usage have

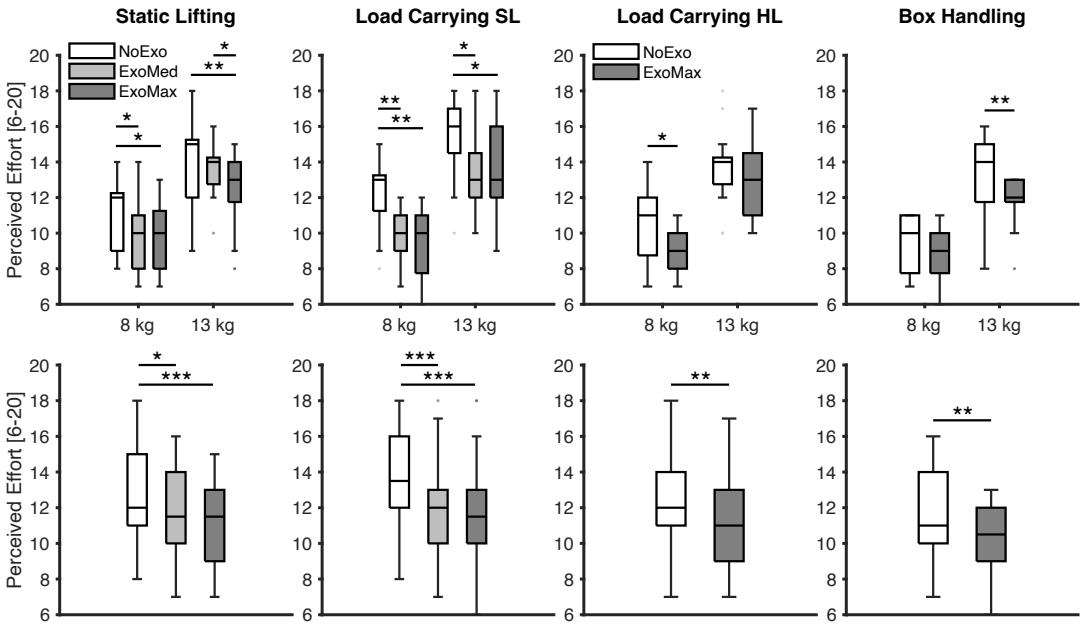

FIGURE 4.9: BORG Rates results for *Assistance* x *Weight* Factors in the top row and *Assistance* Factor in the bottom row. The perceived effort during trials with the exoskeleton was consistently lower compared to trials without it. Additionally, there were no significant differences in perceived effort between the two different levels of assistance provided by the exoskeleton. $*$ indicates p-values ≤ 0.05, $**$ indicates p-values ≤ 0.01, and $***$ indicates p-values ≤ 0.001

been evaluated for a comprehensive understanding and, overall, the results consistently indicate that the exoskeleton reduced muscle activity and lowered the perceived effort by users. Surface electromyography allowed for quantifying the reduction in ten muscles commonly involved in manual handling and lifting. In particular, the task where the best results were obtained is Load Carrying at Shoulder Level (SL). This movement, unlike the others, is of great importance because it represents a task that has been less studied, in which passive upper-limb exoskeletons are likely to be ineffective. The good results achieved by this exoskeleton are mainly due to its semi-active nature. The ability to adjust the level and curve of the provided assistance makes these types of exoskeletons both effective and versatile. Questionnaires, Borg Rates, and NASA-TLX provide valuable insights into user assessments, a crucial aspect of adopting the product in an industrial environment. Lastly, the force platform enabled the evaluation of effects on postural stability and balance. These results confirm that semi-active exoskeletons are a promising field. This outcome holds even if the considered exoskeleton presents a slightly adjustable kinematic structure and the lack of self-aligning mechanisms on the shoulders, which led to low scores in freedom of movement. Finally, despite the weight and bulkiness of the active components and batteries, balance was not compromised.

4.3.1 Effects of the Exoskeleton on Muscular Activity

The statistical analysis conducted to explore the RMS of the EMG signals utilized a two-way ANOVA with *Assistance* and *Weight* as factors. *Weight* Factor was highly significant across all tasks, conditions, and each muscle, as expected (all p-values $<$ .001). This indicates that the EMG signal was higher when the movements were performed by lifting or displacing the 13 *kg* weight. It is intuitive to assume that EMG

levels are higher when carrying 13 *kg* payloads without the exoskeleton. However, it should not be surprising that this difference is also evident in both ExoMax and ExoMed cases: the exoskeleton's function is not to compensate the entire payload to be lifted but rather a relative portion.

TABLE 4.1: Percentage reduction of normalized EMG in muscle activity of Upper Trapezius (UT), Anterior Deltoid (AD), Posterior Deltoid (PD), Infraspinatus (IN), Latissumus Dorsi (LD), Erector Spinae (ES), Rectus Abdominis (RA), Pectoralis Major (PM), Bicep Brachii (BB), and Brachioradialis (BR) of ExoMax compared to trials without the exoskeleton, in tasks with 8 kg

	Static Lifting	Load Carrying SL	Load Carrying HL	Box Handling
UT	-31.7%	-46.4%	-16.6%	-34.5%
AD	-33.3%	-42.6%	-17.7%	-39%
PD	-11.7%	-37.5%	-0.1%	-26.5%
IN	-23.5%	-28.5%	-4.0%	-8.6%
LD	-20.3%	-19.0%	-4.0%	-22.2%
ES	-11.7%	-13.0%	-6.2%	-16.7%
RA	-13.4%	-18.1%	-7.2%	-8.7%
PM	-22.8%	-27.9%	-7.0%	+2.6%
BB	-20.9%	-22.2%	-2.4%	-9.8%
BR	-8.2%	+1.8%	+1.1%	-7.7%

Impact of the Exoskeleton

The findings regarding the *Assistance* factor presented in the Results section underscore the efficacy of the exoskeleton in handling and lifting tasks, resulting in an overall reduction in muscular activity and, consequently, the strain on the musculoskeletal system. The results have been grouped into Tables 4.1 and 4.2, which show the percentage reductions of normalized EMG activation between the ExoMax case and the case without the exoskeleton for 8 kg and 13 kg, respectively, the only case present in all four tasks. It is important to emphasize that these results are specific to the task and weight considered and cannot be used to compare different exoskeletons under different conditions. Anterior Deltoid and Upper Trapezius muscles play a central role in all four tasks, primarily assisting shoulder flexion, elevating the scapula, and sustaining arm elevation [120, 68]. Other studies corroborate this finding [121, 122]. Data consistently shows that these muscles deactivate when wearing the exoskeleton. Reduction for Anterior Deltoid was 33.3%, 42.6%, 17.7%, and 39% in the four Tasks with 8 *kg* and 23.4%, 26.4%, 14.5%, and 25.9% with 13 *kg*. Reduction for Upper Trapezius was 31.7%, 46.4%, 16.6%, and 34.5% in the four Tasks with 8 *kg* and 15.2%, 35.1%, 3.4%, and 22.4% with 13 *kg*. Among them, the Anterior Deltoid stands out as the primary muscle, exhibiting a consistent difference between the two levels of assistance. Similar results can be found in [123]. Literature suggests that this reduced shoulder muscle activity may result in minor compression forces that affect the dynamic stabilization of the glenohumeral joint [124]. Notably, the data also reveals reduced activation of the Rectus Abdominis across all tasks, ranging from 7.2% in Task 3 to 18.1% in Task 2. While the Rectus Abdominis is not directly involved in shoulder stabilization or arm lifting, its activation is implicated in vertebral protection [125].

The muscles that experienced a reduction while using the exoskeleton vary depending on the tasks: there are 9 out of 10 in Static Lifting (Task 1), all of them in Load Carrying SL (Task 2), only 4 in Load Carrying HL (Task 3), and 7 out of 10 in Box Handling (Task 4). Interestingly, the two results at the extremes pertain to the two Load Carrying tasks, with the only variation being the height at which the load was carried. This can be easily explained by examining the required movement. When moving a load at hip level (HL), the angle between the torso and arms is approximately 30°, and most industrial exoskeletons, including this exoskeleton, are expected to provide low assistive forces in this position. However, even in this case, the significant findings coincide with the muscles most involved in the task. Thus, this study illustrates that the exoskeleton tested in this study can alleviate strain on specific shoulder muscles even during tasks conducted beyond the optimal operating configuration of the device. Except for Task 3 (Load Carrying HL), where the exoskeleton operated in a sub-optimal configuration, three other muscles consistently exhibited reduced EMG levels: Latissimus Dorsi, Erector Spinae, and Biceps Brachii. These muscles, in addition to the Anterior Deltoid, Upper Trapezius, and Rectus Abdominis, contribute to an overall decrease in muscular activation when the exoskeleton is used. The findings concerning the Latissimus Dorsi and Erector Spinae, which contribute to back extension, lateral flexion, and shoulder adduction, are also crucial. They indicate that the benefits of the exoskeleton extend beyond the shoulder joint, resulting in reduced trunk activation [126]. Indeed, exoskeletons transfer a portion of the load to more robust areas of the body, particularly the lumbar region of the back. In certain exoskeletons, such as the Hyundai-produced H-VEX, the 70% reduction in shoulder muscle activity during an overhead task was accompanied by a remarkable 97% increase in the signal of the Erector Spinae muscle [127]. This effect is not present in our trials.

Differences between ExoMed and ExoMax Assistance Levels

In Task 1 (Static Lifting) and Task 2 (Load Carrying SL), the only tasks where the medium assistance level (ExoMed) was also used, differences between NoExo and ExoMax conditions were observed in 17 out of 20 muscles, and between NoExo and ExoMed in 15 out of 20 muscles. However, differences between the two assistance levels (ExoMed and ExoMax) appeared in only 7 cases, with 6 of these occurring in Task 2. The Anterior Deltoid was the only muscle consistently showing differences between ExoMed and ExoMax. In Task 1, no other muscles exhibited this behavior. These findings suggest that the impact of assistance level is highly specific to the muscle group and task context. A notable exception emerged in Task 2 (Load Carrying SL), where the Erector Spinae and Brachioradialis showed higher activation under maximum assistance (ExoMax) compared to medium (ExoMed). This unexpected increase may indicate the presence of compensatory motions, where participants adapted their posture or movement patterns in response to the higher assistance. Likely due to the structural constraints of the exoskeleton, users may have adopted altered postures under ExoMax, increasing energy demand in the Erector Spinae and causing greater elbow extension, thus raising the load on the Brachioradialis. These muscles appeared to benefit more from the ExoMed level than from ExoMax. It is also possible that participants required more time to adapt optimally to the higher assistance level, further supporting the idea that compensatory strategies may have been inadvertently introduced.

TABLE 4.2: Percentage reduction of normalized EMG in muscle activity of Upper Trapezius (UT), Anterior Deltoid (AD), Posterior Deltoid (PD), Infraspinatus (IN), Latissumus Dorsi (LD), Erector Spinae (ES), Rectus Abdominis (RA), Pectoralis Major (PM), Bicep Brachii (BB), and Brachioradialis (BR) of ExoMax compared to trials without the exoskeleton, in tasks with 13 kg

	Static Lifting	Load Carrying SL	Load Carrying HL	Box Handling
UT	-15.2%	-35.1%	-3.4%	-22.4%
AD	-23.4%	-26.4%	-14.5%	-25.9%
PD	+2.1%	-22.2%	+5.9%	-17.6%
IN	-14.7%	-20.2%	+7.1%	-1.1%
LD	-8.5%	-9.8%	-1.2%	-8.6%
ES	-6.9%	-11.6%	-4.1%	-10.6%
RA	-14.7%	-15.0%	-13.5%	-13.4%
PM	-21.9%	-22.1%	-23.1%	-6.7%
BB	-12.1%	-21.5%	-10.0%	-6.8%
BR	-7.8%	+7.9%	+0.3%	-5.2%

Further Discussion

Some muscles show no significant differences; this section analyzes and explains these cases. In detail, in Task 1 (Static Lifting), the Posterior Deltoid showed no variations in different conditions. Analyzing the type of movement required, it is evident that this muscle is minimally involved, except for Box Handling (Task 4), where it exhibits a reduction of 26.5% and 17.6% of normalized EMG activity compared to the NoExo trials, for 8 *kg* and 13 *kg* respectively. The decrease in EMG activity of the Posterior Deltoids in Task 4 aligns with the findings of previous studies [128]. This could play an essential role in the long term by reducing biomechanical stress on the shoulder girdle. It can consequently result in significant, enduring effects on the frequency of shoulder tendon disorders. As already discussed above, Task 3 (Load Carrying HL) exhibits few significance because the exoskeleton operates in a sub-optimal configuration. In Box Handling (Task 4), the exoskeleton did not influence the Pectoralis Major, as the activity of the sternocostal part was measured, and the Infraspinatus, a muscle more dedicated to maintaining posture than lifting. Lastly, it is worth mentioning on the Brachioradialis. This muscle does not show significant differences in most tasks, especially when in maximum assistance mode. Furthermore, in Task 2, the Brachioradialis report an increase of 7.9% in the ExoMax compared to NoExo condition. This is expected since the Brachioradialis is a single-joint elbow flexor; thus, its action is relatively unaffected by the exoskeleton. A decrease in Brachioradialis activation is seen only in ExoMed assistance; however, we do not have insights on this result.

Relation with the Existing Literature

The following section highlights how the presented results relate to the existing literature. As anticipated in the introduction, most studies on the effect of industrial upper-limb exoskeletons pertain to passive exoskeletons. These are primarily designed to assist workers in overhead tasks, and the published studies focus on this aspect. This is also the case of H-Pulse, another semi-active exoskeleton found in literature. Grazi et al. [89] recorded decreased muscle activity and heart rate, but their results are not directly comparable to ours. In addition, similar tasks to those

proposed in this study are often tested with exoskeletons that provide back support. Again, the results are not directly comparable. The only exception is the study by Theurel et al. [129], in which a non-anthropomorphic upper-limb passive exoskeleton was tested in similar tasks to those proposed in this study. However, the authors did not record significant differences in the activity of the Anterior Deltoid when comparing walking with and without the exoskeleton. In addition, three other studies have addressed material handling using passive exoskeletons, but none recorded and analyzed electromyographic signals [130, 131, 132].

4.3.2 Effects of the Exoskeleton on Balance and Posture

As discussed in the previous section, wearing the exoskeleton results in a significant reduction in overall muscle activity. Nevertheless, this alone is not enough to establish its effectiveness. Other aspects, such as the impact of the exoskeleton on postural stability and balance, need further investigation and exploration. The analysis of the data collected through the force platform during Task 1 provided valuable insights into the effect of the exoskeleton on balance and postural stability. Total area and Center of Pressure (CoP) migrations along sagittal and coronal planes did not show any impact from the presence of the exoskeleton. This result demonstrates that the studied exoskeleton does not affect the wearer's balance and stability. This is a positive finding, considering that wearing an exoskeleton may shift a wearer's center of mass and increase the likelihood of losing equilibrium [133]. This result is inconsistent with what was achieved with Skel-Ex in a similar task [134]. Furthermore, the average speed of the CoP has decreased. This result is to be considered positive as it could be seen as an indicator of fatigue reduction [135]. On the contrary, some studies have observed an increase in this parameter with other passive exoskeletons [136]. Two other highly significant aspects of exoskeleton use have surfaced. Performing the exercise resulted in a decrease in Center of Pressure velocity when using the exoskeleton. Notably, the maximum force required to lift the weighted bar along the vertical axis decreased under different conditions, with both compensation levels resulting in a reduction in the maximum recorded force compared to trials without the exoskeleton. This is possibly due to a lower load acceleration during lifting. Furthermore, the lifting time has increased when using the exoskeleton with the maximum assistance level, which supports the lower acceleration hypothesis. These three parameters allow us to conclude that the exoskeleton enables lifting the same weight gently while reducing the average effort required and the strain on muscles and articulations. These findings could potentially alleviate fatigue and yield significant benefits in the long term. Obtaining these results with the heavier weight was crucial, representing a higher-risk scenario.

4.3.3 Participants' Subjective Feedback

Before starting the discussion, it is essential to remember that all participants in the study performed the tests shirtless due to the presence of EMG sensors. It is highly plausible that the presence of clothing could lead to better subjective evaluations, alleviating discomfort at the exoskeleton interface.

The decrease in RMS values observed in the analysis of EMG signals under different conditions is strongly supported by all the subjective data collected in the study. The effectiveness of the exoskeleton is evident from the statement in the end-session questionnaire "I felt less tired when I used the exoskeleton", which received

TABLE 4.3: Percentage Reduction in Borg Scales for Perceived Exertion in ExoMax compared to trials without the exoskeleton,

	Static Lifting	Load Carrying SL	Load Carrying HL	Box Handling
8 kg	-12.6%	-19.5%	-14.1%	-11.0%
13 kg	-9.8%	-8.1%	-4.2%	-11.1%

an average rating of 7.9 ± 1.6 (mean ± SD). The results from the BORG Scale also confirmed a reduction in perceived effort. As observed from the muscle analysis, Table 4.3 shows that the exoskeleton was more effective under the conditions with the 8 kg weight. The percentage reductions were 12.6%, 19.5%, 14.1%, and 11.0% for the four tasks with 8 kg and 9.8%, 8.1%, 4.2%, and 11.1% with 13 kg. In addition, participants perceived the few variances observed between the two levels of assistance in the EMG signals, as significance in the Borg Scale is almost absent. This confirms that there don't seem to be any noteworthy differences between ExoMax and ExoMed. The NASA-TLX also confirmed these findings, with differences between NoExo and ExoMax only in Physical Demand and Effort categories. Moreover, inquiries of the end-of-session questionnaire endorsed the absence of divergence in Mental Demand in the NASA-TLX. Participants provided an average rating of 8.0 ± 2.6 for the statement "Using the exoskeleton does not require additional cognitive effort" and 7.9 ± 1.9 for "The exoskeleton does not waste my time." The query "The exoskeleton is easy to use," given his rating of 8.0 ± 1.7, offers insight into the outcomes in the performance category.

A potential critique that can be directed towards semi-active and active exoskeletons is their excessive weight and bulkiness compared to other passive exoskeletons. Participant feedback reflects an acceptance rating of 7.1 ± 2.4 for "The exoskeleton's bulkiness is acceptable" and 7.7 ± 2.2 for "The exoskeleton's weight is acceptable concerning perceived benefits." This semi-active exoskeleton has a higher weight than other passive exoskeletons: for instance, EksoVest weighs 4.3 kg, Levitate 2.4 kg, ShoulderX 3.2 kg, and Paexo 1.9 kg [137]. Despite this, participant responses suggest that the added weight due to actuators and batteries is favorably embraced due to the supplementary support it offers. Another difference between semi-active and passive exoskeletons is the presence of two wireless forearm bracelets to detect loads and enable the motors accordingly. These additional encumbrances might favor the adoption of passive exoskeletons over semi-active and passive ones. However, the participants did not consider the presence of the bracelets unpleasant, as indicated by the statement, "The forearm sensors are not uncomfortable or bothersome," which received a score of 8.7 ± 1.7.

The two inquiries with an average rating lower than six have revealed some issues regarding permitted movements. Similar observations have been made about two other active exoskeletons. Participants wearing the ABLE exoskeleton noted that they were compelled to conform to its movements, which do not necessarily align with their natural movements [138]. Furthermore, misalignment and reduced mobility were found when using the Stuttgart Exo-Jacket [139]. The exoskeleton examined, compared to other passive industrial exoskeletons, features only one passive degree above the shoulder. This lack of a self-centering mechanism for the shoulder joint might elucidate participants' observations concerning mobility constraints [140]. However, participants responded positively when asked if they would like to reuse the exoskeleton to do the same tasks again. This demonstrates how individuals are willing to adapt to the movements facilitated by the exoskeleton and continue using it.

4.3.4 Limitations of the Study and Future Directions

This section identifies certain limitations inherent to the present study. Firstly, the participants were exclusively male and notably younger than the average workforce. In Europe, the proportion of workers over 55 years old increased by 5% between 2014 and 2019, constituting over a quarter of the workforce by 2019 [141]. Furthermore, the participants in this study had no prior experience with the proposed tasks, which might have introduced a learning component during the initial experimental stages. Additionally, the participants were unfamiliar with this exoskeleton, and determining an appropriate duration for the familiarization phase was challenging. This could be a potential area for future research, exploring effective methods for introducing and training individuals in the optimal use of the device. Another limitation revolves around the subjective responses of the participants. The absence of a comparison with other exoskeletons prevents evaluating this semi-active exoskeleton regarding weight, bulkiness, and assistance provided against other passive exoskeletons.

The following limitation concerns the study's restriction to a laboratory rather than a real-world field environment. As extensively documented, findings achieved in a laboratory may not seamlessly extrapolate to practical situations. A controlled environment may yield superior results by eliminating secondary tasks that could potentially impact the user experience of the exoskeleton. Consequently, the extent of electromyographic activity reduction is less well-defined in actual work settings [142]. Nevertheless, considering this marks the inaugural study involving a commercially available semi-active exoskeleton, conducting experiments in a controlled environment was deemed suitable. Additionally, to uniformly compare the individuals who participated in the test, all the shelf heights were adjusted, which is not always possible in an actual workplace. Lastly, the exoskeleton was used for a limited duration, which cannot be compared to a regular work shift.

In conclusion, assessing one of the most common drawbacks of industrial exoskeletons was impossible. The need to exert force to lower the arms, effectively working against the exoskeleton, can lead to heightened Triceps Brachii activity in specific scenarios [123]. Moreover, users might also need to perform eccentric actions to decelerate arm flexion during the forward phase. Some participants in this study also noted this aspect. However, as the activation of the Triceps Brachii was not measured, it remains indeterminate whether there was a general increase in this muscle group or a perception limited to specific individuals. Furthermore, akin to other active exoskeletons, this might occur only at the maximum assistance level [143]. Nevertheless, semi-active (and active) exoskeletons could potentially mitigate this issue. Such exoskeletons can modulate assistance based on movement, potentially making the arm-lowering phase easier.

4.4 Conclusions

The results indicate that the semi-active upper-limb exoskeleton tested in this study effectively reduced muscular activity and strain on articulations due to lower acceleration and perceived effort across four different tasks in a simulated industrial environment. This demonstrates that using a semi-active exoskeleton helps reduce musculoskeletal overload, which has proven effective in the prevention of work-related musculoskeletal disorders (WRMSDs).

Using two different weights in each task and choosing to test two different levels of assistance allowed us to observe the versatility and adaptability of a semi-active

exoskeleton in all different experimental conditions. With the maximum assistance level and in the most challenging task, the reduction of the Anterior Deltoid, Upper Trapezius, Posterior Deltoid, and Pectoralis Major was 42.6%, 46.4%, 37.5%, and 27.9%, respectively. In addition, no cases of overburdening of other parts of the body were found. Participants also perceived this reduction in muscle effort, as demonstrated by the results of the Borg scale, with a reduction up to 19.5% in perceived exertion, and the NASA-TLX, which reports a 44.9% reduction in their Effort category and a 34.0% reduction in Physical Demand. The perceived effort decreased thanks to using the exoskeleton without increasing the required cognitive effort and without affecting the overall performance. The postural stability analysis indicates that participants extend the duration of actions when using the exoskeleton and avoid fast movements. Balance was not altered. Overall, although some negative comments were reported by the participants regarding freedom of movement, all participants were positively inclined toward using the exoskeleton and would reuse it for the same exercises.

The study highlights the potential of semi-active exoskeletons to contribute to ergonomic interventions in occupational settings. In particular, the greater assistance provided by this type of exoskeleton proved to be effective in tasks involving heavy and repetitive lifting at shoulder level. Since passive upper-limb exoskeletons would not be as effective, according to this study integrating motors and developing semi-active exoskeletons represent a viable direction for research. However, further work is still necessary to explore the long-term effects, user adaptability, and the potential impact of semi-active exoskeletons on diverse occupational scenarios.

Chapter 5

AGtuator, the Anti-Gravity Actuator

The contribution of this chapter is to introduce the concept of an Anti-Gravity actuator, which we briefly name AGtuator [144]. The AGtuator concept uses active motors and passive elastic elements to compensate for the weight of a structure and external payloads that may vary during use. Unlike other semi-active systems, the active and passive elements work in series and are driven by a low-level torque control module. In this way, the AGtuator is not only able to compensate for variable gravity forces but also to generate arbitrary torque profiles. In this chapter, the AGtuator concept based on electromagnetic motors and ideal springs, in the sense of zero free length, is explored.

5.1 General Concept

The AGtuator is defined here as a semi-active actuation system composed of one or two controlled motors combined with a Gravity Compensation System (GCS). The main motor of the AGtuator is responsible for regulating the force generated by the elastic element of the GCS, changing its kinematic configuration by increasing and decreasing its length. The second motor could provide torque directly to the link as in traditional robotic systems.

An AGtuator acts on a generic robotic link in such a way that the following properties hold:

1. the AGtuator is capable of compensating the robot-induced gravitational forces with near-zero power expenditure;

2. the AGtuator is capable of compensating the gravitational forces of a variable payload fixed to the robot link with minimal power expenditure;

3. the AGtuator is capable of applying an arbitrary torque profile to the robot link, within a certain bandwidth.

While Property 1 belongs to standard passive GCS, Property 2 characterizes mechanically adjustable passive GCS, and Property 3 is a typical feature of torque-controlled actuators. The AGtuator combines the features of these three solutions, providing a power-efficient and versatile actuation system useful for a variety of payload-lifting and payload-carrying tasks. It is important to note that every robotic task involves payload lifting and carrying, as the robot must, at a minimum, support its own weight. From the power-efficiency point of view, an AGtuator uses power only in the instant when the payload changes or when an arbitrary torque profile is

requested. In the first case, a power shot is spent to re-configure the passive GCS. In the second case, a continuous power flow may be required.

The system could be intended as an improvement over existing gravity compensation systems, as it adapts quickly and precisely, but, in practice, it provides an additional and extremely versatile feature: it can be used as an actuator to control different physical quantities such as torque, position, velocity, impedance, etc. Such versatility is unparalleled by existing semi-active systems, even if proposed mechanical structures are inspired by well-known passive GCS [145]. However, their focus was merely on gravitational compensation for external payloads and not on the possibility of automatically adapting or generating torque profiles.

Possible mechanical architectures and sizing are described in section 5.1. As explained in this section, the AGtuator mechanics unavoidably introduce non-linear dynamics, which control must handle. Section 5.4 introduces a possible non-linear control architecture with theoretically proven stability on a reference mechanical design. Section 5.5 presents a prototype that is built to demonstrate the proposed concept and three experiments that are conducted to validate its properties.

5.2 Mechanical Design

AGtuator is a flexible concept that can be applied in various configurations. Some of the many alternatives are mentioned in this section. The explanation of the system's operating principle refers to its simplest version, namely the single-motor version applied to a planar robotic link, represented in Figure 5.1.

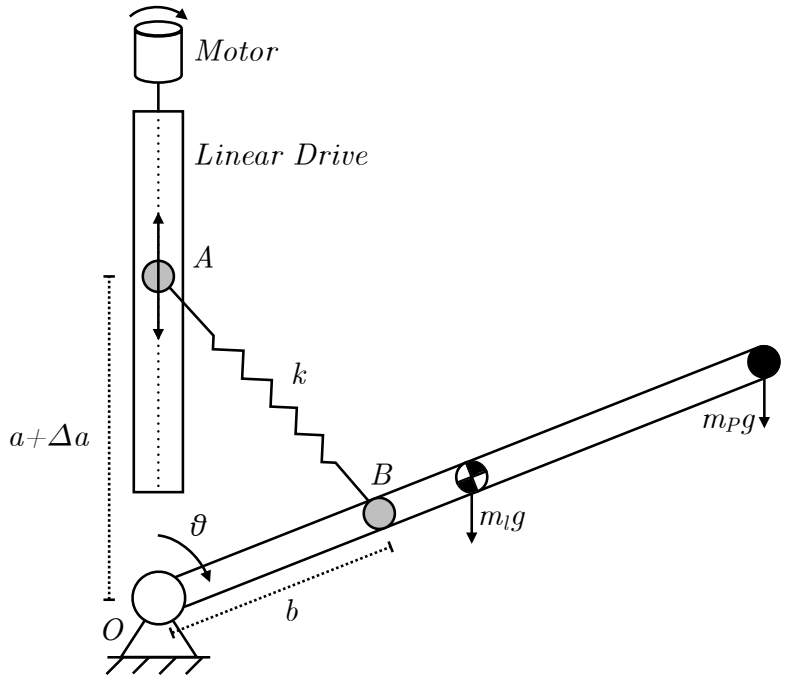

FIGURE 5.1: Single-motor AGtuator scheme: the system, consisting of a motor and a linear drive, allows for adjusting the distance between the hinge in O and point A, thus controlling the elastic force provided by the spring with elastic constant k. This system compensates for the gravitational forces for any value of angle θ due to the weight of the link itself, denoted by m_l, and any variable payloads, denoted by m_p.

The system is a link with 1 rotational DOF defined by a hinge in O. The link has a length l and mass m_l. The system is balanced by a spring, with the spring stiffness k carefully selected, extending between points A and B. The length of the spring is indicated by the letter x. Point B is fixed on the link at a distance b from the origin O of the system. Point A is grounded and must be above the hinge O. The distance between points O and A is indicated as a. The angle between segments $\overline{OA}$ and $\overline{OB}$ is denoted as θ and the convention is positive clockwise. The spring used is an ideal zero-free-length spring, therefore, the elastic force F_e exerted by the spring on the link is:

$$F_e = k \cdot x \tag{5.1}$$

Choosing a spring with a specific constant factor is necessary to achieve a system in equilibrium for any position. The process begins by writing the mechanical equilibrium of the system, in terms of momentum. The total torque, calculated at the hinge located at O, is as follows:

$$\sum M_i|_O \Rightarrow F_{en} \cdot b - m_l \cdot g \cdot \frac{l}{2} \cdot \sin\theta = 0 \tag{5.2}$$

where F_{en} is the elastic force normal to the link, as shown in Figure 5.2. F_{en} can also be written as:

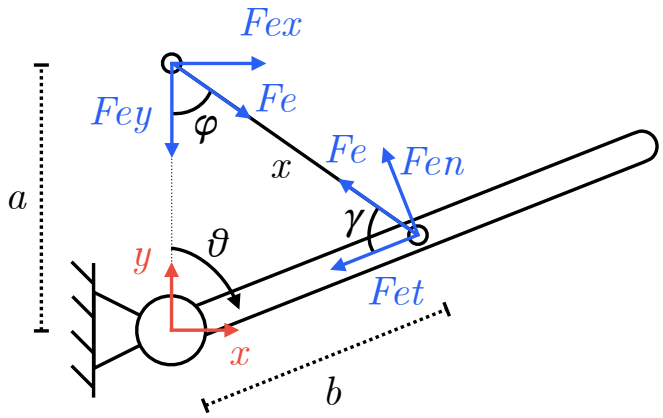

FIGURE 5.2: Diagram of the elastic forces acting on the link due to the spring. F_{en} indicates the elastic force perpendicular to the link, F_{et} the elastic force tangential to the link, F_{ex} indicates the elastic force in the horizontal direction, and F_{ey} the elastic force in the vertical direction. See Appendix B for the complete analysis.

$$\begin{aligned} F_{en} &= F_e \cdot \sin\gamma \\ F_{en} &= k \cdot x \cdot \sin\gamma \end{aligned} \tag{5.3}$$

where γ represents the angle between the spring and the link. Using the law of sines, that is $\frac{a}{\sin\gamma} = \frac{x}{\sin\theta} = \frac{b}{\sin\varphi}$, the following equality can be written:

$$x \cdot \sin\gamma = a \cdot \sin\theta \tag{5.4}$$

By substituting the newly obtained expression into Eq. 5.3, F_{en} becomes:

$$F_{en} = k \cdot a \cdot \sin\theta \tag{5.5}$$

Substituting the expression of the elastic normal force to the link and generalizing for other masses that may be present in the system, we obtain:

$$\sum M_i|_O \Rightarrow kab \sin\theta - m^* g \sin\theta = 0 \tag{5.6}$$

where $m^* = \sum m_i d_{COM,i}$ indicates the summation of masses multiplied by the distance of their respective centers of mass, with respect to the point O. In the system with only the mass of a uniform rigid link, as in the case under consideration, m^* corresponds to $m_l \frac{l}{2}$. The term may also include torques due to other masses, such as additional links when using a parallelogram structure, or the weight of a person's arm connected to the link of an exoskeleton. To maintain the system in equilibrium for any value of the angle θ, it is necessary to impose that $d\sum M_i|_O / d\theta = 0$. The derivative of the total torque corresponds to $kab = m^* g$, given that $\cos\theta$ simplifies. From this last equation, we can obtain the value of the spring constant k that keeps the system in equilibrium regardless of the position θ, which corresponds to:

$$k = \frac{m^* g}{ab} \tag{5.7}$$

Once a spring with the just calculated spring constant is installed, the system is, therefore, in equilibrium for all positions θ. However, in real systems, it is difficult to find an application where the external payload remains unchanged. Adding a mass m_p at the end of the link will disrupt the system's equilibrium. This is precisely the task of the AGtuator concept: to re-establish the equilibrium by reconfiguring the system, thus controlling the elastic torque provided by the spring through the linear drive. For instance, the amount of displacement Δa to be imposed on point A can be easily calculated using the same previous procedure. The new total torque of the system, with the addition of a known payload mass m_p at a distance l from the hinge O, is as follows:

$$\sum M_i|_O \Rightarrow F_{en} \cdot b - M^* g \sin\theta = 0 \tag{5.8}$$

where $M^* = m^* + \sum m_{p,i} d_{p,i}$, with $m_{p,i}$ indicating multiple payloads and $d_{p,i}$ their distance with respect to the hinge in O. In this new system, the elastic normal force to the link corresponds to:

$$F_{en} = k \cdot (a + \Delta a) \cdot \sin\theta \tag{5.9}$$

This value can be substituted into Equation 5.8. The static torque equilibrium derivative with respect to θ is equal to:

$$kb(a + \Delta a) = M^* g \tag{5.10}$$

From this expression, by substituting the previously found value of $k = \frac{m^* g}{ab}$, it is possible to determine how much the position of the motor (Δa) needs to be modified to balance the system:

$$\Delta a = \left(\frac{M^*}{m^*} - 1 \right) a \tag{5.11}$$

with the term $(\frac{M^*}{m^*} - 1)$ always greater (or equal) than zero. By applying such a displacement, the system is in equilibrium regardless of the position θ and for any additional mass included in M^*. The displacement linearly depends on the initial

choice of a, indicating that choosing a small a requires only a small motor adjustment. As a drawback, a higher spring constant, as denoted by eq 5.7, is requested.

A system in equilibrium for any position and payload can only be achieved if the segment $\overline{OA}$ is vertical and the motor moves the attachment point of the spring along this direction. If the $\overline{OA}$ segment is inclined at an angle α, as in Figure 5.3, it is still possible to achieve a system in equilibrium but no longer independently of the position of the link θ. In this latter case, equilibrium can be achieved by knowing the angle of inclination α and moving the attachment point of the spring by a position equal to:

$$\Delta a = \frac{M^* \sin(\theta + \alpha) - m^* \sin\theta}{m^* \sin\theta} a \tag{5.12}$$

recalling that θ indicates the angle between the link and the linear drive. As can be seen, the displacement depends on the tilt angle α. By setting $\alpha = 0°$, the solution is equivalent to Equation 5.11.

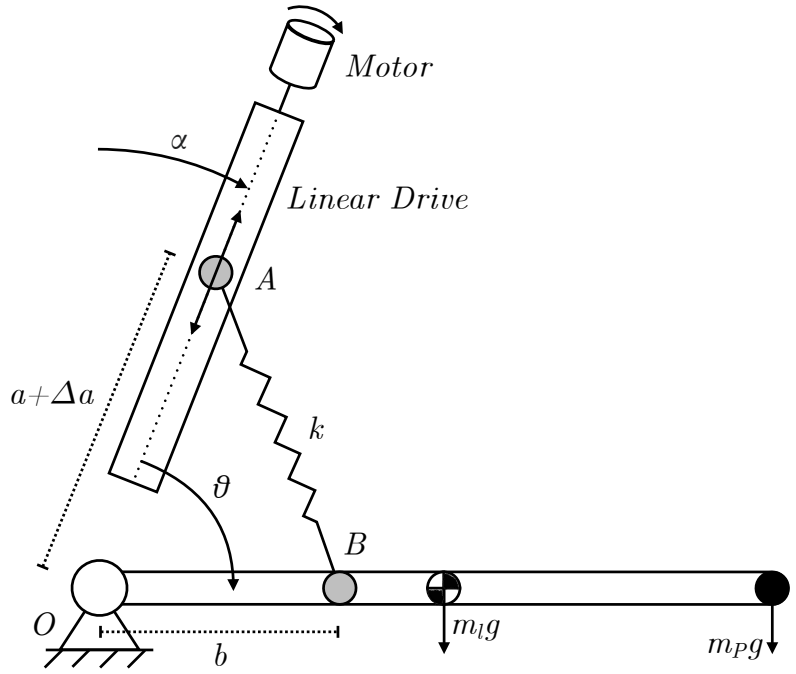

FIGURE 5.3: Diagram of AGtuator with the linear drive rotated by an angle α relative to the vertical. In this case, AGtuator is still capable of compensating for a variable payload but only by continuously supplying power to the system.

Finally, we highlight that equations 5.11 and 5.12 are reported here just to show their feasibility, their dependency on certain physical quantities, and the existence of equilibrium configurations. However, the proposed control module will not explicitly use these expressions. Instead, and differently from existing approaches, the computation of displacements Δa implicitly arises thanks to the action of force feedback, see section 5.4 for details.

5.3 Implementations

AGtuator is a versatile concept that can be applied to various structures. For example, in the same 1 DOF system, an equivalent solution can also be achieved by moving point B, thus modifying the length of segment b, as shown in Figure 5.4. The related displacement is similar to Equation 5.11: $\Delta b = \left(\frac{M^*}{m^*} - 1\right) b$.

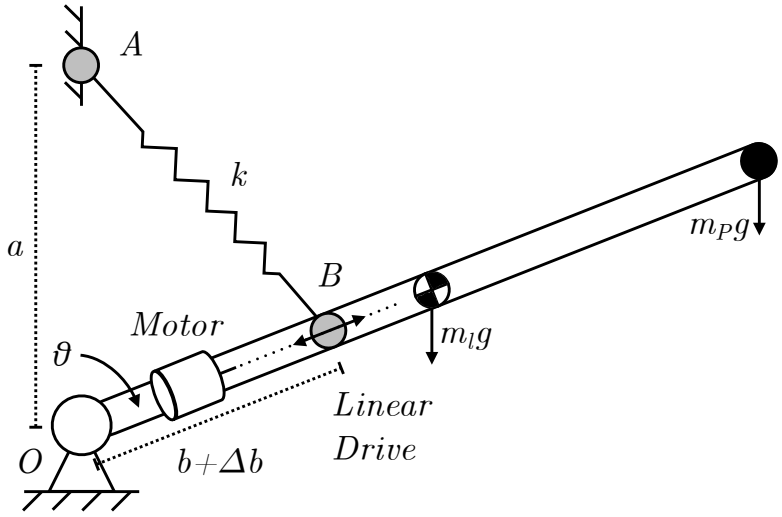

FIGURE 5.4: Diagram of AGtuator with the motor and linear drive mounted on the link adjusting the length of the elastic element moving point B.

Having demonstrated that regulating either of the two attachment points of the elastic element is equivalent, the AGtuator concept can also be implemented using other configurations as well. For example, the AGtuator concept can be applied to parallelogram structures, as shown in a) of Figure 5.5. Using a four-bar mechanism allows multiple AGtuators to be combined in series, as shown in panel b). The use of this structure is necessary due to the verticality constraint for the point A discussed in the previous section to minimize motor adjustments and mechanical power generation. Alternatively, the AGtuator can be configured by mirroring the spring position below the link to be compensated. In this case, the linear drive and the elastic element must be installed on the extension of the link. 5.5 c) illustrates two solutions by moving either of the two attachment points of the elastic element.

5.3.1 Dual Motor Solution

A possible evolution of the AGtuator concept involves adding a second motor directly to the joint to provide additional torque. In this case, the linear drive remains responsible for adjusting the spring configuration, while the second motor, along with its associated control algorithms, generates the additional torque required to accomplish various control tasks, such as gravity compensation, position control, impedance control, and interaction control. The combined action of the two motors can be managed by MISO optimal control algorithms, which minimize power consumption and thermal dissipation of both motors while maximizing performance metrics such as responsiveness and/or maximum force generation.

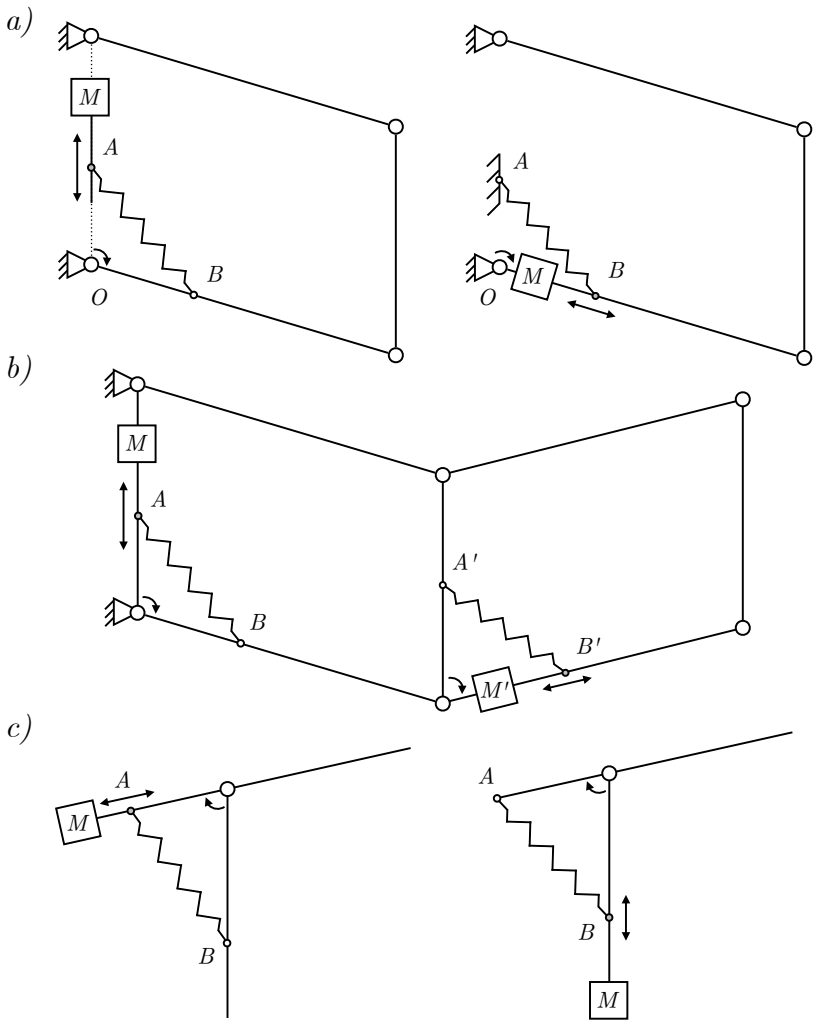

FIGURE 5.5: Other possible implementations of AGtuator. Panel a shows AGtuator applied to a parallelogram mechanism, Panel b shows two AGtuators combined in a parallelogram mechanism, while in Panel c it is applied below the link to be balanced, acting on its extension.

This dual-motor solution could lead to significant advantages regarding controllability, performance, energy efficiency and related trade-offs and can be applied to all possible implementations proposed in the previous paragraph. For example, Figure 5.6 a) illustrates a possible implementation using a parallelogram structure. This family of solutions and their control will be explored in the future.

5.3.2 Double Spring Solution

Another possible implementation of the AGtuator concept involves using multiple elastic elements in the system, not all of which are re-configured by the linear drive. For certain heavy systems, it may be efficient to have one spring dedicated to balancing the weight of the structure itself and another dedicated to compensating for the variable load. This will reduce the effort for generating displacements Δa or Δb thus minimizing power expenditure when the payload change. An illustrative diagram is shown in Figure 5.6 b).

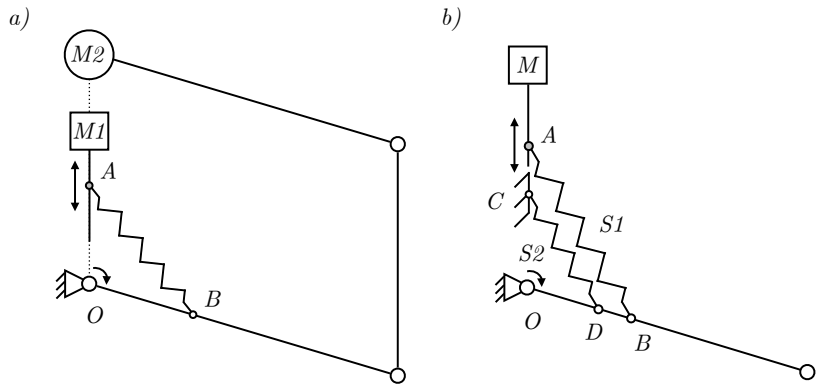

FIGURE 5.6: Panel a shows the dual motor solution, with the second one (M2) placed at one of the two fixed hinges. The auxiliary motor M2 handles the peak torque, while the principal one (M1) adjusts the spring configuration. Panel b illustrated the double spring solution. The main spring S1 is connected to the linear drive and compensates for the variable payload, while the secondary spring S2 is fixed and balances the weight of the robotic link in an unloaded condition.

5.3.3 Implementation of Zero Free Length

As already mentioned in Section 5.2, the proposed AGtuator concept requires a zero-free-length elastic element. If this type of spring is undesirable due to its high cost and limited availability, a non-zero-free-length elastic element can be used instead with additional linkages incorporated into the structure. Some examples are shown in Figure 5.7.

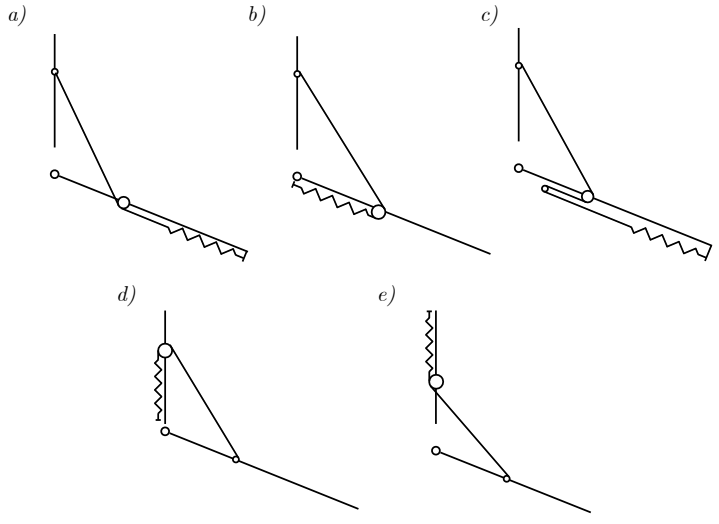

FIGURE 5.7: Some possible solutions to emulate the behavior of a zero-free-length spring using a standard spring.

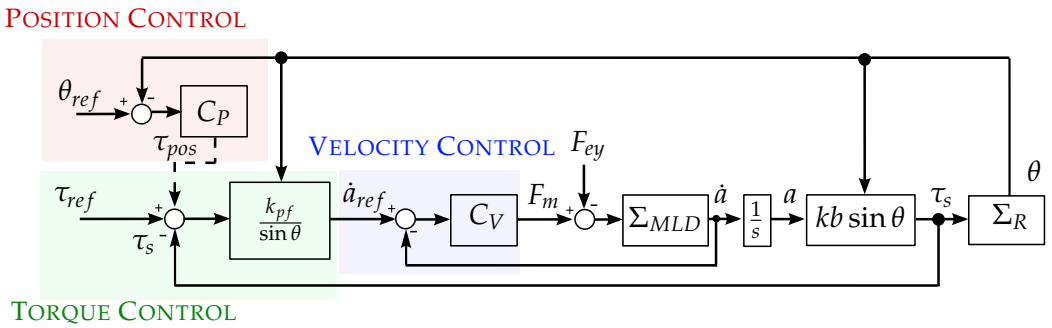

FIGURE 5.8: Block diagram representation of the proposed control architecture

5.4 Control Design

The key advantage of the proposed AGtuator system over existing semi-active solutions [115] lies in its versatile control capabilities. Similarly to the state-of-technology actuation systems, the AGtuator concept relies on a cascaded control architecture with an innermost torque control loop and different possible controllers implemented on top, e.g., gravity compensation, velocity, position, interaction or myography-driven control. While in traditional electromagnetic actuators, the inner torque loop regulates the motor current, here, the same loop will regulate the kinematic configuration of the spring k. Of course, because of the involvement of mechanics, we cannot expect the same bandwidth of current control, and there exists a trade-off between bandwidth and efficiency which will be thoroughly examined in future research.
This Section introduces the low-level torque controller for the AGtuator configuration in Figure 5.1, assumed here as a reference design and provides a stability analysis of the controlled system. It is important to highlight that the control algorithm introduced in this Section is independent of the AGtuator configuration and can be applied to any of the possible implementations discussed in Section 5.3 with minor changes.
The dynamics of AGtuator configuration represented in Figure 5.1 can be described as the combination of the motor and linear drive system dynamics (referred here as Σ_{MLD}) and the robot link system dynamics (referred here as Σ_R).
The dynamics of Σ_{MLD} can be described with the following equations:

$$\begin{aligned} F_m - F_{ey} &= I\ddot{a} + f_v\dot{a} + f_c\text{sign}(\dot{a}) \\ F_{ey} &= k(a - b\cos\theta) \end{aligned} \tag{5.13}$$

where F_m is the force generated by the linear drive, F_{ey} is the elastic force exerted by the spring on the linear drive axis (as shown in Figure 5.2), I denotes the inertia of the linear drive, θ is the angular position of the joint and f_v and f_c represent the viscous friction force and the Coulomb friction force respectively.
The dynamics of Σ_R can be described as:

$$\begin{aligned} M^*g\sin\theta - \tau_s &= J\ddot{\theta} + \tau_v\dot{\theta} + \tau_c\text{sign}(\dot{\theta}) \\ \tau_s &= kab\sin\theta \end{aligned} \tag{5.14}$$

where J represents the inertia of the AGtuator link, including any additional payload, τ_v and τ_c represent the overall viscous and Coulomb friction parameters, τ_s is the torque exerted by the spring , and $M^*g\sin\theta$ is the gravity-induced torque.

A block diagram of the proposed control architecture is shown in Figure 5.8. This design includes a torque control loop (depicted in green) that allows dynamic compensation time-varying gravity torques, an inner velocity loop (depicted in blue) to control the linear drive, and an optional position loop (depicted in red) to track a desired position reference θ_{ref}.
In this Section we focus on torque control only, fed by a gravity compensation reference. Gravity compensation represents indeed a fundamental feature of the AGtuator concept. The proposed control law is defined as:

$$\dot{a}_{ref} = \frac{k_{pf}}{\sin\theta}(\tau_{ref} - \tau_s) \tag{5.15}$$

where $\dot{a}_{ref}$ is the speed command reference for the velocity controller, k_{pf} is a proportional gain, τ_{ref} is the torque reference and the ratio $\frac{1}{\sin\theta}$ is introduced to linearize the torque loop.

5.4.1 Stability analysis

This subsection provides a stability analysis of the reference AGtuator system (5.13)-(5.14) under the torque control law (5.15). The analysis is based on the following assumptions:

(A1) the AGtuator system performs a gravity compensation task, i.e. $\tau_{ref} = M^* g \sin\theta$;

(A2) the inner velocity controller C_V is a simple proportional controller, i.e. $F_m = k_{pv}(\dot{a}_{ref} - \dot{a})$, where k_{pv} is the proportional velocity gain.

Additionally, the analysis relies on the following error definition:

$$\tilde{a} = a^* - a \tag{5.16}$$

Lemma 1. *The AGtuator system described by (5.13)-(5.14) and controlled by the torque control law (5.15) is stable with $\dot{\theta} \to 0$ and $\dot{a} \to 0$.*

Proof. Let us consider the following Lyapunov candidate function:

$$V(\theta, \dot{\theta}, a, \dot{a}) = \frac{1}{2}k(a^2 + b^2 - 2ab\cos\theta) + M^* g(1 + \cos\theta) + \frac{1}{2}J\dot{\theta}^2 + \frac{1}{2}I\dot{a}^2 + \frac{1}{2}\beta k\tilde{a}^2 \tag{5.17}$$

which is positive definite, and includes the potential energy of the spring, the potential energy of gravity, the kinetic energy of the robotic link (payload included), and the kinetic energy of the motor and linear drive. Additionally, the term $\frac{1}{2}\beta k\tilde{a}^2$ with $\beta > 0$ is a positive contribution.
The time derivative of V is computed as:

$$\dot{V} = ka\dot{a} - k\dot{a}b\cos\theta + kab\sin\theta\dot{\theta} - M^* g\sin\theta\dot{\theta} + J\dot{\theta}\ddot{\theta} + I\dot{a}\ddot{a} + \beta k\tilde{a}\dot{\tilde{a}} \tag{5.18}$$

Substituting $\ddot{a}$ and $\ddot{\theta}$ using the system dynamics (5.13) and (5.14) yields:

$$\dot{V} = F_m\dot{a} - f_v\dot{a}^2 - f_c|\dot{a}| + \beta k\tilde{a}\dot{\tilde{a}} - \tau_v\dot{\theta}^2 - \tau_c|\dot{\theta}| \tag{5.19}$$

According to Assumption (**A2**), one can rewrite (5.19) as:

$$\dot{V} = k_{pv}(\dot{a}_{ref} - \dot{a})\dot{a} - f_v\dot{a}^2 - f_c|\dot{a}| + \beta k\tilde{a}\dot{\tilde{a}} - \tau_v\dot{\theta}^2 - \tau_c|\dot{\theta}| \tag{5.20}$$

and by considering the Assumption (**A1**) and the definition of $\tilde{a}$ from (5.16) one obtains:

$$\dot{V} = k_{pv}k_{pf}k\tilde{a}b\dot{a} - k_{pv}\dot{a}^2 - f_v\dot{a}^2 - f_c|\dot{a}| + \beta k\tilde{a}\dot{\tilde{a}} - \tau_v\dot{\theta}^2 - \tau_c|\dot{\theta}| \tag{5.21}$$

Finally, since $\dot{\tilde{a}} = -\dot{a}$ and choosing $\beta = k_{pv}k_{pf}b$ the equation simplifies to:

$$\dot{V} = -k_{pv}\dot{a}^2 - f_v\dot{a}^2 - f_c|\dot{a}| - \tau_v\dot{\theta}^2 - \tau_c|\dot{\theta}| < 0 \tag{5.22}$$

All terms are negative, thus guaranteeing stability. □

5.5 Validation

This Section describes the developed prototype and the experimental validation of the AGtuator concept.

5.5.1 Experimental Setup

A picture of the prototype with the AGtuator concept realized for the experimental validation is shown in Figure 5.9. It consists of a parallelogram structure as in Figure 5.5 a). The spring used is a non-zero-free-length spring. Various configurations of the system can be adopted to emulate a zero-free-length spring. In our system, a double pulley solution was used, with routing as in Figure 5.7 c). All Mechanical parameters are summarized in Table 5.1. The prototype was designed with a parallelogram structure to take advantage of the fact that the vertical link does not rotate during use. This made it easier to integrate support for inserting disk weights to simulate an external payload. All links were manufactured using 3D printing, with the Bambu Lab X1C printer and PLA CF (Carbon Fiber) material produced by the same company. The mechanical properties of the material are: density $\rho = 1.22\,\mathrm{g/cm^3}$, Young's modulus in the xy direction $E_{xy} = 2790 \pm 120\,\mathrm{MPa}$ and in the z direction $E_z = 2160 \pm 90\,\mathrm{MPa}$, and tensile strength in the xy direction $\sigma_{xy} = 38 \pm 4\,\mathrm{MPa}$ and in the z direction $\sigma_z = 26 \pm 2\,\mathrm{MPa}$. Between the two hinges the linear drive manufactured by THK (model KR15) has been inserted and connected to the electric motor produced by Faulhaber, model 4490-H-048-BS. Knowing that the quantity a cannot be negative, the linear drive was installed so that its lowest point coincides with the hinge at O. The linear drive has a ball screw with a screw step of 1 mm and an effective stroke length of 85 mm. This was the main constraint in the prototype's construction. By imposing a maximum allowable payload of $m_{p,\max} = 2\,\mathrm{kg}$, the elastic constant k of the spring and the distance $\overline{OB}$ were calculated using Equations (5.7) and (5.11), ensuring that the displacements of point A remained within the linear drive, operating with m_p between 0 and $m_{p,\max}$. The computed value of m^* is 0.141 kgm. The obtained values were $k = 983\,\mathrm{N/m}$ and $b = 0.06\,\mathrm{m}$. However, a length adjustment system for b was incorporated into the lower link to correct any calculation errors of the parameter m^*.
The control algorithms run on an embedded board (Nucleo L432KC) as periodic 2 kHz real-time processes and the electric motor is driven in velocity control mode using a commercial driver (ESCON module 50/5). The joint angle θ is measured using an incremental encoder with a resolution of 0.0015 rad. Finally, we used a force sensor (Futek LCM300) arranged on the parallelogram structure to directly measure the weight of an external payload, allowing us to compute M^* for the torque reference $\tau_s = M^* g \sin\theta$. Integrating force sensor-less strategies for online payload estimation will be a matter of future research.

Description	Symbol	Value
MECHANICAL PARAMETERS		
Spring Attachment Point	b	0.06 m
Link Length	l	0.02 m
Height of the Parallelogram	h	0.1 m
Equivalent Mass-COM	m^*	0.141 kgm
Elastic Constant	k	983 N/m
Maximum Payload Admissible	$m_{p,max}$	2 kg
Inclination Angle Exp 3	α	25 deg
ACTUATION PARAMETERS		
Effective Stroke Length	S_l	0.085 m
Screw Pitch	S_p	0.001 m
Torque constant	k_T	0.17 Nm/A
Terminal resistance	R	2.1 Ω
CONTROL PARAMETERS		
Proportional Force Gain Exp 1 and 2	k_{pf}	550
Proportional Force Gain Exp 3	k_{pf}	300
Proportional Velocity Gain Exp 1, 2, and 3	k_{pv}	0.006
Integrative Velocity Gain Exp 1, 2, and 3	k_{iv}	1.0
Proportional Position Gain Exp 3	k_{pp}	2.0
Integrative Position Gain Exp 3	k_{ip}	1.0
Derivative Position Gain Exp 3	k_{dp}	1.0

TABLE 5.1: Mechincal, Actuation, and Control Parameters used in experimental trials.

5.5.2 Experimental Description and Results

Three different experiments are designed to validate the AGtuator properties presented in Section 5.2. In the first two experiments, the electric motor is driven by a torque control architecture represented in green in Figure 5.8. In the third experiment, an external position control loop is added, represented in red in Figure 5.8. Control parameters are reported in Table 5.1. A detailed description of the experiments is presented in the following.

Experiment 1

The first experiment was conducted to verify properties 1 and 2, which are the capability of compensating the robot-induced gravitational forces and compensating the gravitational forces of a variable payload fixed to the robot link, both with minimal power expenditure. Therefore, the torque reference of the torque control architecture is $\tau_{ref} = M^* g \sin\theta$. The system starts without any external payload. To demonstrate that the system is in equilibrium for any angle θ, the link is manually moved to four different positions and left for a few moments to verify the gravitational balance. Subsequently, a 0.5 kg external payload is added, and the process is repeated to show that the AGtuator system effectively balances the added weight. An additional 0.5 kg payload is then added, increasing the total payload to 1 kg, and the procedure is repeated once more. Finally, the two disks are removed individually,

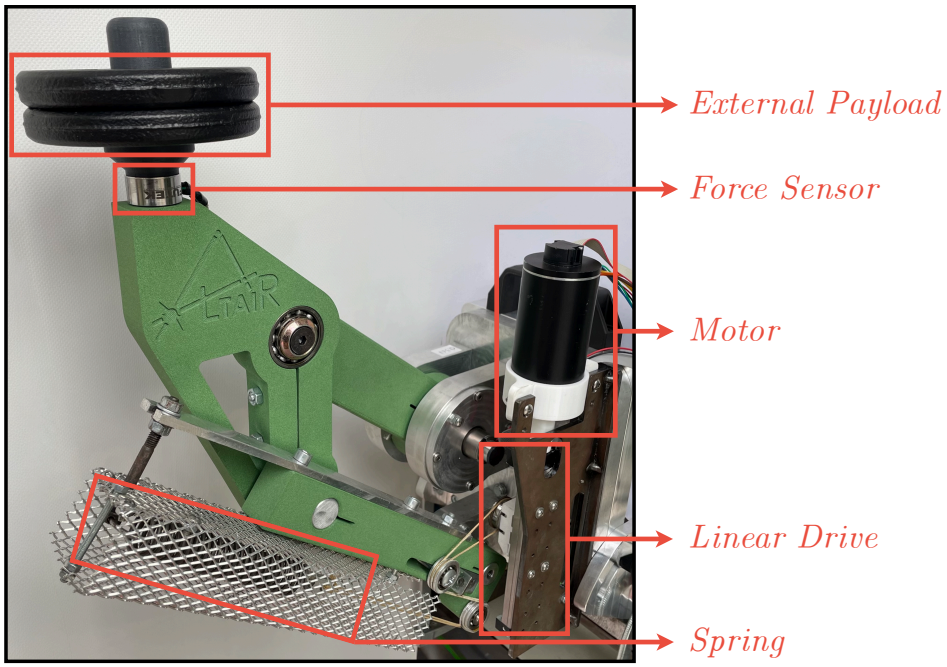

FIGURE 5.9: A picture of the AGtuator prototype, with the main components highlighted in red. The parallelogram structure can accommodate a payload of up to $2kg$, measured by the force sensor. The motor and linear drive move the guide and adjust the spring tension, which is enclosed in a metal cage for safety reasons.

returning the system to its original unloaded state. Experimental results are shown in Figure 5.10 where external payload changes are highlighted with vertical dark lines.

The first plot shows the torque tracking performance where τ_s, depicted in blue, represents the feedback torque produced by the spring, computed as in Eq. (5.14), and τ_{ref}, in orange, represents the torque reference. The second plot represents the angular position θ of the link, showing that the system is balanced in different positions. The third plot compares the linear drive position a, depicted in blue, and the expected position a_e, depicted with a black dashed line, derived from eq. (5.10). The last plot shows the overall motor power, which includes the mechanical power generated by the motor and the electrical power dissipated, and it is computed as:

$$Power = \tau_m \dot{\theta}_m + R(\tau_m / k_T)^2 \tag{5.23}$$

where τ_m is the motor torque read from the ESCON module, $\dot{\theta}_m$ is the motor velocity, computed by numerical differentiation, K_T is the torque constant and R is the motor terminal resistance.

Experiment 2

The second experiment was designed to validate Property 3, namely to verify that the AGtuator can apply an arbitrary torque profile to the robot link, within a certain bandwidth. In this experiment, the system is tilted by an angle of $\alpha = 25°$ and no additional payload was added. Thus, the torque reference was computed as $\tau_{ref} = m^* g \sin(\theta + \alpha)$. The system was manually stopped and left in eight different positions. Experimental results are shown in Figure 5.11.

Again, the four plots respectively show the torque tracking performance, the angular position of the link, the expected and measured positions of the linear guide, and the mechanical and electrical power of the motor. Although in this configuration the gravitational forces on the link are properly compensated, there is no single position of the linear drive that keeps the system in equilibrium for each angle (as one can observe from the third plot of Figure 5.11). This is expected since, in this case, the equilibrium position is a function of both α and θ, as one can observe from eq. (5.12) in Section 5.2.

Experiment 3

The third experiment was carried out to verify property 3. The goal of this experiment is to demonstrate that the AGtuator system can apply an arbitrary torque profile. In this experiment, we use this property to track a desired position reference, using an outermost position loop. The considered control architecture is the one shown in Figure 5.8 with C_P designed as a PID controller (control gains are reported in Table 5.1). The reference θ_{ref} was generated using a potentiometer. Experimental results are shown in Figure 5.12. The first plot shows the torque tracking result with

$$\tau_{ref} = M^* g \sin\theta + \tau_{pos}$$

with

$$\tau_{pos} = k_{pp}(\theta_{ref} - \theta) + k_{dp}\dot{\theta} + k_{ip}\int(\theta_{ref} - \theta).$$

The second plot shows the position tracking result. One can observe how, with small adjustments of the spring torque, the AGtuator system can track the position reference.

5.6 Discussion

The results of Experiment 1 confirmed the first two properties of the AGtuator, demonstrating that the proposed concept is an adaptive gravity compensator capable of adjusting to changes in external load. The system remained in equilibrium for any loading condition and angle θ. This is evident by observing the power, in the last panel of Figure 5.10, which remains close to zero when the system is perturbed. This demonstrates that the AGtuator can compensate the robot and the payload gravitational forces with near-to-zero power expenditure. The same plot shows that a power shot is only required when the payload changes. Once the system has reconfigured itself, the power required to move freely returns close to zero.

The second experiment confirmed Property 3, showing that, by using a modified reference including the angle α, the AGtuator can compensate for gravity forces even when the linear drive is non-vertical. In this case, equilibrium is not achieved with minimal power expenditure, as expected. A comparison of the power required in the ideal case, with a vertically oriented linear drive, and in the inclined case can be made by analyzing the zoomed-in section of Figure 5.10 and the power graph in Figure 5.11.

In these first two experiments, the expected position a_e of the linear drive that balances the system could be calculated a priori using Equations (5.11) and (5.12). As previously mentioned, the system does not explicitly use these equations but computes them through the control loop. The comparison between the expected

position a_e and the actual value a, shown in the third panel of Figures 5.10 and 5.11, demonstrates that the two values are extremely similar.

The objective of the third experiment is mainly to demonstrate the great versatility of the AGtuator concept. The AGtuator allows the tracking of generic torque references, including those coming from outer control loops. The case of position control is just an example to showcase this opportunity. The second graph in Figure 5.12 shows that position tracking is maintained.

5.6.1 Potential Applications and Future Works

The proposed AGtuator concept proved to be a dynamic gravity compensation system and also a semi-active versatile actuator with potential applications in industrial robotics, such as industrial and collaborative manipulators, mobile assistive robotics, and wearable exoskeletons. Minimal power expenditure when lifting and carrying different payloads allows us to meet the energy-efficiency requirements of modern industrial plants and to reduce the size and weight of battery packs in mobile or wearable applications. The outcomes of experiment 2 show how the system can work even in the case of imperfect vertical alignment of the linear drive, demonstrating applicability even in those applications where such verticality constraints cannot be precisely met. Typical examples are wearable exoskeletons. The system's versatility is mostly due to property 3, which allows the generation of arbitrary torque profiles. This represents the main enabling factor for application to different contexts, including the implementation of assistive strategies based, for example, on the amplification of muscular activations or other advanced assistive applications. Also, AGtuator systems require motors with smaller sizes compared to traditional robots, which are usually linked to lower mass, inertia, and cost, further promoting portability and wearable applications.

Single-motor AGtuator designs are mainly tailored for assistive robotics tasks typical of assistive or industrial exoskeletons, where accurate torque generation is more important than accurate positioning. In different designs, combining two motors, to both accurate torque generation and positioning are possible, satisfying different application requirements. This may be the case, for example, in industrial applications, such as manipulators or co-bots, where the (series chain of) quadrilateral solution with dual springs and dual motor configurations could be the most effective to combine energy efficiency and quality position control.

In our future work, we plan to better characterize the friction effects due to the high system internal forces, i.e. due to the spring tension, and to investigate optimization and control aspects of dual-motor solutions. Regarding applications, we plan to exploit the AGtuator concept in the design of assistive exoskeletons and mobile assistive robots to further demonstrate the concept's versatility.

5.7 Conclusions

This paper introduced the concept of AGtuator, a semi-active actuation system with low-power gravity compensation capability. The primary feature of the AGtuator is its ability to self-adjust the passive compensation system not only to balance variable external payloads but also to generate arbitrary torque profiles. The concept can be applied in various forms and fields, and to demonstrate its feasibility, a prototype was developed and tested. The experimental results highlighted the potential and versatility of the system.

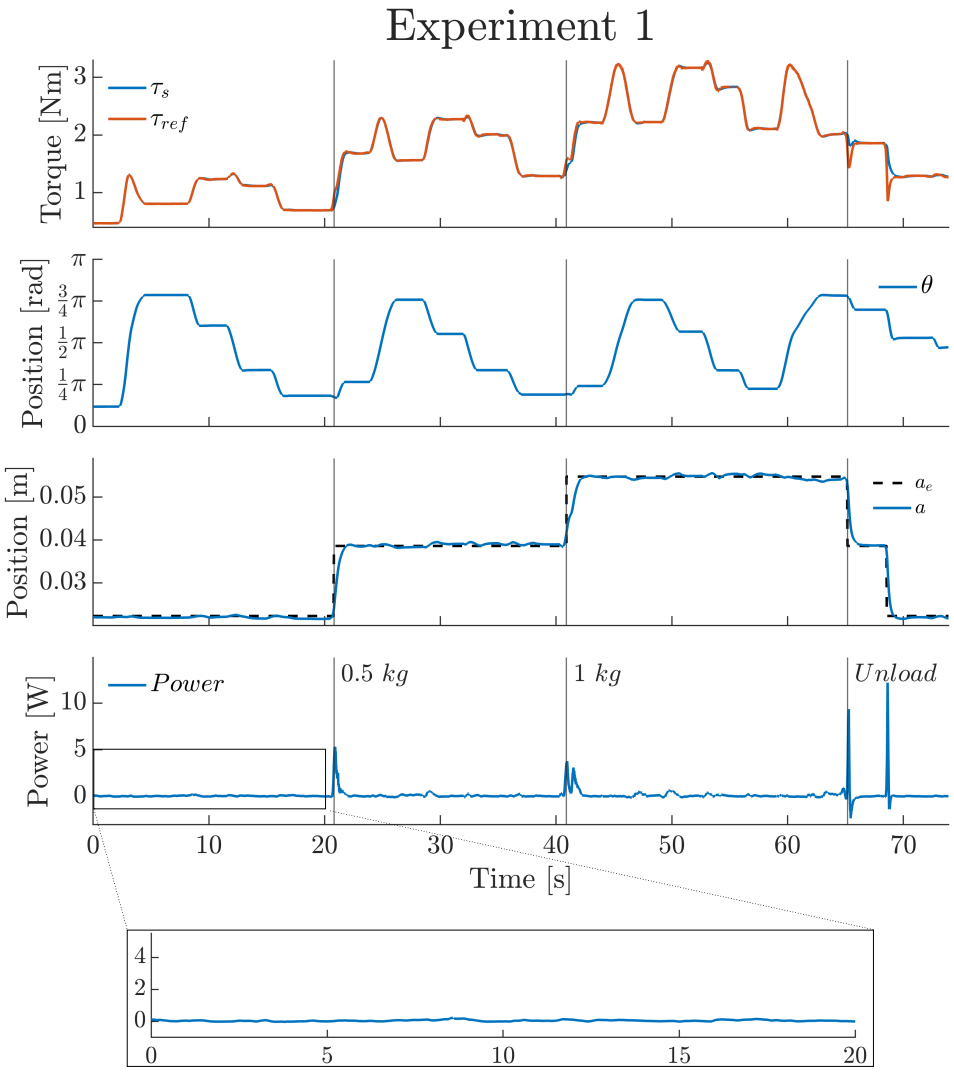

FIGURE 5.10: Experimental results of Experiment 1. The four panels show force tracking, the position θ of the link, the real and theoretical position of the linear drive, and the power output of the AGtuator system. The system starts with no payload, which is then increased first to 0.5 kg and subsequently to 1 kg. Ultimately, the system returns to the unloaded state by removing the two disks one at a time.

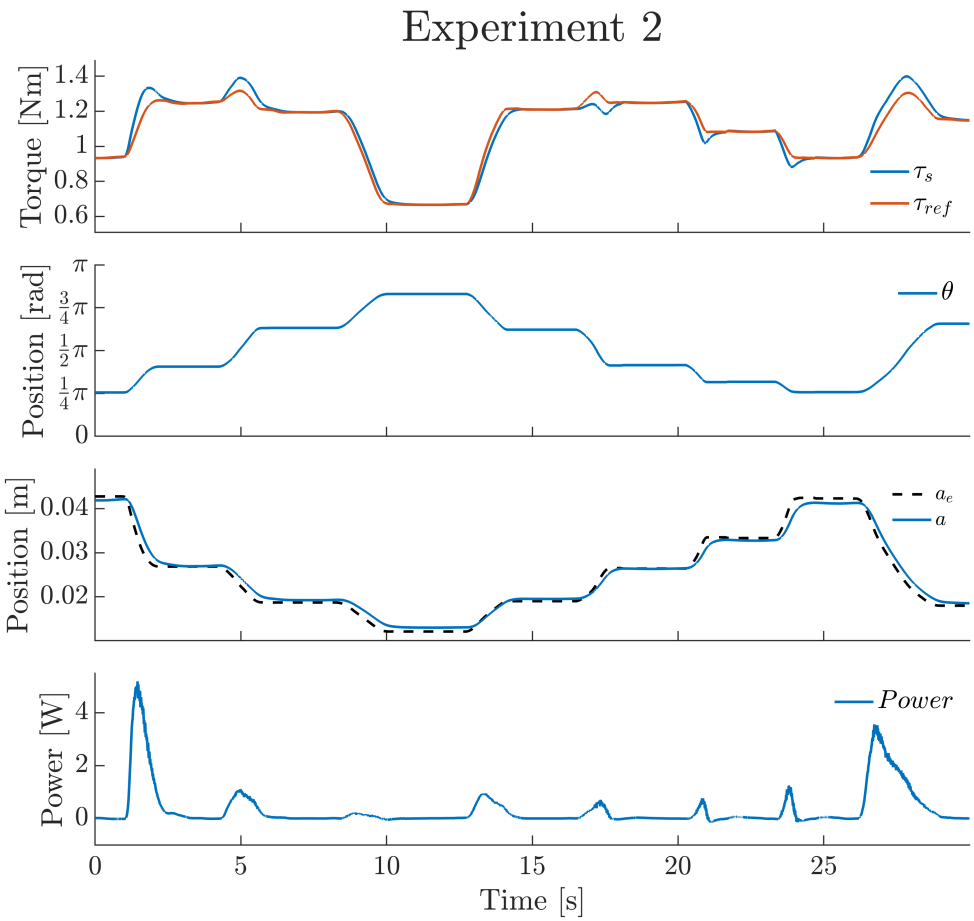

FIGURE 5.11: Experimental results of Experiment 2. The four panels show force tracking, the position θ of the link, the real and theoretical position of the linear drive, and the power output of the AGtuator system. AGtuator's ability to apply an arbitrary torque profile is confirmed, as gravitational forces are compensated even when the system is tilted at an angle $\alpha = 25°$.

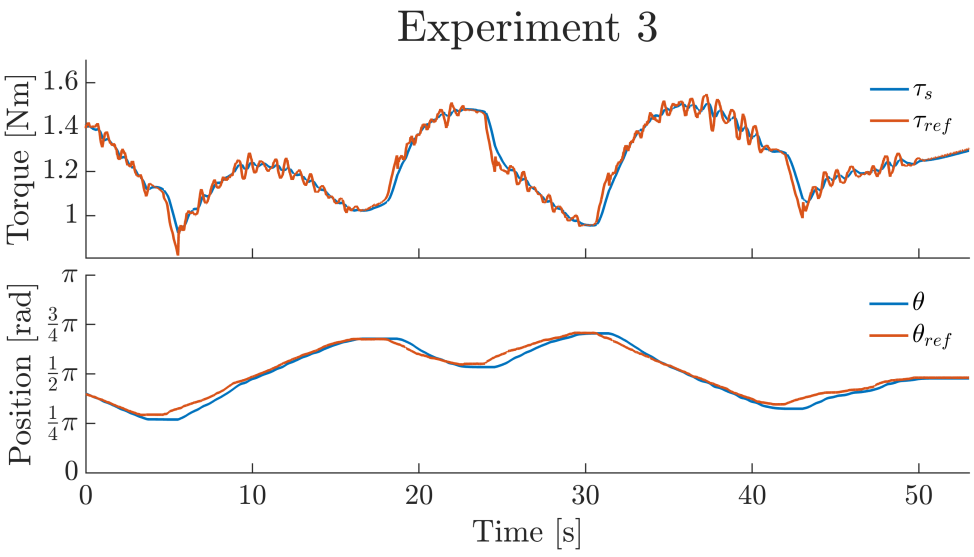

FIGURE 5.12: Experimental results of Experiment 3. The two panels show the torque tracking performance and the position tracking performance.

Chapter 6

Design of a Semi-Active Industrial Exoskeleton

The AGtuator actuation and gravity compensation system, presented in the previous chapter, can be used in various fields. In the following chapter, a possible application to industrial exoskeletons is presented.

6.1 From Passive to Semi-Active

One of the most popular and appreciated industrial exoskeletons is the Paexo Shoulder, produced by Ottobock. The Paexo is a passive shoulder-support exoskeleton based on a bungee cord, ideal for overhead tasks. The main strength of this device lies in its kinematic compatibility, achieved through a patented mechanism consisting of a spherical joint positioned on the lumbar belt [146]. Like other passive exoskeletons, the level of support it provides is not adjusted during use but can be preset in advance. The adjustment can be made in two ways: using the bungee cord in a single or double configuration and by rotating the screw to modify the tension of the cord itself. Even in the single configuration, the elastic cord is doubled: it is fixed at the lower part, loops around a pulley near the shoulder joint, and returns to be fixed at the base. Therefore, we have a total of 2 elastic cords in the single configuration and 4 elastic cords in the double configuration. However, despite the various adjustment options, the issue of passive exoskeletons remains: the lack of adaptability to the load. A semi-active solution could be implemented to address this issue. In addition, as mentioned in Chapter 3, semi-passive systems can overcome approximations of the gravitational model by adjusting residual gravity forces with the usage of the actuator. To achieve the advantages of a semi-active exoskeleton, it is first necessary to analyze the structure of the Paexo to understand its kinematics and the torques provided.

6.1.1 Analysis of Ottobock Paexo

The Paexo exoskeleton by Ottobock is mainly composed of two rods hinged together. On one side, they are connected to the user's arm, while on the other, they are attached to a belt via a ball joint. Between the rear rod and the extension of the rod fixed to the arm is positioned the bungee cord, which provides the assistance delivered by the exoskeleton. Figure 6.1 shows the exoskeleton worn by a person performing an overhead task. Superimposed on the person's figure and placed alongside for clarity, an arbitrary nomenclature of the various segments is provided to facilitate the analysis of the structure. Table 6.1 lists all the measurements of the various segments. The measurements were taken directly from an exoskeleton, as no details are provided by the company.

Segment	$\overline{OD}$	$\overline{AD}$	$\overline{DE}$	$\overline{CE}$	$\overline{BC}$	$\overline{CF}$	$\overline{FG}$	l_0	l_{cord}
Length [m]	0.115	0.02	0.33	0.007	0.052	0.026	0.26	0.155	0.13

TABLE 6.1: Measurements of the various segments that make up the Paexo by Ottobock. l_{cord} and l_0 represent, respectively, the length of the inextensible metal cord and the resting length of the bungee cord.

FIGURE 6.1: The Paexo by Ottobock worn while performing an overhead task and the proposed nomenclature for analyzing the exoskeleton [68]. The bungee cord is installed between Points A and B. The image was taken from the company's website [68].

The elastic torque provided by the exoskeleton is proportional to the elongation of the elastic cord, fixed between Points A and B, and can be calculated using the formula:

$$\tau_{Elastic} = n_{cord} \cdot k \cdot (\Delta l \times r) \tag{6.1}$$

where k is the elastic constant of the bungee cord, Δl is the elongation of the bungee cord, $\times$ denotes the cross product, and r is the position vector, ranging from the hinge to the point where the force is applied. n_{cord} can be a value between 1 and 2, depending on whether the configuration is used. The bungee cord is placed directly between the two segments, without rerouting, and thus has a resting length of l_0. The effective elongation Δl can be defined as the distance between points A and B, subtracting the resting length l_0 and the length of the metal cord l_{cord} that attaches the bungee cord to one of the two links:

$$\Delta l = \overline{AB} - l_{cord} - l_0 \tag{6.2}$$

The length of the segment $\overline{AB}$ can be written as:

$$\overline{BE} = \sqrt{(x_A - x_B)^2 + (y_A - y_B)^2} \tag{6.3}$$

The coordinates of point A are fixed, while the coordinates of point B vary as the angle θ changes. The result of the cross product, the vector perpendicular both to r and to the elastic force, can be identified with $r_\perp$ and can be calculated using the distance from a point to a line distance. In particular, with the following formula, it is possible to calculate the shortest distance between the hinge (point C) and the segment $\overline{AB}$, representing the direction of the elastic force.

$$r_\perp = \frac{||\overline{AC} \times \overline{AB}||}{||\overline{AB}||} \tag{6.4}$$

$\overline{AC} \times \overline{AB}$ denotes the cross product between the two vectors and $||\overline{AB}||$ the vector norm. The formula can be written, using the coordinates of points, as:

$$r_\perp = \frac{|(x_C - x_A)(y_B - y_A) - (y_C - y_A)(x_B - x_A)|}{\sqrt{(x_A - x_B)^2 + (y_A - y_B)^2}} \tag{6.5}$$

Considering the formulas mentioned above, it is possible to rewrite the $\tau_{Elastic}$ provided by the Ottobock Paexo as follows:

$$\tau_{Elastic} = n_{cord} \cdot k \cdot \left(\sqrt{(x_A - x_B)^2 + (y_A - y_B)^2} - l_{cord} - l_0 \right) \cdot \\ \cdot \frac{|(x_C - x_A)(y_B - y_A) - (y_C - y_A)(x_B - x_A)|}{\sqrt{(x_A - x_B)^2 + (y_A - y_B)^2}} \tag{6.6}$$

The chosen convention considers a negative angle of $-90°$ as if the exoskeleton were worn by a person with their arms resting along their sides. The various configurations of the exoskeleton at the corresponding angles are shown in Figure 6.2. Since

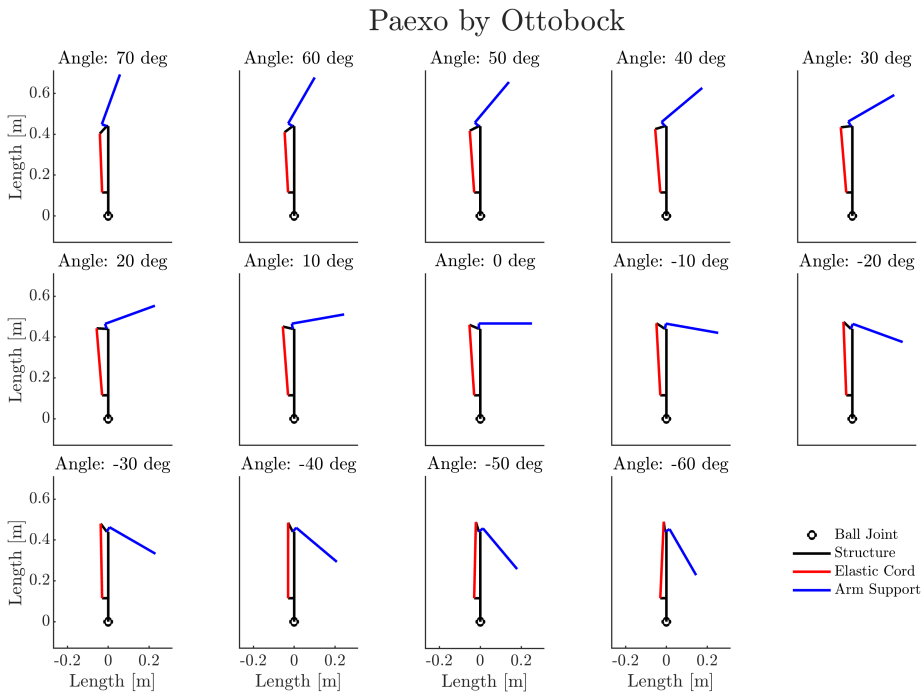

FIGURE 6.2: Various configurations of the Paexo exoskeleton by Ottobock as the arm inclination angle, indicated in blue, varies. The circle represents the ball joint attached to the belt. The exoskeleton structure is shown in black, while the bungee cord is depicted in red.

the characteristics of the bungee cord are unknown and Ottobock does not provide accurate measurements of the torque supplied by the Paexo, the maximum value was taken from a study in the literature [147]. Watterworth et al. proposed this experimental profile of the elastic torque, referred to as $\tau_{ExpProfile}$, using a fourth-order polynomial:

$$\tau_{ExpProfile} = 2.339203 \cdot 10^{-1} - 1.453055 \cdot 10^{-1} \cdot \theta_{deg} + 9.489930 \cdot 10^{-3} \cdot \theta_{deg}^2 - 9.519813 \cdot 10^{-5} \cdot \theta_{deg}^3 + 2.598484 \cdot 10^{-7} \cdot \theta_{deg}^4 \quad (6.7)$$

where θ_{deg} represents the rotation of the arm link expressed in degrees. To study a possible adaptive Paexo, it was necessary to calculate the torque starting from the geometry. Therefore, the formula presented in (6.1) was used, with $n_{cord} = 2$. The missing value of k was computed to obtain the same maximum value of $\tau_{ExpProfile}$. Figure 6.3 shows the assistance torque as a function of the angle provided by the Paexo, calculated using both the previous formula and the geometric formula. The

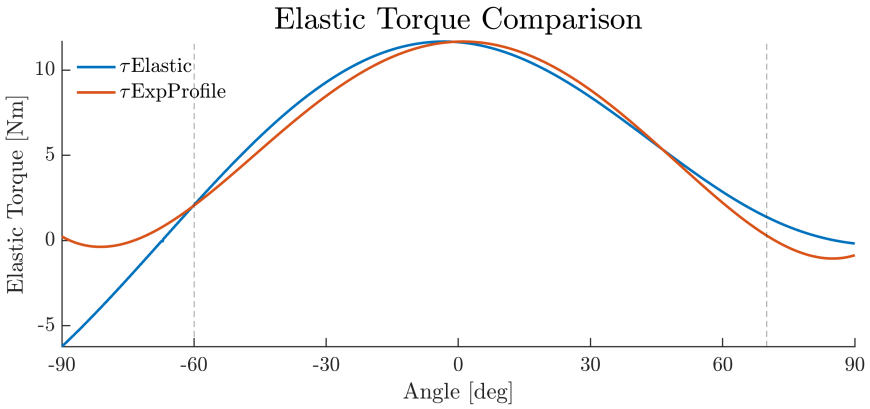

FIGURE 6.3: Comparison between the elastic torque provided by the Ottobock Paexo according to experimental validation, shown in orange, and according to the geometry, shown in blue. The correlation between the two curves has an R^2 value of 0.984 in the range from $-60°$ to $70°$.

two curves exhibit a similar trend, with a difference at the peak value. The experimentally derived curve has a maximum of approximately 1°, whereas the curve calculated based on geometry peaks at around -3.3°. However, computing the correlation between the two curves yields a value of $R^2 = 0.925$, which increases to $R^2 = 0.984$ when considering only the range between -60° and 70°. The evident differences in the range of motion between $-90°$ and $-60°$ are due to a mechanism in the Paexo that blocks the rotation of the bungee cord. This mechanism was not included in the geometric model. It can, therefore, be concluded that the calculation of the torque provided from the geometry, at least within the aforementioned interval, is a good approximation and can thus be used to compute the displacements in a hypothetical semi-active and adaptive Paexo.

6.1.2 Analysis of an adaptive Paexo Implementation

As mentioned in the previous paragraph, the adjustment of the assistance provided by the Paexo, being a passive exoskeleton, can only be made before wearing the exoskeleton, and there is no way to make it adapt to the load. Applying a semi-active

and adaptive system to the load represents a possible solution to this problem, allowing energy-efficient and precise compensation throughout the entire range of motion. In [148], this has been done by mounting a linear drive to modify the distance $\overline{BC}$. Here on we analyze such proposed solution. The coordinates of Point B modify the elastic torque, as can be seen from equation 6.6. Thus, referring to Figure 6.1, if the goal is the precise compensation throughout the entire range of motion, by imposing the equality $\tau_{Elastic} = \tau_{Gravity}$, it is possible to compute the new coordinates of point B that satisfy the equation. The gravitational torque reference $\tau_{Gravity}$ has been calculated by taking the maximum elastic torque that the Paexo can provide:

$$\tau_{Gravity,max} = max(\tau_{ExpProfile}) \cos\theta \tag{6.8}$$

Figure 6.4 shows the trends of the gravitational torque and the maximum elastic torque that can be produced by the Paexo. An ideal force controller will adjust the elastic torque produced by the exoskeleton to follow the required torque profile. To simulate the position changes that the linear drive will make, four different gravitational torque profiles were chosen, corresponding to 40%, 60%, 80%, and 100% of the previously calculated maximum. The top row of Figure 6.5 shows the required displacement to achieve full compensation as the angle θ varies, in the range -60° to 70°.

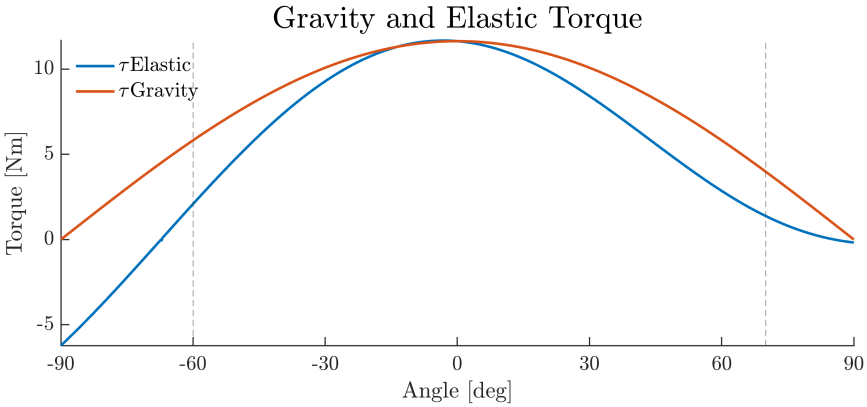

FIGURE 6.4: Comparison between the maximum elastic torque provided by the Paexo and a gravitational torque, a function that exhibits a co-sinusoidal behavior in the range from $-90°$ to $90°$.

As can be seen, Paexo's structure results in a system that constantly needs to move to balance a weight, even within the range of interest. The movements of point B were confined within a range from 0.052 m to 0.02 m, corresponding to the pretension adjustment available on the Adaptive Paexo proposed in [148]. Given this limitation, the system was not always able to provide an elastic torque equal to the required gravitational torque reference. Figure 6.5, in the bottom row, shows these trends in the four cases. The system can exactly balance the gravitational forces only in the first case, corresponding to 40% of the maximum torque that the Paexo can provide. However, this is achieved through continuous movement across the entire range, resulting in precise compensation but requiring the system to operate continuously. As the gravitational torques increase, in the cases of 60%, 80%, and 100%, an adequate elastic torque can only be produced for angles close to 0°. Such bad behavior is surely because the Paexo exoskeleton is intended to assist workers with overhead tasks, making it suboptimal for lifting or carrying payloads where GC is required within a wide Range of Motion (RoM). We highlight that a semi-active

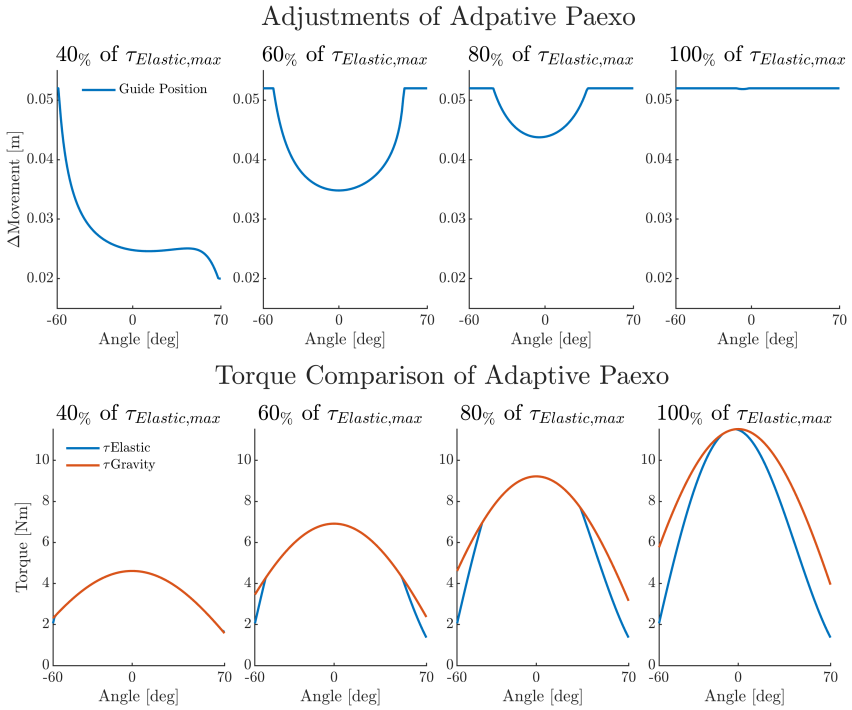

FIGURE 6.5: *Top Row* - Required displacement of the bungee cord anchor point to achieve different assistance curves, varying between 40% and 100% of the required torque curves. The displacement is confined between 0.02 m and 0.052 m, as in the Paexo structure used in [148]. *Bottom Row* - Comparison between the gravitational torque profile and the assistance provided by the adaptive Paexo, obtained through the force control of the AGtuator. Complete overlap between the two curves occurs only in the case of 40% of the maximum payload, at the cost of continuous movement of the guide throughout the entire range of motion.

Paexo proposed in [148] was not meant for load lifting, therefore it lacks the torque control capabilities that allow for uniform assistance throughout a wide range of motion.

This section has shown that it is not possible to achieve an adaptive Paexo system capable of providing complete assistance with low energy consumption. In the next section, a modification to the structure will be introduced to implement the AGtuator concept introduced in Chapter 5, to achieve an adaptive and energy-efficient system. Additionally, by incorporating an active component, an attempt will be made to increase the maximum torque of the exoskeleton compared to the Paexo by Ottobock.

6.2 Design of a new exoskeleton with AGtuator concept

As shown in the previous chapter, the geometric constraints required to achieve a system that remains in equilibrium in all positions are well-defined. The most significant modification, however, involves the cord used, which must behave like a zero-free-length cord to function effectively. This means the rigid, non-deformable metal cord must be removed, and a redirecting mechanism must be incorporated to ensure the elastic force is proportional to the distance $\overline{AB}$.

Segment	$\overline{OA}$	$\overline{AA'}$	$\overline{AC}$	$\overline{CD}$	$\overline{DE}$	$\overline{EB}$	$\overline{EF}$	$\overline{DG}$
Length [m]	0.35	0.30	0.15	0.02	0.09	0.02	0.08	0.40

TABLE 6.2: Measurements of the various segments of the exoskeleton prototype built with the AGtuator concept.

Effective geometry is given by the AGtuator concept and has already been presented in the previous chapter in Figure 5.5.

Here, we introduce a slight modification that mainly concerns the shoulder link area. The chosen geometry is shown in Figure 6.6. As in [148], we decided to place

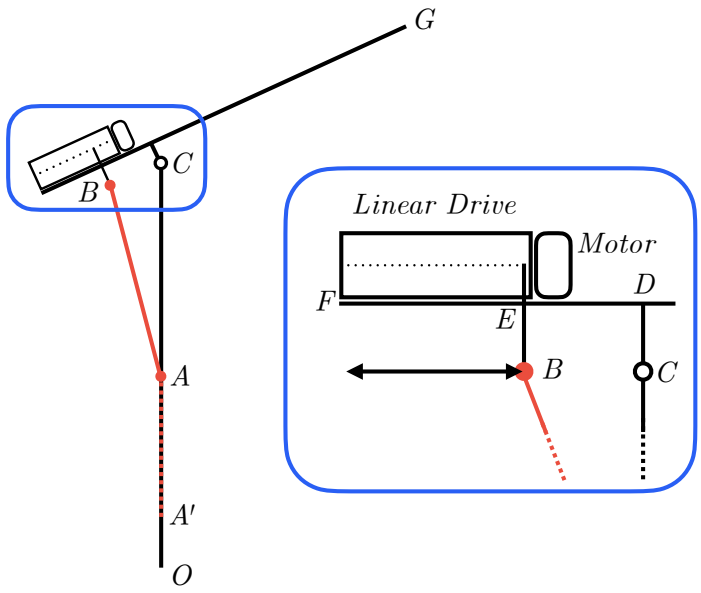

FIGURE 6.6: Structure of the shoulder exoskeleton prototype with the AGtuator concept that will be built. The motor and the linear drive, responsible for controlling the elastic force, are placed on the extension of the link that connects to the arm. In blue, a zoom-in of the actuation system with the nomenclature of the various segments is shown.

the motor and the linear drive near the shoulder joint. This way, the additional weight of these components can act as a counterweight and aid in compensation. To achieve a 180° range of motion, it was necessary to introduce an offset between the two links, denoted as $\overline{CD}$ in the figure. The linear drive has a motion range equal to $\overline{EF}$. It is important to emphasize that the distance $\overline{BE}$ must be chosen so that point B aligns with the hinge at C. Only in this way will it be possible to meet the geometric requirements imposed by the AGtuator concept. The segment AA' represents the redirection of the cord, necessary to achieve the zero-free-length behavior. The dimensions of all segments are listed in Table 6.2. Figure 6.7 shows the exoskeleton as the angle θ varies, similar to the case of the Paexo.

Once the geometry has been defined, it is possible to calculate the elastic torque this exoskeleton provides. In the case of a zero-free length spring (l_0 = 0) and l_{cord} = 0, where the segment $\overline{AB}$ is equal to the elongation in 6.1 of the bungee cord, the

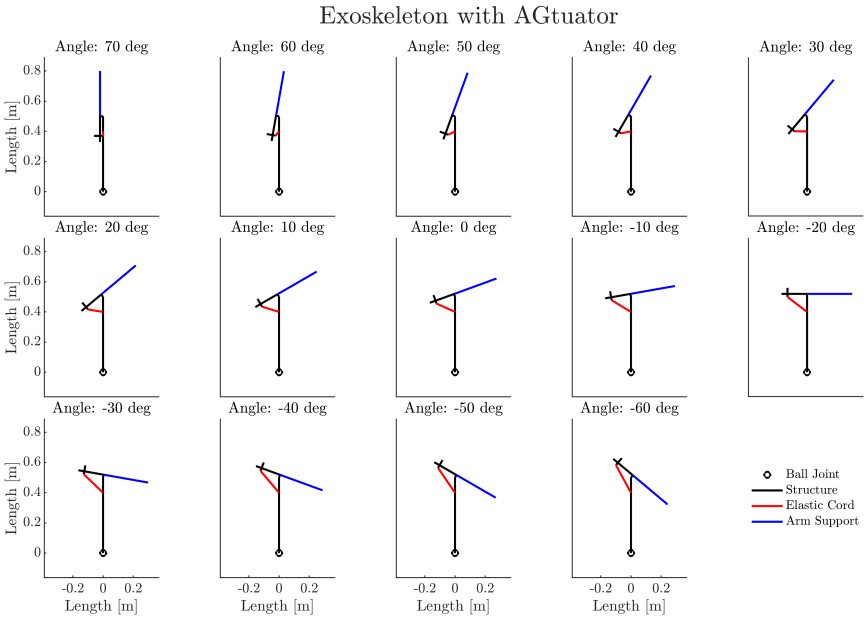

FIGURE 6.7: Various configurations of the proposed new exoskeleton with AGtuator concept as the arm inclination angle, indicated in blue, varies. The circle represents the ball joint attached to the belt. The exoskeleton structure is shown in black, while the bungee cord is depicted in red.

formula simplifies:

$$\tau_{Elastic} = k \cdot |(x_C - x_A)(y_B - y_A) - (y_C - y_A)(x_B - x_A)| \tag{6.9}$$

The elastic constant of the bungee has been estimated using the following formula:

$$k = \frac{A}{l_r} E \tag{6.10}$$

where A denotes the cross-sectional area of the cord, l_r is the length $\overline{AA'}$ of the cord in the redirection, and E is equal to $6.9 \cdot 10^6\ MPa$, as specified by the manufacturer. The cord has a diameter of $d = 6mm$, thus an $Area = 2.826 \cdot 10^{-5} m$. Figure 6.8 shows the elastic torques obtainable as the position of the guide varies. As can be seen, the torque curve is only shifted up and down and corresponds exactly to a cosine function, as expected for perfect gravity compensation of a payload. The minimum torque that can be provided is approximately equal to the maximum torque that the Paexo can generate, while the maximum torque is about twice as much. This allows for a system that adapts to the payload present in the structure without requiring additional adjustments as the angle varies.

Wearability, comfort, and shoulder self-alignment are achieved through a belt arranged on the pelvis and a spherical joint on the point O connecting to the main structure of the exoskeleton, similarly to the Paexo exoskeleton.

6.2.1 Prototype Development

Given the potential of a semi-active AGtuator exoskeleton system, it was decided to develop a prototype. The progress at the time of writing this work is shown in Figure 6.9. The exoskeleton, built according to the scheme and dimensions of Figure

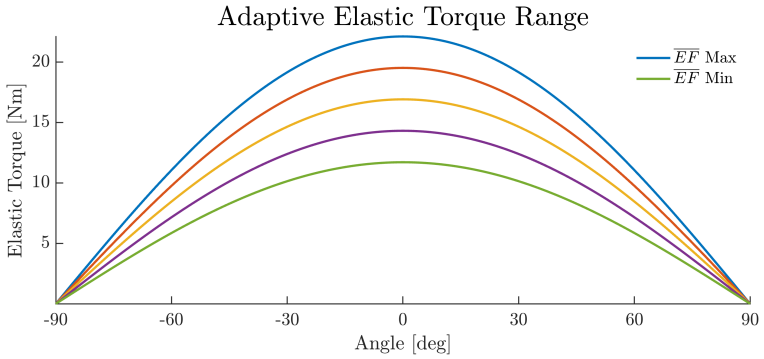

FIGURE 6.8: Comparison of the assistance profiles achievable with the exoskeleton prototype using the AGtuator concept. The linear drive has an active stroke of 0.008 m, and the curves represent five possible profiles. In blue, the maximum assistance is provided with the carriage positioned at the end of the guide, while in green, the minimum assistance is shown with the carriage positioned at the beginning of the guide.

6.6 and Table 6.2, consists of two hollow aluminum tubes with a square cross-section, hinged together. The rod corresponding to the back area has dimensions of 20 × 20 mm, while the one supporting the arm has dimensions of 16 × 16 mm. The back tube will be attached to a belt through a spherical joint, shown in red in Figure 6.9. Also in red, mounted on the extension of the tube supporting the arm, is the housing for the linear drive. Two pulleys with corresponding bearings ensure the correct sliding of the bungee cord, minimizing friction.

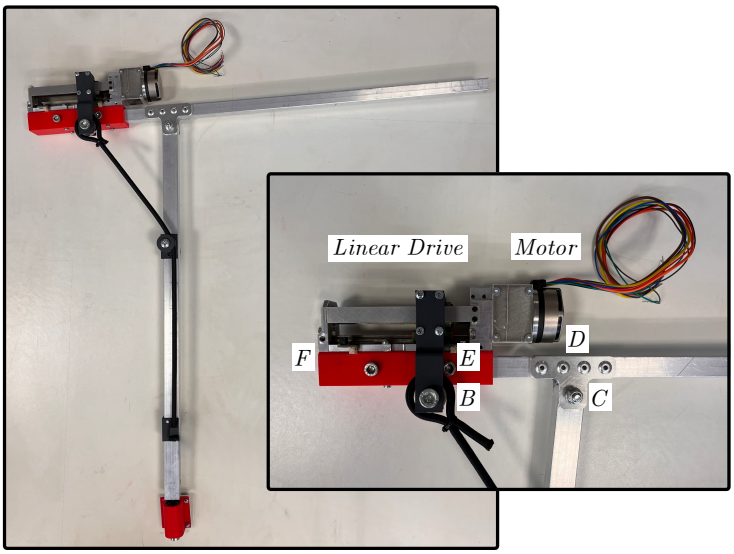

FIGURE 6.9: Photo of the upper limb exoskeleton prototype with the AGtuator system. In the zoomed-in section, the actuation system that makes the exoskeleton semi-active.

The actuation part, the focus of this semi-active exoskeleton, is shown in the zoomed section of Figure 6.9 along with its nomenclature. The motor chosen to control the linear drive, manufactured by THK, is a 4221G048BXTR produced by Faulhaber, Germany. As mentioned earlier, to ensure an optimal torque curve, point B was aligned with the hinge at C. Due to time constraints, it was not possible to

actuate the exoskeleton and test its effectiveness. Furthermore, the best interface for connecting the arm is still under study.

6.3 Adding of Elbow Joint

The AGtuator concept, and therefore the proposed exoskeleton, requires the estimation or measurement of gravitational torques measuring the payload. The AGtuator prototype built in Chapter 5 was measuring the payload using a load cell. In the case of an exoskeleton, such a solution is not convenient, and an algorithm for load estimation based on the electromyographic signal is available in our lab [90, 149]. Without further details, achieving this requires an exoskeleton that includes an actuated elbow joint.

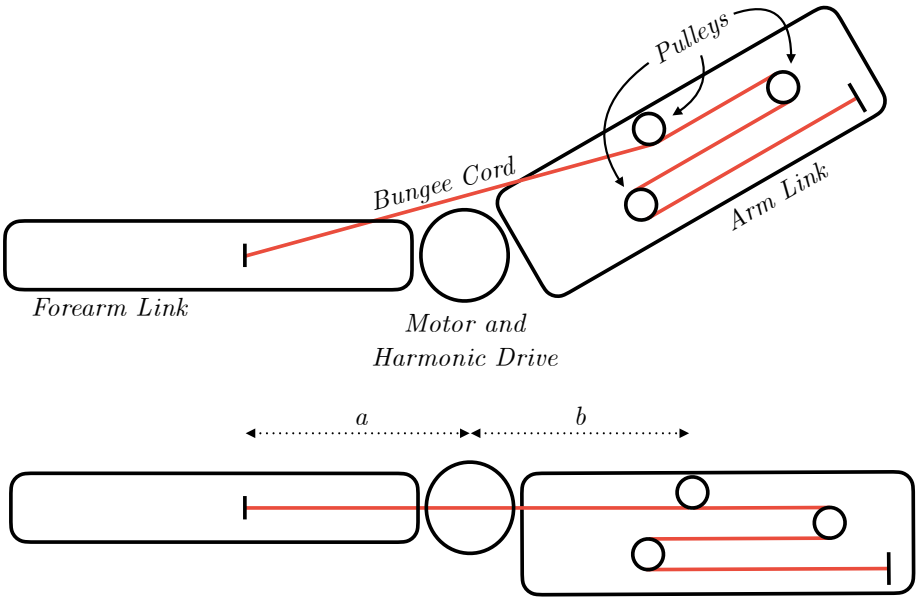

FIGURE 6.10: Schematic of the elbow exoskeleton. The bungee cord, connected to the exoskeleton at distances a and b relative to the motor at the joint, provides additional assistance during elbow flexion. A pulley system, hidden within the arm link, optimizes the behavior of the passive elastic element.

The elbow exoskeleton was designed using a joint-mounted motor and an elastic element in parallel to increase the total torque produced while keeping the weight low and the dimensions compact. The elastic element assists the elbow flexion. Figure 6.10 shows a schematic view of the exoskeleton. To achieve the lightest possible system, a Harmonic Drive reducer has been chosen. The motor is a 4221G048BXTR produced by Faulhaber. The reducer is a LHD-III series model 17 manufactured by Leaderdrive [150]. The specifications are listed in the Table 6.3. A bungee cord with a diameter of 6 mm, the same as before, has been chosen as the elastic element.

The elastic force produced by the bungee cord must be as high as possible but must not exceed the torque generated by the motor. The motor must be capable of "overcoming" the force of the cord to allow elbow extension. Therefore, the torque provided by the elastic element is a crucial parameter. The required torque profile, following the convention where angles vary between $-90°$ and $90°$, is asked to follow a cosine pattern. The maximum value, obtained at position $\theta = 0°$, corresponds

Faulhaber Series 4221G048BXTR		LeaderDrive LHD-III series model 17	
Nominal Torque [Nm]	0.112	Reduction Ratio	80
Nominal Rotational Speed [rpm]	4380	Max Input Speed [rpm]	7000
Nominal Voltage [V]	24	Max Avg Output Torque [Nm]	21
Weight [g]	142	Weight [g]	450

Electric Motor + Harmonic Drive	
Nominal Torque Output [Nm]	8.96
Nominal Speed Output [rpm]	54.88
Total Weight [g]	592

TABLE 6.3: Parameters of the motor, the gearbox, and the combined motor and gearbox used for the realization of the elbow exoskeleton.

to:

$$\tau_{Elastic} = k \cdot ab \tag{6.11}$$

where a and b represent the distances between the hinge and the two attachment points of the elastic cord. The elastic constant, on the other hand, can be expressed as:

$$k = \frac{Area}{l_r} E \tag{6.12}$$

with Area $= 2.826 \cdot 10^{-5}\,\mathrm{m}^2$ and $E = 6.9 \cdot 10^6$ MPa.

6.3.1 Optimization of Bungee Cord

To build the most compact elbow exoskeleton possible, it is necessary to optimize its dimensions as much as possible. An important factor in the overall size, especially if a passive component is added to enhance the provided assistance, is the routing of the bungee cord, denoted as l_r in the previous formula. l_r must therefore be as small as possible while still ensuring the proper functioning of the system. To determine this value, two system properties must be considered: the maximum elongation capability of the cord and the maximum elongation required by the system. The first parameter is an intrinsic property of the selected cord, which in our case corresponds to 100%, meaning the cord can reach a length equal to twice its initial length. The maximum elongation of the cord in our system, denoted as Δl_{max}, occurs when the arm is fully extended, i.e., at $\theta = 90°$. Therefore, it can be stated that:

$$\begin{aligned} Elongation_{max} = \frac{l_{max}}{l_r} = \frac{l_r + \Delta l_{max}}{l_r} = 2 \\ \Rightarrow \Delta l_{max} = l_r \end{aligned} \tag{6.13}$$

The value of l_r is equal to the sum of segments a and b.

$$\begin{aligned} \Delta l_{max}(\theta = \frac{\pi}{2}) = a + b \\ a + b = l_r \end{aligned} \tag{6.14}$$

Now, it is possible to rewrite equation 6.12, substituting the newly obtained value. The new value of k can then be replaced in equation 6.11 to express the elastic torque

provided by the exoskeleton as a function of the distances a and b:

$$\tau_{Elastic} = k \cdot ab = E \cdot \frac{Area}{a+b} \cdot ab \tag{6.15}$$

In minimizing l_r, which represents the redirection of the elastic cord and corresponds to the sum $a + b$, it is crucial to ensure that the following equation holds:

$$\tau_m > \tau_{Elastic}. \tag{6.16}$$

It can be shown that l_r is minimized when a and b are equal.

Proof. By combining equations 6.15 and 6.16, we obtain:

$$\tau_m > \tau_{Elastic} = E \cdot \frac{Area}{a+b} \cdot ab \tag{6.17}$$

Now, by imposing the limiting case in which τ_{elastic} is equal to τ_m and defining the ratio $\tau_m/(E \cdot \text{Area}) = T$, we can write:

$$T = \frac{ba}{b+a} \tag{6.18}$$

From this equation, we can explicitly express a as

$$a = \frac{Tb}{b-T} \tag{6.19}$$

and substitute it into our function to be minimized, namely $l_r = a + b$:

$$(a+b) = (\frac{Tb}{b-T} + b) = \frac{Tb + b^2 - Tb}{b-T} = \frac{b^2}{b-T} \tag{6.20}$$

To find the minimum, we can differentiate the obtained equation and set the derivative equal to zero.

$$\frac{d\left(\frac{b^2}{b-T}\right)}{db} = 0 \Rightarrow \frac{b(b-2T)}{(b-T)^2} = 0 \tag{6.21}$$

The equation has two solutions: the first corresponds to $b = 0$, which is not acceptable, while the second is $b = 2T$. Substituting this value into Eq. 6.19, we obtain:

$$a = \frac{Tb}{b-T} = \frac{2T^2}{2T-T} = \frac{2T^2}{T} = 2T \tag{6.22}$$

Demonstrating that the minimum is obtained when a and b are equal and, in the limiting case, both are equal to $2T$.

□

By reintroducing this condition into 6.16, we obtain that $a < 2T$ and $b < 2T$, with $T = \frac{\tau_m}{E \cdot \text{Area}}$. Substituting the values and assuming a 90% efficiency for the harmonic drive, the maximum length of segments a and b is obtained as 0.092 m.

6.4 Further Work and Limitations

The next steps involve the realization of the whole exoskeleton and the validation of some simplifications that have been made. In particular, for the shoulder joint, it will be necessary to verify the linearity and behavior of the elastic cord. A bungee cord has been chosen instead of a spring primarily for safety reasons. If non-linearity compromises the proper functioning of the AGtuator concept, a spring-based solution will be reconsidered. The development of the prototype will require testing to determine the most ergonomic solution, from positioning the structure on the belt to designing the interfaces with the user's arm.

For the elbow joint, the behavior of the bungee cord will also need to be evaluated. However, for this degree of freedom, the cord's behavior is less critical, as it works in parallel with the motor. The main tasks involve optimizing the dimensions, including housing the electronics and finding ergonomic interfaces for wearing the device.

Appendix A

Complete Results of Agadexo Evaluation

A.1 EMG Results

A.1.1 Task 1 - Static Lifting

	UT	AD	PD	IN	LD
p-value	<.001	<.001	=.497	<.001	<.001
F-ratio	15.15	52.07	0.701	23.03	16.18

	ES	RA	PM	BB	BR
p-value	<.001	<.001	<.001	<.001	=.02
F-ratio	7.27	23.59	15.59	11.05	3.94

TABLE A.1: p-values and F-ratio of Muscle Activity (RMS) in Task 1 - Static Lifting for *Assistance* Factor. Muscles: Upper Trapezius (UT), Anterior Deltoid (AD), Posterior Deltoid (PD), Infraspinatus (IN), Latissimus Dorsi (LD), Erector Spinae (ES), Rectus Abdominis (RA), Pectoralis Major (PM), Biceps Brachii (BB), and Brachioradialis (BR)

	UT	AD	PD	IN	LD
NoExo - ExoMax	<.001	<.001	=.722	<.001	<.001
NoExo - ExoMed	<.001	<.001	=.911	<.001	<.001
ExoMax - ExoMed	=.492	=.02	=.472	=.965	=.291

	ES	RA	PM	BB	BR
NoExo - ExoMax	=.004	<.001	<.001	<.001	=.088
NoExo - ExoMed	=.002	<.001	<.001	=.007	=.021
ExoMax - ExoMed	=.961	=.342	=.823	=.252	=.84

TABLE A.2: p-values of Muscle Activity (RMS) in Task 1 - Static Lifting for *Assistance* Factor. Muscles: Upper Trapezius (UT), Anterior Deltoid (AD), Posterior Deltoid (PD), Infraspinatus (IN), Latissimus Dorsi (LD), Erector Spinae (ES), Rectus Abdominis (RA), Pectoralis Major (PM), Biceps Brachii (BB), and Brachioradialis (BR)

	UT	AD	PD	IN	LD
p-value	=.447	=.73	=.373	=.892	=.199
F-ratio	0.81	0.32	0.99	0.11	1.62

	ES	RA	PM	BB	BR
p-value	=.963	=.558	=.563	=.771	=.895
F-ratio	0.04	0.58	0.57	0.26	0.11

TABLE A.3: p-values and F-ratio of Muscle Activity (RMS) in Task 1 - Static Lifting for *Assistance* x *Weight* Factors. Muscles: Upper Trapezius (UT), Anterior Deltoid (AD), Posterior Deltoid (PD), Infraspinatus (IN), Latissimus Dorsi (LD), Erector Spinae (ES), Rectus Abdominis (RA), Pectoralis Major (PM), Biceps Brachii (BB), and Brachioradialis (BR)

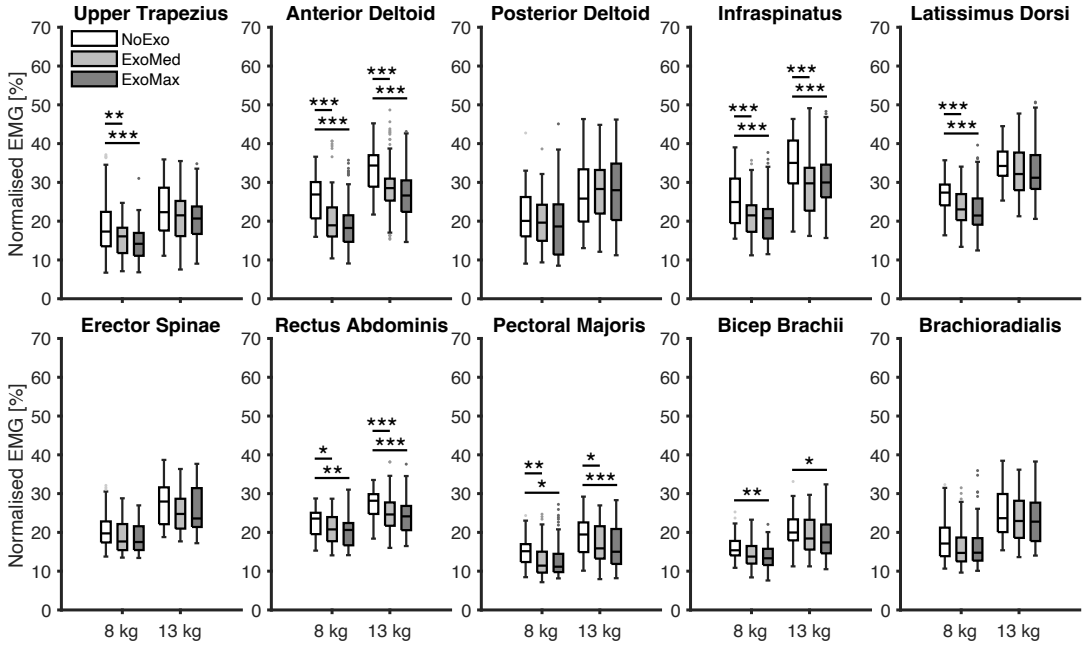

FIGURE A.1: EMG results *Assistance* x *Weight* Factors for Task 1 - Static Lifting. $*$ indicates p-values ≤ 0.05, $**$ indicates p-values ≤ 0.01, and $***$ indicates p-values ≤ 0.001

8 kg	UT	AD	PD	IN	LD
NoExo - ExoMax	<.001	<.001	=.678	<.001	<.001
NoExo - ExoMed	=.002	<.001	=.996	<.001	<.001
ExoMax - ExoMed	=.938	=.642	=.928	=.996	=.907

13 kg	UT	AD	PD	IN	LD
NoExo - ExoMax	=.056	<.001	=.999	<.001	=.059
NoExo - ExoMed	=.25	<.001	=.889	<.001	=.504
ExoMax - ExoMed	=.985	=.21	=.983	=.999	=.887

8 kg	ES	RA	PM	BB	BR
NoExo - ExoMax	=.138	=.001	=.021	=.003	=.832
NoExo - ExoMed	=.138	=.022	=.007	=.077	=.578
ExoMax - ExoMed	=.999	=.976	=.999	=.927	=.998

13 kg	ES	RA	PM	BB	BR
NoExo - ExoMax	=.316	<.001	<.001	=.043	=.488
NoExo - ExoMed	=.163	<.001	=.036	=.598	=.27
ExoMax - ExoMed	=.999	=.824	=.857	=.802	=.999

TABLE A.4: p-values of Muscle Activity (RMS) in Task 1 - Static Lifting for *Assistance* x *Weight* Factors. Muscles: Upper Trapezius (UT), Anterior Deltoid (AD), Posterior Deltoid (PD), Infraspinatus (IN), Latissimus Dorsi (LD), Erector Spinae (ES), Rectus Abdominis (RA), Pectoralis Major (PM), Biceps Brachii (BB), and Brachioradialis (BR)

A.1.2 Task 2 - Load Carrying SL

	UT	AD	PD	IN	LD
p-value	<.001	<.001	<.001	<.001	<.001
F-ratio	84.95	50.45	19.36	33.97	12.3

	ES	RA	PM	BB	BR
p-value	<.001	<.001	<.001	<.001	=.002
F-ratio	21.6	23.81	9.69	10.68	6.74

TABLE A.5: p-values and F-ratio of Muscle Activity (RMS) in Task 2 - Load Carrying SL for *Assistance* Factor. Muscles: Upper Trapezius (UT), Anterior Deltoid (AD), Posterior Deltoid (PD), Infraspinatus (IN), Latissimus Dorsi (LD), Erector Spinae (ES), Rectus Abdominis (RA), Pectoralis Major (PM), Biceps Brachii (BB), and Brachioradialis (BR)

	UT	AD	PD	IN	LD
NoExo - ExoMax	<.001	<.001	<.001	<.001	<.001
NoExo - ExoMed	<.001	<.001	=.007	<.001	<.001
ExoMax - ExoMed	=.077	<.001	=.04	=.841	=.991

	ES	RA	PM	BB	BR
NoExo - ExoMax	<.001	<.001	<.001	<.001	=.477
NoExo - ExoMed	<.001	<.001	=.712	=.389	=.027
ExoMax - ExoMed	=.003	=.16	=.014	=.021	=.001

TABLE A.6: p-values of Muscle Activity (RMS) in Task 2 - Load Carrying SL for *Assistance* Factor. Muscles: Upper Trapezius (UT), Anterior Deltoid (AD), Posterior Deltoid (PD), Infraspinatus (IN), Latissimus Dorsi (LD), Erector Spinae (ES), Rectus Abdominis (RA), Pectoralis Major (PM), Biceps Brachii (BB), and Brachioradialis (BR)

	UT	AD	PD	IN	LD
p-value	=.938	=.604	=.645	=.885	=.767
F-ratio	0.06	0.5	0.44	0.12	0.26

	ES	RA	PM	BB	BR
p-value	=.404	=.962	=.022	=.471	=.503
F-ratio	0.91	0,04	3.86	0.753	0.69

TABLE A.7: p-values and F-ratio of Muscle Activity (RMS) in Task 2 - Load Carrying SL for *Assistance* x *Weight* Factors. Muscles: Upper Trapezius (UT), Anterior Deltoid (AD), Posterior Deltoid (PD), Infraspinatus (IN), Latissimus Dorsi (LD), Erector Spinae (ES), Rectus Abdominis (RA), Pectoralis Major (PM), Biceps Brachii (BB), and Brachioradialis (BR)

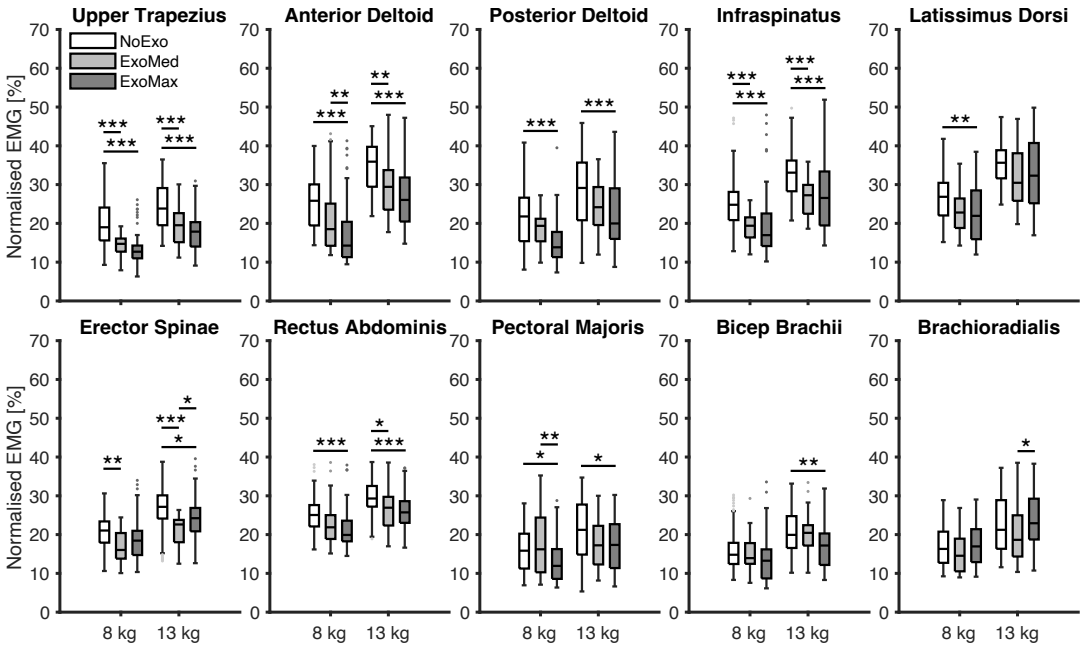

FIGURE A.2: EMG results *Assistance* x *Weight* Factors for Task 2 - Static Lifting. $*$ indicates p-values ≤ 0.05, $**$ indicates p-values ≤ 0.01, and $***$ indicates p-values ≤ 0.001

8 kg	UT	AD	PD	IN	LD
NoExo - ExoMax	<.001	<.001	<.001	<.001	=.004
NoExo - ExoMed	<.001	=.054	=.442	<.001	=.061
ExoMax - ExoMed	=.755	=.004	=.173	=.999	=.999

13 kg	UT	AD	PD	IN	LD
NoExo - ExoMax	<.001	<.001	<.001	<.001	=.088
NoExo - ExoMed	<.001	=.006	=.147	<.001	=.078
ExoMax - ExoMed	=.525	=.22	=.893	=.981	=.998

8 kg	ES	RA	PM	BB	BR
NoExo - ExoMax	=.164	<.001	=.041	=.054	=.999
NoExo - ExoMed	=.004	=.082	=.721	=.76	=.597
ExoMax - ExoMed	=.595	=.69	=.001	=.9	=.467

13 kg	ES	RA	PM	BB	BR
NoExo - ExoMax	=.032	<.001	=.024	=.004	=.742
NoExo - ExoMed	<.001	=.031	=.215	=.995	=.322
ExoMax - ExoMed	=.033	=.87	=.999	=.081	=.016

TABLE A.8: p-values of Muscle Activity (RMS) in Task 2 - Load Carrying SL for *Assistance* x *Weight* Factors. Muscles: Upper Trapezius (UT), Anterior Deltoid (AD), Posterior Deltoid (PD), Infraspinatus (IN), Latissimus Dorsi (LD), Erector Spinae (ES), Rectus Abdominis (RA), Pectoralis Major (PM), Biceps Brachii (BB), and Brachioradialis (BR)

A.1.3 Task 3 - Load Carrying HL

	UT	AD	PD	IN	LD
p-value	=.018	<.001	=.395	=.462	=.544
F-ratio	5.67	12.16	0.73	0.54	0.37

	ES	RA	PM	BB	BR
p-value	=.103	<.001	<.001	=.503	=.858
F-ratio	2.67	16.97	17.81	3.86	0.03

TABLE A.9: p-values and F-ratio of Muscle Activity (RMS) in Task 3 - Load Carrying HL for *Assistance* Factor. Muscles: Upper Trapezius (UT), Anterior Deltoid (AD), Posterior Deltoid (PD), Infraspinatus (IN), Latissimus Dorsi (LD), Erector Spinae (ES), Rectus Abdominis (RA), Pectoralis Major (PM), Biceps Brachii (BB), and Brachioradialis (BR)

	UT	AD	PD	IN	LD
p-value	0.19	=.571	=.382	=.135	=.827
F-ratio	1.75	0.32	0.76	2.24	0.05

	ES	RA	PM	BB	BR
p-value	=.926	=.129	=.004	=.151	=.955
F-ratio	0.01	2.32	8.41	2.07	0.00

TABLE A.10: p-values and F-ratio of Muscle Activity (RMS) in Task 3 - Load Carrying HL for *Assistance* x *Weight* Factors. Muscles: Upper Trapezius (UT), Anterior Deltoid (AD), Posterior Deltoid (PD), Infraspinatus (IN), Latissimus Dorsi (LD), Erector Spinae (ES), Rectus Abdominis (RA), Pectoralis Major (PM), Biceps Brachii (BB), and Brachioradialis (BR)

8 kg	UT	AD	PD	IN	LD
NoExo - ExoMax	=.042	=.163	=.999	=.949	=.935

13 kg	UT	AD	PD	IN	LD
NoExo - ExoMax	=.879	=.022	=.629	=.398	=.993

8 kg	ES	RA	PM	BB	BR
NoExo - ExoMax	=.61	=.246	=.782	=.98	=.998

13 kg	ES	RA	PM	BB	BR
NoExo - ExoMax	=.698	<.001	<.001	=.095	=1

TABLE A.11: p-values of Muscle Activity (RMS) in Task 3 - Load Carrying HL for *Assistance* x *Weight* Factors. Muscles: Upper Trapezius (UT), Anterior Deltoid (AD), Posterior Deltoid (PD), Infraspinatus (IN), Latissimus Dorsi (LD), Erector Spinae (ES), Rectus Abdominis (RA), Pectoralis Major (PM), Biceps Brachii (BB), and Brachioradialis (BR)

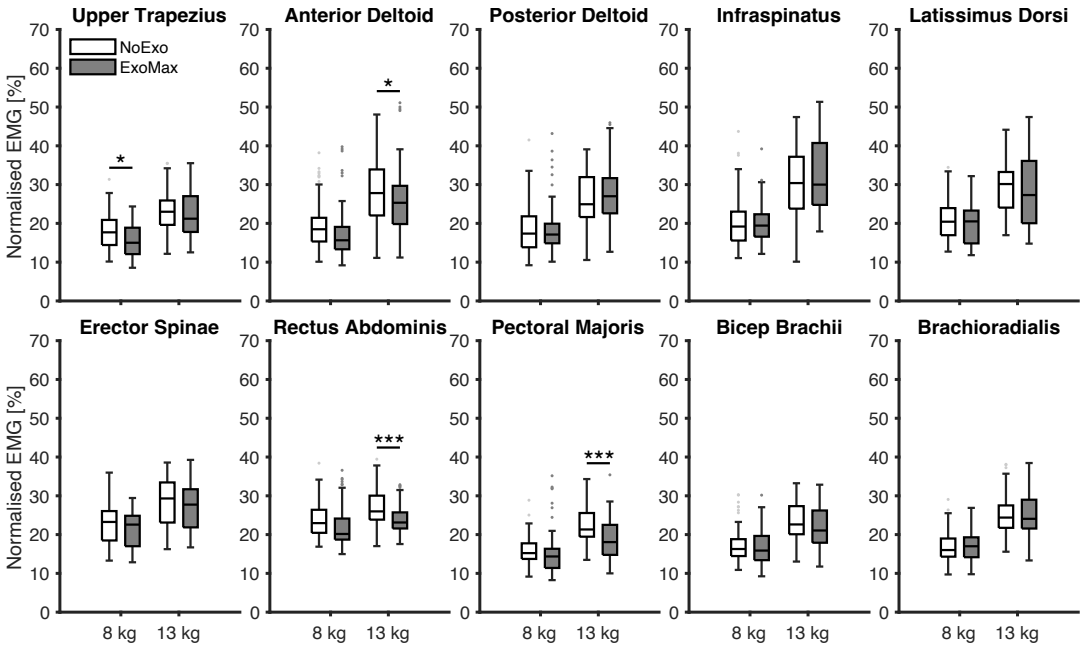

FIGURE A.3: EMG results *Assistance* x *Weight* Factors for Task 3 - Load Carrying HL. $*$ indicates p-values ≤ 0.05, $**$ indicates p-values ≤ 0.01, and $***$ indicates p-values ≤ 0.001

A.1.4 Task 4 - Box Handling

	UT	AD	PD	IN	LD
p-value	<.001	<.001	<.001	=.11	<.001
F-ratio	70.43	102.56	21.79	2.57	36.68

	ES	RA	PM	BB	BR
p-value	<.001	<.001	=.483	=.04	0.17
F-ratio	25.4	13.6	0.49	4.24	1.86

TABLE A.12: p-values and F-ratio of Muscle Activity (RMS) in Task 4 - Box Handling for *Assistance* Factor. Muscles: Upper Trapezius (UT), Anterior Deltoid (AD), Posterior Deltoid (PD), Infraspinatus (IN), Latissimus Dorsi (LD), Erector Spinae (ES), Rectus Abdominis (RA), Pectoralis Major (PM), Biceps Brachii (BB), and Brachioradialis (BR)

	UT	AD	PD	IN	LD
p-value	=.529	=.523	=.712	=.241	=.036
F-ratio	0.4	0.41	0.14	1.38	4.45

	ES	RA	PM	BB	BR
p-value	=.699	=.266	=.176	=.898	=.986
F-ratio	0.15	1.24	1.84	0.02	0.00

TABLE A.13: p-values and F-ratio of Muscle Activity (RMS) in Task 4 - Box Handling for *Assistance* x *Weight* Factors. Muscles: Upper Trapezius (UT), Anterior Deltoid (AD), Posterior Deltoid (PD), Infraspinatus (IN), Latissimus Dorsi (LD), Erector Spinae (ES), Rectus Abdominis (RA), Pectoralis Major (PM), Biceps Brachii (BB), and Brachioradialis (BR)

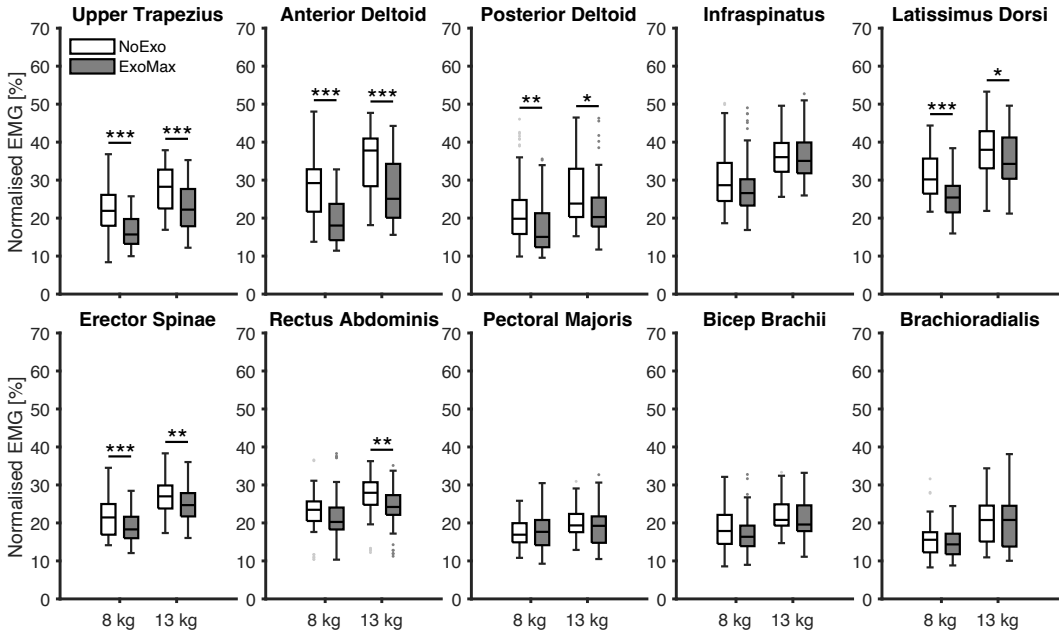

FIGURE A.4: EMG results *Assistance* x *Weight* Factors for Task 4 - Box Handling. $*$ indicates p-values ≤ 0.05, $**$ indicates p-values ≤ 0.01, and $***$ indicates p-values ≤ 0.001

8 kg	UT	AD	PD	IN	LD
NoExo - ExoMax	<.001	<.001	=.001	=.184	<.001

13 kg	UT	AD	PD	IN	LD
NoExo - ExoMax	<.001	<.001	=.015	=.991	=.029

8 kg	ES	RA	PM	BB	BR
NoExo - ExoMax	<.001	=.253	=.966	=.353	=.769

13 kg	ES	RA	PM	BB	BR
NoExo - ExoMax	=.005	=.004	=.478	=.568	=.771

TABLE A.14: p-values of Muscle Activity (RMS) in Task 4 - Box Handling for *Assistance* x *Weight* Factors. Muscles: Upper Trapezius (UT), Anterior Deltoid (AD), Posterior Deltoid (PD), Infraspinatus (IN), Latissimus Dorsi (LD), Erector Spinae (ES), Rectus Abdominis (RA), Pectoralis Major (PM), Biceps Brachii (BB), and Brachioradialis (BR)

A.2 Force Platform Results

	NoExo ExoMax	NoExo ExoMed	ExoMax ExoMed
Ellipse Area	=.839	=.562	=.879
CoP Length	=.465	=.996	=.367
CoP Velocity	=.392	=.016	=.264
CoP Migration Sagittal	=.997	=.764	=.689
CoP Migration Coronal	=.324	=.236	=.988
Max Vertical Force	=.002	=.044	=.506
Lifting Time	<.001	=.278	=.523

TABLE A.15: Force Platform results for *Assistance* Factor

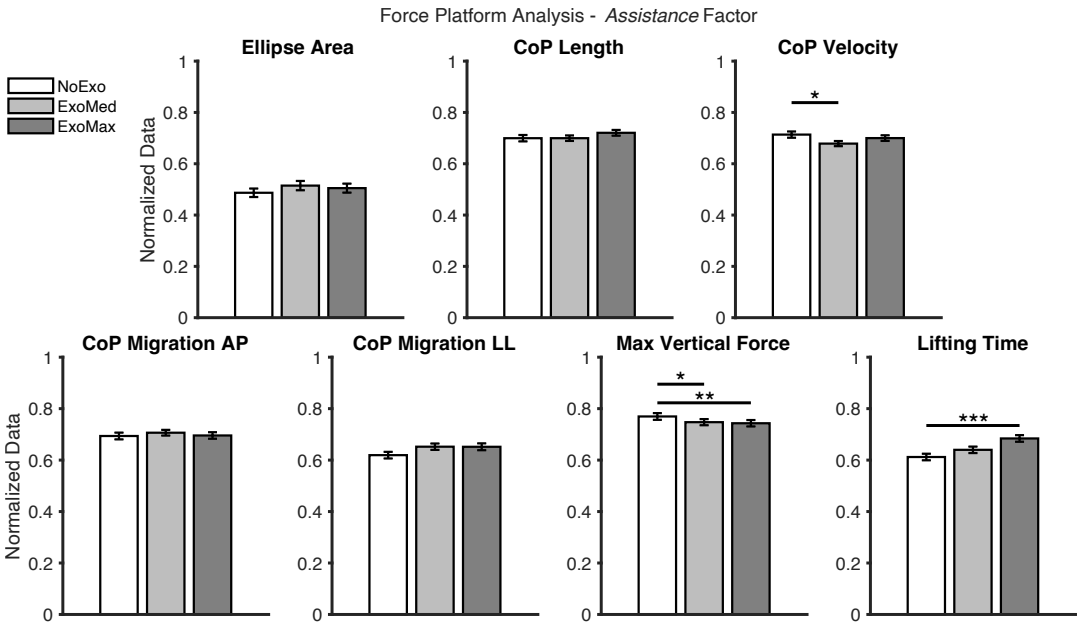

FIGURE A.5: Force Platform results for *Assistance* Factor. $*$ indicates p-values ≤ 0.05, $**$ indicates p-values ≤ 0.01, and $***$ indicates p-values ≤ 0.001

	Assistance		*Assistance* x *Weight*	
	p-value	F-ratio	p-value	F-ratio
1)	=.593	0.52	=.143	1.95
2)	=.333	1.10	=.242	1.42
3)	=.021	3.86	=.003	5.8
4)	=.669	0.4	=.214	1.55
5)	=.24	1.43	=.964	0.04
6)	=.002	6.12	=.026	3.69
7)	<.001	7.32	=.71	0.34

TABLE A.16: p-values and F-ratio of Force Platform results for *Assistance* x *Weight* Factors. 1) Ellipse Area, 2) CoP Length, 3) CoP Velocity, 4) CoP Migration AP, 5) CoP Migration LL, 6) Max Vertical Force, and 7) Lifting Time.

	NoExo - ExoMax		NoExo - ExoMed		ExoMax - ExoMed	
	8 kg	13 kg	8 kg	13 kg	8 kg	13 kg
1)	=1	=.994	=.449	=.999	=.569	=.932
2)	=.587	=1	=.867	=.82	=.995	=.735
3)	=.924	=.057	=.999	<.001	=.985	=.645
4)	=1	=1	=.616	=.993	=.563	=.997
5)	=.9	=.925	=.782	=.944	=1	=1
6)	=.793	=.004	=.999	=.004	=.595	=.999
7)	=.209	=.025	=.817	=.942	=.887	=.243

TABLE A.17: Force Platform results for *Assistance* x *Weight* Factors. 1) Ellipse Area, 2) CoP Length, 3) CoP Velocity, 4) CoP Migration AP, 5) CoP Migration LL, 6) Max Vertical Force, and 7) Lifting Time.

A.3 Borg Rates Results

	NoExo - ExoMax	NoExo - ExoMed	ExoMax - ExoMed
Task 1	<.001	=.014	=.078
Task 2	<.001	<.001	=.442
Task 3	=.003	Not present	Not present
Task 4	=.002	Not present	Not present

TABLE A.18: p-values of BORG Rates of Perceived Effort for *Assistance* Factor

	NoExo - ExoMax		NoExo - ExoMed		ExoMax - ExoMed	
	8 kg	13 kg	8 kg	13 kg	8 kg	13 kg
Task 1	=.011	=.003	=.019	=.315	=1	=.039
Task 2	=.001	=.019	=.005	=.031	=.402	=.992
Task 3	=.016	=.158	Not present		Not present	
Task 4	=.074	=.007	Not present		Not present	

TABLE A.19: p-values of BORG Rates of Perceived Effort for *Assistance* x *Weight* Factors

Appendix B

AGtuator Internal Forces

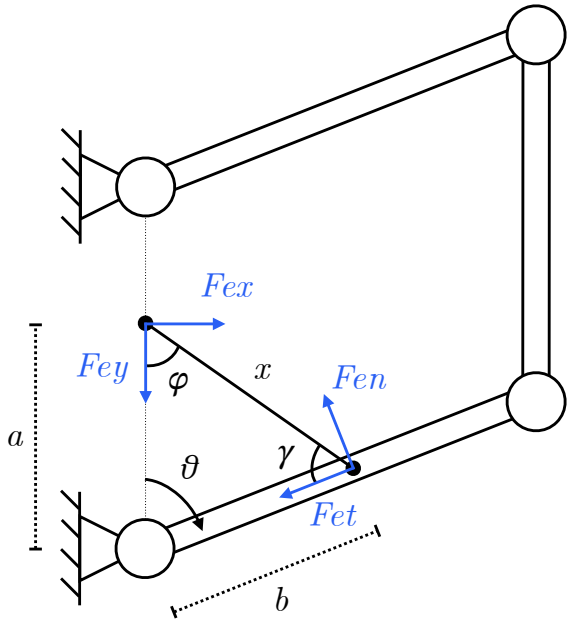

FIGURE B.1: Decomposition of the elastic force F_e into normal F_{en} and tangential F_{et} forces with respect to the link, and into horizontal F_{ex} and vertical F_{ey} forces.

B.1 Elastic Force

Elastic Force:

$$F_{el} = k \cdot x \tag{B.1}$$

And law of sines:

$$\frac{a}{\sin\gamma} = \frac{x}{\sin\theta} = \frac{b}{\sin\varphi} \tag{B.2}$$

B.1.1 Horizontal Elastic Force F_{ex}

$$\begin{aligned} F_x &= F_{el} \cdot \sin\varphi \\ F_x &= k \cdot x \cdot \sin\varphi \\ x \cdot \sin\varphi &= b \cdot \sin\theta \\ F_x &= k \cdot b \cdot \sin\theta \end{aligned} \tag{B.3}$$

B.1.2 Vertical Elastic Force F_{ey}

$$\begin{aligned} F_y &= F_{el} \cdot \cos\varphi \\ F_y &= k \cdot x \cdot \cos\varphi \\ F_y &= k \cdot x \cdot \sqrt{1 - \sin^2\varphi} \\ F_y &= k \cdot \sqrt{x^2 - x^2 \cdot \sin^2\varphi} \\ x^2 \cdot \sin^2\varphi &= b^2 \cdot \sin^2\theta \\ x^2 &= a^2 + b^2 - 2ab \cdot \cos\theta \\ F_y &= k \cdot \sqrt{a^2 + b^2 - 2ab \cdot \cos\theta - b^2 \cdot \sin^2\theta} \\ F_y &= k \cdot \sqrt{a^2 + b^2 \cdot (1 - \sin^2\theta) - 2ab \cdot \cos\theta} \\ F_y &= k \cdot \sqrt{a^2 + b^2 \cdot \cos^2\theta - 2ab \cdot \cos\theta} \\ F_y &= k \cdot \sqrt{(a - b\cos\theta)^2} \\ F_y &= k \cdot (a - b\cos\theta) \end{aligned} \tag{B.4}$$

B.1.3 Normal Elastic Force F_{en}

$$\begin{aligned} F_n &= F_{el} \cdot \sin\gamma \\ F_n &= k \cdot x \cdot \sin\gamma \\ x \cdot \sin\gamma &= a \cdot \sin\theta \\ F_n &= k \cdot a \cdot \sin\theta \end{aligned} \tag{B.5}$$

B.1.4 Tangential Elastic Force F_{et}

$$
\begin{aligned}
F_t &= F_{el} \cdot \cos\gamma \\
F_t &= k \cdot x \cdot \cos\gamma \\
F_t &= k \cdot x \cdot \sqrt{1 - \sin^2\gamma} \\
F_t &= k \cdot \sqrt{x^2 - x^2 \cdot \sin^2\gamma} \\
x^2 \cdot \sin^2\gamma &= a^2 \cdot \sin^2\theta \\
x^2 &= a^2 + b^2 - 2ab \cdot \cos\theta \\
F_t &= k \cdot \sqrt{a^2 + b^2 - 2ab \cdot \cos\theta - a^2 \cdot \sin^2\theta} \\
F_t &= k \cdot \sqrt{b^2 + a^2 \cdot (1 - \sin^2\theta) - 2ab \cdot \cos\theta} \\
F_t &= k \cdot \sqrt{b^2 + a^2 \cdot \cos^2\theta - 2ab \cdot \cos\theta} \\
F_t &= k \cdot \sqrt{(b - a\cos\theta)^2} \\
F_t &= k \cdot (b - a\cos\theta)
\end{aligned}
\tag{B.6}
$$

B.2 Summary

$$
\begin{cases}
F_x = & k \cdot b \cdot \sin\theta \\
F_y = & k \cdot (a - b \cdot \cos\theta)
\end{cases}
\tag{B.7}
$$

$$
\begin{cases}
F_n = & k \cdot a \cdot \sin\theta \\
F_t = & k \cdot (b - a \cdot \cos\theta)
\end{cases}
\tag{B.8}
$$

Bibliography

[1] *Agade, Milan, Italy*. https://agade-exoskeletons.com/en/product/. Accessed: 2023-12-11.

[2] Vigen Arakelian. "Gravity compensation in robotics". In: *Advanced Robotics* 30 (Nov. 2015), pp. 1–18. DOI: 10.1080/01691864.2015.1090334.

[3] Just L. Herder. "Design of spring force compensation systems". In: *Mechanism and Machine Theory* 33.1 (1998), pp. 151–161. ISSN: 0094-114X. DOI: https://doi.org/10.1016/S0094-114X(97)00027-X. URL: https://www.sciencedirect.com/science/article/pii/S0094114X9700027X.

[4] N. Ulrich and V. Kumar. "Passive mechanical gravity compensation for robot manipulators". In: *Proceedings. 1991 IEEE International Conference on Robotics and Automation*. 1991, 1536–1541 vol.2. DOI: 10.1109/ROBOT.1991.131834.

[5] Jehyeok Kim et al. "Compact Variable Gravity Compensation Mechanism With a Geometrically Optimized Lever for Maximizing Variable Ratio of Torque Generation". In: *IEEE/ASME Transactions on Mechatronics* 25.4 (Aug. 2020), pp. 2019–2026. ISSN: 1083-4435, 1941-014X. DOI: 10.1109/TMECH.2020.2998291. (Visited on 10/11/2024).

[6] Andrea Calanca et al. "Enhancing Force Controllability by Mechanics in Exoskeleton Design". In: *Mechatronics* 86 (1 2022), pp. 1–9. ISSN: 0957-4158. DOI: 10.1016/j.mechatronics.2022.102867. URL: https://doi.org/10.1016/j.mechatronics.2022.102867.

[7] Volkert van der Wijk and Just Herder. "Force balancing of variable payload by active force-balanced reconfiguration of the mechanism". In: *Proceedings of the 2009 ASME/IFToMM International Conference on Reconfigurable Mechanisms and Robots, ReMAR 2009* (Jan. 2009).

[8] Sushant Veer and S. Sujatha. "Approximate Spring Balancing of Linkages to Reduce Actuator Requirements". In: *Mechanism and Machine Theory* 86 (Apr. 2015), pp. 108–124. ISSN: 0094114X. DOI: 10.1016/j.mechmachtheory.2014.11.014. (Visited on 10/25/2024).

[9] Simon Lessard et al. "Optimum Static Balancing of a Parallel Robot for Medical 3D-Ultrasound Imaging". In: 5 (June 2007).

[10] Basilio Lenzo et al. "Trackhold: A Novel Passive Arm-Support Device". In: *Journal of Mechanisms and Robotics* 8 (Oct. 2015). DOI: 10.1115/1.4031716.

[11] Omar Mendoza-Trejo et al. "Exploring the Design of Highly Energy Efficient Forestry Cranes Using Gravity Compensation". In: *Croatian journal of forest engineering* 43.2 (June 2022), pp. 257–270. ISSN: 18489672, 18455719. DOI: 10.5552/crojfe.2022.1303. (Visited on 11/27/2024).

[12] N. Ulrich and V. Kumar. "Passive Mechanical Gravity Compensation for Robot Manipulators". In: *Proceedings. 1991 IEEE International Conference on Robotics and Automation*. Sacramento, CA, USA: IEEE Comput. Soc. Press, 1991, pp. 1536–1541. ISBN: 978-0-8186-2163-5. DOI: 10.1109/ROBOT.1991.131834.

[13] Albert Bayer and Ginther Merk. "(54) INDUSTRIAL ROBOT WITH A WEIGHT". In: (2011), p. 6.

[14] Nicolas Schmit and Masafumi Okada. "Optimal Design of Nonlinear Springs in Robot Mechanism: Simultaneous Design of Trajectory and Spring Force Profiles". In: *Advanced Robotics* 27.1 (Jan. 2013), pp. 33–46. ISSN: 0169-1864, 1568-5535. DOI: 10.1080/01691864.2013.751162. (Visited on 10/25/2024).

[15] Ruprecht Altenburger, Daniel Scherly, and Konrad S. Stadler. "Design of a Passive, Iso-Elastic Upper Limb Exoskeleton for Gravity Compensation". In: *ROBOMECH Journal* 3.1 (Apr. 2016), p. 12. ISSN: 2197-4225. DOI: 10.1186/s40648-016-0051-5. (Visited on 10/25/2023).

[16] F.L.S. Riele and Just Herder. "Perfect static balance with normal springs". In: (Jan. 2001), pp. 9–12.

[17] SLABINA Petr. "CONSTANT FORCE INDUCING EQUIPMENT". WO/2001/020211. Mar. 2001. URL: https://www.sumobrain.com/patents/WO2001020211A1.html.

[18] R. H. Nathan. "A constant force generation mechanism". English. In: *Journal of Mechanical Design, Transactions Of the ASME* 107.4 (Jan. 1985), pp. 508–512. ISSN: 1050-0472. DOI: 10.1115/1.3260755.

[19] Emanuele Palazzi et al. "An Affordable Upper-Limb Exoskeleton Concept for Rehabilitation Applications". In: *Technologies* 10.1 (Jan. 2022), p. 22. ISSN: 2227-7080. DOI: 10.3390/technologies10010022. (Visited on 09/07/2022).

[20] Diego Franchetti, Giovanni Boschetti, and Basilio Lenzo. "Passive Gravity Balancing with a Self-Regulating Mechanism for Variable Payload". In: *Machines* 9.8 (July 2021), p. 145. ISSN: 2075-1702. DOI: 10.3390/machines9080145. (Visited on 10/25/2023).

[21] Dexter Chew, Kristin Wood, and U-Xuan Tan. "Design of a Passive Self-Regulating Gravity Compensator for Variable Payloads". In: *Journal of Mechanical Design* 141 (Feb. 2019). DOI: 10.1115/1.4043582.

[22] Yu-Lin Chu and Chin-Hsing Kuo. "A Single-Degree-of-Freedom Self-Regulated Gravity Balancer for Adjustable Payload". In: *Journal of Mechanisms and Robotics* 9.2 (Apr. 2017), p. 021006. ISSN: 1942-4302, 1942-4310. DOI: 10.1115/1.4035561. (Visited on 02/01/2024).

[23] Dexter Chew, Kristin Wood, and U-Xuan Tan. "Design of a Passive Self-Regulating Gravity Compensator for Variable Payloads". In: *Journal of Mechanical Design* 141 (Feb. 2019). DOI: 10.1115/1.4043582.

[24] Zong-Wei Yang and Chao-Chieh Lan. "An Adjustable Gravity-Balancing Mechanism Using Planar Extension and Compression Springs". In: *Mechanism and Machine Theory* 92 (Oct. 2015), pp. 314–329. ISSN: 0094114X. DOI: 10.1016/j.mechmachtheory.2015.05.006. (Visited on 10/25/2024).

[25] Just Herder. "Energy-free Systems; Theory, conception and design of statically balanced spring mechanisms". PhD thesis. Nov. 2001. DOI: 10.13140/RG.2.1.3942.8966.

[26] W.D. van Dorsser et al. "Balancing Device". NL1029989C, WO2007035096, US2008210842. 2005.

[27] Wouter D. Van Dorsser et al. "Gravity-Balanced Arm Support With Energy-Free Adjustment". In: *Journal of Medical Devices* 1.2 (June 2007), pp. 151–158. ISSN: 1932-6181, 1932-619X. DOI: 10.1115/1.2736400.

[28] J L Herder et al. "Efficiently Variable Zero Stiffness Mechanisms". 2011.

[29] Boudewijn M. Wisse et al. "Energy-Free Adjustment of Gravity Equilibrators Using the Virtual Spring Concept". In: *2007 IEEE 10th International Conference on Rehabilitation Robotics*. Noordwijk, Netherlands: IEEE, June 2007, pp. 742–750. DOI: 10.1109/ICORR.2007.4428508. (Visited on 11/13/2023).

[30] Rogier Barents et al. "Spring-to-Spring Balancing as Energy-Free Adjustment Method in Gravity Equilibrators". In: *Journal of Mechanical Design* 133.6 (June 2011), p. 061010.

[31] W D Van Dorsser et al. "Energy-Free Adjustment of Gravity Equilibrators by Adjusting the Spring Stiffness". In: *Proceedings of the Institution of Mechanical Engineers, Part C: Journal of Mechanical Engineering Science* 222.9 (Sept. 2008), pp. 1839–1846. ISSN: 0954-4062, 2041-2983. DOI: 10.1243/09544062JMES832. (Visited on 03/12/2024).

[32] Wei-Hsuan Chiang and Dar-Zen Chen. "Design of planar variable-payload balanced articulated manipulators with actuated linear ground-adjacent adjustment". In: *Mechanism and Machine Theory* 109 (Mar. 2017), pp. 296–312. DOI: 10.1016/j.mechmachtheory.2016.12.001.

[33] Mahdi Bamdad and Farhad Parivash. "Integrated Active and Passive Gravity Compensation Method for a Cable-Actuated Elbow Rehabilitation Robot". In: *2015 3rd RSI International Conference on Robotics and Mechatronics (ICROM)*. Tehran, Iran: IEEE, Oct. 2015, pp. 079–084. ISBN: 978-1-4673-7234-3. DOI: 10.1109/ICRoM.2015.7367764. (Visited on 10/11/2024).

[34] Cédric Baradat et al. "Design and Prototyping of a New Balancing Mechanism for Spatial Parallel Manipulators". In: *Journal of Mechanical Design - J MECH DESIGN* 130 (July 2008). DOI: 10.1115/1.2901057.

[35] Julien Boisclair et al. "Gravity Compensation of Robotic Manipulators Using Cylindrical Halbach Arrays". In: *IEEE/ASME Transactions on Mechatronics* 22.1 (2017), pp. 457–464. DOI: 10.1109/TMECH.2016.2614386.

[36] William Montalvo et al. "Low-Cost Automation for Gravity Compensation of Robotic Arm". In: *Applied Sciences* 10 (May 2020), p. 3823. DOI: 10.3390/app10113823.

[37] Hugh Herr. "Exoskeletons and Orthoses: Classification, Design Challenges and Future Directions". In: *Journal of NeuroEngineering and Rehabilitation* 6.1 (June 2009), p. 21. ISSN: 1743-0003. DOI: 10.1186/1743-0003-6-21.

[38] Priyanshu Agarwal and Ashish Deshpande. "Exoskeletons: State-of-the-Art, Design Challenges, and Future Directions". In: Feb. 2019, pp. 234–259. ISBN: 9780190455132. DOI: 10.1093/oso/9780190455132.003.0011.

[39] Robert Bogue. "Robotic exoskeletons: A review of recent progress". In: *Industrial Robot: An International Journal* 42 (Jan. 2015), pp. 5–10. DOI: 10.1108/IR-08-2014-0379.

[40] Antonio Frisoli et al. "Arm Rehabilitation with a Robotic Exoskeleleton in Virtual Reality". In: *2007 IEEE 10th International Conference on Rehabilitation Robotics*. Noordwijk, Netherlands: IEEE, June 2007, pp. 631–642. ISBN: 978-1-4244-1319-5 978-1-4244-1320-1. DOI: 10.1109/ICORR.2007.4428491.

[41] H.I. Krebs et al. "Robot-aided neurorehabilitation". In: *IEEE Transactions on Rehabilitation Engineering* 6.1 (1998), pp. 75–87. DOI: 10.1109/86.662623.

[42] Marian Schoone, Peter van Os, and Antonet Campagne. "Robot-mediated Active Rehabilitation (ACRE) A user trial". In: *2007 IEEE 10th International Conference on Rehabilitation Robotics*. 2007, pp. 477–481. DOI: 10.1109/ICORR.2007.4428469.

[43] S. J. Spencer et al. "A low cost parallel robot and trajectory optimization method for wrist and forearm rehabilitation using the Wii". In: *2008 2nd IEEE RAS EMBS International Conference on Biomedical Robotics and Biomechatronics*. 2008, pp. 869–874. DOI: 10.1109/BIOROB.2008.4762902.

[44] Hermano Krebs et al. "Rehabilitation Robotics: Pilot Trial of a Spatial Extension for MIT-Manus". In: *Journal of NeuroEngineering and Rehabilitation* 1.1 (2004), p. 5. ISSN: 17430003. DOI: 10.1186/1743-0003-1-5.

[45] José Pons. "Witnessing a wearables transition". In: *Science* 365 (Aug. 2019), pp. 636–637. DOI: 10.1126/science.aaw9407.

[46] Alan T. Asbeck et al. "Stronger, Smarter, Softer: Next-Generation Wearable Robots". In: *IEEE Robotics & Automation Magazine* 21.4 (Dec. 2014), pp. 22–33. ISSN: 1070-9932, 1558-223X. DOI: 10.1109/MRA.2014.2360283.

[47] Michele Xiloyannis et al. "Soft Robotic Suits: State of the Art, Core Technologies, and Open Challenges". In: *IEEE Transactions on Robotics* 38.3 (2022), pp. 1343–1362. DOI: 10.1109/TRO.2021.3084466.

[48] Daegeun Park and Kyu-Jin Cho. "Development and evaluation of a soft wearable weight support device for reducing muscle fatigue on shoulder". In: *PLOS ONE* 12 (Mar. 2017), pp. 1–24. DOI: 10.1371/journal.pone.0173730. URL: https://doi.org/10.1371/journal.pone.0173730.

[49] Elena Bardi et al. "Upper Limb Soft Robotic Wearable Devices: A Systematic Review". In: *Journal of NeuroEngineering and Rehabilitation* 19.1 (Aug. 2022), p. 87. ISSN: 1743-0003. DOI: 10.1186/s12984-022-01065-9.

[50] Michele Xiloyannis et al. "Soft Robotic Suits: State of the Art, Core Technologies, and Open Challenges". In: *IEEE Transactions on Robotics* 38.3 (June 2022), pp. 1343–1362. ISSN: 1552-3098, 1941-0468. DOI: 10.1109/TRO.2021.3084466.

[51] Ciarán T. O'Neill et al. "A soft wearable robot for the shoulder: Design, characterization, and preliminary testing". In: *2017 International Conference on Rehabilitation Robotics (ICORR)*. 2017, pp. 1672–1678. DOI: 10.1109/ICORR.2017.8009488.

[52] Nathanaël Jarrassé et al. "Robotic exoskeletons: a perspective for the rehabilitation of arm coordination in stroke patients". In: *Frontiers in Human Neuroscience* 8 (2014), p. 947. DOI: 10.3389/fnhum.2014.00947. URL: https://hal.sorbonne-universite.fr/hal-01320175.

[53] AléErkan Engín. "On the biomechanics of the shoulder complex". In: *Journal of Biomechanics* 13.7 (1980), pp. 575–590. ISSN: 0021-9290. DOI: https://doi.org/10.1016/0021-9290(80)90058-5. URL: https://www.sciencedirect.com/science/article/pii/0021929080900585.

[54] R. A. R. C. Gopura and Kazuo Kiguchi. "Mechanical Designs of Active Upper-Limb Exoskeleton Robots: State-of-the-art and Design Difficulties". In: *2009 IEEE International Conference on Rehabilitation Robotics*. Kyoto, Japan: IEEE, June 2009, pp. 178–187. ISBN: 978-1-4244-3788-7. DOI: 10.1109/ICORR.2009.5209630.

[55] F.H. Martini, M.J. Timmons, and R.B. Tallitsch. *Human Anatomy*. Pearson Education, 2013. ISBN: 9781292038834. URL: https://books.google.it/books?id=EL6pBwAAQBAJ.

[56] CrossFit. *Movement About Joints, Part 1: The Shoulder*. Accessed: 2025-03-13. 2025. URL: https://www.crossfit.com/essentials/movement-about-joints-part-1-shoulder.

[57] CrossFit. *Movement About Joints, Part 2: The Elbow*. Accessed: 2025-03-13. 2025. URL: https://www.crossfit.com/essentials/movement-about-joints-part-2-the-elbow.

[58] JT London. "Kinematics of the elbow". In: *The Journal of bone and joint surgery. American volume* 63.4 (Apr. 1981), pp. 529–535. ISSN: 0021-9355. URL: http://europepmc.org/abstract/MED/7217119.

[59] *World population ageing, 1950-2050*. eng. New York: United Nations, 2002. ISBN: 9210510925.

[60] Ronald Lee and Yi Zhou. "Does Fertility or Mortality Drive Contemporary Population Aging? The Revisionist View Revisited". In: *Population and Development Review* 43.2 (June 2017), pp. 285–301. URL: https://ideas.repec.org/a/bla/popdev/v43y2017i2p285-301.html.

[61] E. Fuller-Thomson et al. "Basic ADL Disability and Functional Limitation Rates Among Older Americans From 2000–2005: The End of the Decline?" In: *The Journals of Gerontology: Series A* 64A.12 (Sept. 2009), pp. 1333–1336. ISSN: 1079-5006. DOI: 10.1093/gerona/glp130. eprint: https://academic.oup.com/biomedgerontology/article-pdf/64A/12/1333/1517543/glp130.pdf. URL: https://doi.org/10.1093/gerona/glp130.

[62] Akim Kapsalyamov, Shahid Hussain, and Prashant K. Jamwal. "State-of-the-Art Assistive Powered Upper Limb Exoskeletons for Elderly". In: *IEEE Access* 8 (2020), pp. 178991–179001. ISSN: 2169-3536. DOI: 10.1109/ACCESS.2020.3026641.

[63] MyoPro. *MyoPro - Myoelectric Arm Orthosis*. Accessed: 2025-03-13. 2025. URL: https://myopro.com/.

[64] Lynne M. Weber and Joel Stein. "The Use of Robots in Stroke Rehabilitation: A Narrative Review". In: *NeuroRehabilitation* 43.1 (July 2018). Ed. by Richard L. Harvey, pp. 99–110. ISSN: 10538135, 18786448. DOI: 10.3233/NRE-172408.

[65] Hyunchul Kim et al. "Kinematic Data Analysis for Post-Stroke Patients Following Bilateral Versus Unilateral Rehabilitation With an Upper Limb Wearable Robotic System". In: *IEEE Transactions on Neural Systems and Rehabilitation Engineering* 21.2 (2013), pp. 153–164. DOI: 10.1109/TNSRE.2012.2207462.

[66] Joel C. Perry, Jacob Rosen, and Stephen Burns. "Upper-Limb Powered Exoskeleton Design". In: *IEEE/ASME Transactions on Mechatronics* 12.4 (Aug. 2007), pp. 408–417. ISSN: 1941-014X. DOI: 10.1109/TMECH.2007.901934.

[67] Bruno R. da Costa and Edgar Ramos Vieira. "Risk Factors for Work-Related Musculoskeletal Disorders: A Systematic Review of Recent Longitudinal Studies". In: *American Journal of Industrial Medicine* (2009), n/a–n/a. ISSN: 02713586, 10970274. DOI: 10.1002/ajim.20750.

[68] *Ottobock, Duderstadt, Germany*. https://ottobockexoskeletons.com/. Accessed: 2023-12-11.

[69] *Levitate Technologies, San Diego, California*. https://www.levitatetech.com/. Accessed: 2023-12-11.

[70] Andrea Galeazzi. *ESOSCHELETRO - Ho provato MATE di COMAU*. Accessed: 2025-03-13. 2025. URL: https://andreagaleazzi.com/esoscheletro-mate-di-comau/.

[71] *SuitX Emeryville, California*. https://www.suitx.com/. Accessed: 2023-12-11.

[72] Heedon Lee et al. "The technical trend of the exoskeleton robot system for human power assistance". In: *International Journal of Precision Engineering and Manufacturing* 13 (Aug. 2012). DOI: 10.1007/s12541-012-0197-x.

[73] Md Rasedul Islam et al. "A Brief Review on Robotic Exoskeletons for Upper Extremity Rehabilitation to Find the Gap between Research Porotype and Commercial Type". In: *Advances in Robotics & Automation* 06.03 (2017). ISSN: 21689695. DOI: 10.4172/2168-9695.1000177.

[74] Tobias Nef et al. "Effects of arm training with the robotic device ARMin I in chronic stroke: three single cases". In: *Neuro-degenerative diseases* 6.5-6 (2009), pp. 240–251. ISSN: 1660-2854. DOI: 10.1159/000262444. URL: https://doi.org/10.1159/000262444.

[75] Hyung Soon Park, Yupeng Ren, and Li-Qun Zhang. "IntelliArm: An exoskeleton for diagnosis and treatment of patients with neurological impairments". English (US). In: *Proceedings of the 2nd Biennial IEEE/RAS-EMBS International Conference on Biomedical Robotics and Biomechatronics, BioRob 2008*. Proceedings of the 2nd Biennial IEEE/RAS-EMBS International Conference on Biomedical Robotics and Biomechatronics, BioRob 2008. 2nd Biennial IEEE/RAS-EMBS International Conference on Biomedical Robotics and Biomechatronics, BioRob 2008 ; Conference date: 19-10-2008 Through 22-10-2008. Dec. 2008, pp. 109–114. ISBN: 9781424428830. DOI: 10.1109/BIOROB.2008.4762876.

[76] Elvira Pirondini et al. "Evaluation of a New Exoskeleton for Upper Limb Post-stroke Neuro-rehabilitation: Preliminary Results". In: *Replace, Repair, Restore, Relieve – Bridging Clinical and Engineering Solutions in Neurorehabilitation*. Ed. by Winnie Jensen, Ole Kæseler Andersen, and Metin Akay. Vol. 7. Cham: Springer International Publishing, 2014, pp. 637–645. DOI: 10.1007/978-3-319-08072-7_91.

[77] Ruwan Gopura, Kazuo Kiguchi, and Sanjaya Bandara. "A brief review on upper extremity robotic exoskeleton systems". In: Aug. 2011, pp. 346–351. DOI: 10.1109/ICIINFS.2011.6038092.

[78] Michiel P. de Looze et al. "Exoskeletons for Industrial Application and Their Potential Effects on Physical Work Load". In: *Ergonomics* 59.5 (May 2016), pp. 671–681. ISSN: 0014-0139, 1366-5847. DOI: 10.1080/00140139.2015.1081988.

[79] Sander De Bock et al. "Passive Shoulder Exoskeletons: More Effective in the Lab Than in the Field?" In: *IEEE Transactions on Neural Systems and Rehabilitation Engineering* 29 (2021), pp. 173–183. ISSN: 1534-4320, 1558-0210. DOI: 10.1109/TNSRE.2020.3041906.

[80] Simona Crea et al. "Occupational exoskeletons: A roadmap toward large-scale adoption. Methodology and challenges of bringing exoskeletons to workplaces". In: *Wearable Technologies* 2 (2021), e11. DOI: 10.1017/wtc.2021.11.

[81] Anthony Voilqué et al. "Industrial Exoskeleton Technology: Classification, Structural Analysis, and Structural Complexity Indicator". In: Mar. 2019. DOI: 10.1109/WEARRACON.2019.8719395.

[82] Sander De Bock et al. "Benchmarking occupational exoskeletons: An evidence mapping systematic review". In: *Applied Ergonomics* 98 (Sept. 2021). DOI: 10.1016/j.apergo.2021.103582.

[83] Tobias Möller et al. "Effects of Upper-Limb Exoskeletons Designed for Use in the Working Environment-A Literature Review". In: *Frontiers in Robotics and AI* 9 (Apr. 2022), p. 1. DOI: 10.3389/frobt.2022.858893.

[84] Michiel Looze et al. "Exoskeletons for industrial application and their potential effects on physical work load". In: *Ergonomics* 59 (Oct. 2015), pp. 1–11. DOI: 10.1080/00140139.2015.1081988.

[85] John Howard et al. "Industrial exoskeletons: Need for intervention effectiveness research". In: *American Journal of Industrial Medicine* 63.3 (), pp. 201–208. DOI: https://doi.org/10.1002/ajim.23080. eprint: https://onlinelibrary.wiley.com/doi/pdf/10.1002/ajim.23080. URL: https://onlinelibrary.wiley.com/doi/abs/10.1002/ajim.23080.

[86] Ashley Stewart et al. "Review of Upper Limb Hybrid Exoskeletons". In: *IFAC-PapersOnLine* 50 (July 2017), pp. 15169–15178. DOI: 10.1016/j.ifacol.2017.08.2266.

[87] Emanuele Palazzi et al. "An Affordable Upper-Limb Exoskeleton Concept for Rehabilitation Applications". In: *Technologies* 10 (Jan. 2022). DOI: 10.3390/technologies10010022.

[88] Zhenhua Zhu, Amrita Dutta, and Fei Dai. "Exoskeletons for manual material handling – A review and implication for construction applications". In: *Automation in Construction* 122 (Feb. 2021), p. 103493. DOI: 10.1016/j.autcon.2020.103493.

[89] Lorenzo Grazi et al. "Design and Experimental Evaluation of a Semi-Passive Upper-Limb Exoskeleton for Workers With Motorized Tuning of Assistance". In: *IEEE Transactions on Neural Systems and Rehabilitation Engineering* PP (Aug. 2020), pp. 1–1. DOI: 10.1109/TNSRE.2020.3014408.

[90] Emanuele Feola et al. "A Neuromechanical Model-Based Strategy to Estimate the Operator's Payload in Industrial Lifting Tasks". In: *IEEE Transactions on Neural Systems and Rehabilitation Engineering* 31 (2023), pp. 4644–4652. ISSN: 15580210. DOI: 10.1109/TNSRE.2023.3334993.

[91] Agnès Parent-Thirion et al. "Sixth European working conditions survey–overview report". In: (2016).

[92] Jeremy Beach, Ambikaipakan Senthilselvan, and Nicola Cherry. "Factors affecting work-related shoulder pain". In: *Occupational medicine (Oxford, England)* 62 (July 2012), pp. 451–4. DOI: 10.1093/occmed/kqs130.

[93] Jason Grieve and Clark Dickerson. "Overhead work: Identification of evidence-based exposure guidelines". In: *Occupational Ergonomics* 8 (Sept. 2008), pp. 53–66. DOI: 10.3233/OER-2008-8105.

[94] Arun Garg, Kurt Hegmann, and Jay Kapellusch. "Short-cycle overhead work and shoulder girdle muscle fatigue". In: *International Journal of Industrial Ergonomics* 36 (June 2006), pp. 581–597. DOI: 10.1016/j.ergon.2006.02.002.

[95] Glenn Terry and Thomas Chopp. "Functional Anatomy of the Shoulder". In: *Journal of athletic training* 35 (Feb. 2000), pp. 248–55.

[96] Stephen Bevan. "Economic impact of musculoskeletal disorders (MSDs) on work in Europe". In: *Best Practice & Research Clinical Rheumatology* 29 (Oct. 2015). DOI: 10.1016/j.berh.2015.08.002.

[97] J Bos, P Paul Kuijer, and Monique Frings-Dresen. "Definition and assessment of specific occupational demands concerning lifting, pushing, and pulling based on a systematic literature search". In: *Occupational and environmental medicine* 59 (Jan. 2003), pp. 800–6. DOI: 10.1136/oem.59.12.800.

[98] Aijse de Vries and Michiel Looze. "The Effect of Arm Support Exoskeletons in Realistic Work Activities: A Review Study". In: *Journal of Ergonomics* 9 (Nov. 2019), p. 255. DOI: 10.35248/2165-7556.19.9.255.

[99] David Romero et al. "Towards an Operator 4.0 Typology: A Human-Centric Perspective on the Fourth Industrial Revolution Technologies". In: Oct. 2016.

[100] Tjaša Kermavnar et al. "Effects of Industrial Back-Support Exoskeletons on Body Loading and User Experience: An Updated Systematic Review". In: *Ergonomics* 64.6 (June 2021), pp. 685–711. ISSN: 0014-0139, 1366-5847. DOI: 10.1080/00140139.2020.1870162. (Visited on 07/28/2023).

[101] Robert Bogue. "Exoskeletons - a review of industrial applications". In: *Industrial Robot: An International Journal* 45 (July 2018). DOI: 10.1108/IR-05-2018-0109.

[102] Jean Theurel and Kevin Desbrosses. "Occupational Exoskeletons: Overview of Their Benefits and Limitations in Preventing Work-Related Musculoskeletal Disorders". In: *IISE Transactions on Occupational Ergonomics and Human Factors* 7 (July 2019), pp. 1–21. DOI: 10.1080/24725838.2019.1638331.

[103] Stephen Fox et al. "Exoskeletons: Comprehensive, comparative and critical analyses of their potential to improve manufacturing performance". In: *Journal of Manufacturing Technology Management* 31 (June 2019). DOI: 10.1108/JMTM-01-2019-0023.

[104] Ali Golabchi, U Chao, and Mahdi Tavakoli. "A Systematic Review of Industrial Exoskeletons for Injury Prevention: Efficacy Evaluation Metrics, Target Tasks, and Supported Body Postures". In: *Sensors* 22 (Apr. 2022). DOI: 10.3390/s22072714.

[105] Verena Kopp et al. "Exoworkathlon: A prospective study approach for the evaluation of industrial exoskeletons". In: *Wearable Technologies* 3 (Sept. 2022). DOI: 10.1017/wtc.2022.17.

[106] Gjulio Ashta et al. "Passive Exoskeletons to Enhance Workforce Sustainability: Literature Review and Future Research Agenda". In: *Sustainability* 15.9 (Apr. 2023), p. 7339. ISSN: 2071-1050. DOI: 10.3390/su15097339. URL: http://dx.doi.org/10.3390/su15097339.

[107] Thomas Schmalz et al. "Biomechanical and Metabolic Effectiveness of an Industrial Exoskeleton for Overhead Work". In: *International Journal of Environmental Research and Public Health* 16 (2019).

[108] Ilaria Pacifico et al. "An Experimental Evaluation of the Proto-MATE: A Novel Ergonomic Upper-Limb Exoskeleton to Reduce Workers' Physical Strain". In: *IEEE Robotics Automation Magazine* 27.1 (2020), pp. 54–65. DOI: 10.1109/MRA.2019.2954105.

[109] Lorenzo Grazi et al. "Design and Experimental Evaluation of a Semi-Passive Upper-Limb Exoskeleton for Workers With Motorized Tuning of Assistance". In: *IEEE Transactions on Neural Systems and Rehabilitation Engineering* 28.10 (Oct. 2020), pp. 2276–2285. ISSN: 1558-0210. DOI: 10.1109/TNSRE.2020.3014408.

[110] Pauline Maurice et al. "Objective and Subjective Effects of a Passive Exoskeleton on Overhead Work". In: *IEEE Transactions on Neural Systems and Rehabilitation Engineering* 28.1 (Jan. 2020), pp. 152–164. ISSN: 1534-4320, 1558-0210. DOI: 10.1109/TNSRE.2019.2945368.

[111] Andrea Blanco et al. "The Effect of an Active Upper-Limb Exoskeleton on Metabolic Parameters and Muscle Activity During a Repetitive Industrial Task". In: *IEEE Access* 10 (2022), pp. 16479–16488. ISSN: 2169-3536. DOI: 10.1109/ACCESS.2022.3150104.

[112] Tobias Moeller et al. "Effects of Upper-Limb Exoskeletons Designed for Use in the Working Environment—A Literature Review". In: *Frontiers in Robotics and AI* 9 (Apr. 2022), p. 858893. ISSN: 2296-9144. DOI: 10.3389/frobt.2022.858893.

[113] Gabriela Ferreira et al. "Piloting the Use of an Upper Limb Passive Exoskeleton in Automotive Industry: Assessing User Acceptance and Intention of Use". In: *Advances in Human Factors and Systems Interaction*. Ed. by Isabel L. Nunes. Cham: Springer International Publishing, 2020, pp. 342–349. ISBN: 978-3-030-51369-6.

[114] Hermie Hermens et al. "Development of recommendations for SEMG sensors and sensor placement procedures". In: *Journal of electromyography and kinesiology : official journal of the International Society of Electrophysiological Kinesiology* 10 (Oct. 2000), pp. 361–74. DOI: 10.1016/S1050-6411(00)00027-4.

[115] Lorenzo Aquilante et al. *LOAD COMPENSATION DEVICE, IN PARTICULAR OF GRAVITATIONAL LOADS, APPLICABLE TO EXOSKELETONS*. Apr. 2022.

[116] Gunnar Borg. *Borg's Perceived Exertion And Pain Scales*. July 1998. ISBN: 0-88011-623-4.

[117] Sandra Hart and L. Stavenland. "Development of NASA-TLX (Task Load Index): Results of empirical and theoretical research". In: vol. 52. Dec. 1988, pp. 139–. ISBN: 9780444703880. DOI: 10.1016/S0166-4115(08)62386-9.

[118] Hsien-Min Wang, Dang Le, and Wei-Chih Lin. "Evaluation of a Passive Upper-Limb Exoskeleton Applied to Assist Farming Activities in Fruit Orchards". In: *Applied Sciences* 11 (Jan. 2021), p. 757. DOI: 10.3390/app11020757.

[119] Flavien Quijoux et al. "A review of center of pressure (COP) variables to quantify standing balance in elderly people: Algorithms and open-access code*". In: *Physiological Reports* 9 (Nov. 2021). DOI: 10.14814/phy2.15067.

[120] V Phadke, PR Camargo, and PM Ludewig. "Scapular and rotator cuff muscle activity during arm elevation: a review of normal function and alterations with shoulder impingement". In: *Brazilian Journal of Physical Therapy* 13.1 (Jan. 2009), pp. 1–9. ISSN: 1413-3555. DOI: 10.1590/S1413-35552009005000012. URL: https://doi.org/10.1590/S1413-35552009005000012.

[121] Kirsten Huysamen et al. "Assessment of an Active Industrial Exoskeleton to Aid Dynamic Lifting and Lowering Manual Handling Tasks". In: *Applied Ergonomics* 68 (Apr. 2018), pp. 125–131. ISSN: 0003-6870. DOI: 10.1016/j.apergo.2017.11.004. (Visited on 10/18/2022).

[122] Tessy Luger et al. "A Passive Back Exoskeleton Supporting Symmetric and Asymmetric Lifting in Stoop and Squat Posture Reduces Trunk and Hip Extensor Muscle Activity and Adjusts Body Posture – A Laboratory Study". In: *Applied Ergonomics* 97 (Nov. 2021), p. 103530. ISSN: 00036870. DOI: 10.1016/j.apergo.2021.103530. (Visited on 11/28/2023).

[123] Logan Engelhoven et al. "Evaluation of an adjustable support shoulder exoskeleton on static and dynamic overhead tasks". In: *Proceedings of the Human Factors and Ergonomics Society Annual Meeting* 62 (Sept. 2018), pp. 804–808. DOI: 10.1177/1541931218621184.

[124] Seok-Beom Lee and Kai-Nan An. "Dynamic Glenohumeral Stability Provided by Three Heads of the Deltoid Muscle". In: *Clinical orthopaedics and related research* 400 (Aug. 2002), pp. 40–7. DOI: 10.1097/00003086-200207000-00006.

[125] K.M. Tesh. *Abdominal Muscle and Vertebral Stability: (the Contributions of a Raised Intra-abdominal Pressure and Tension in the Thoracolumbar Fascia to Stabilising the Lumbar Spine)*. University of Strathclyde, 1986. URL: https://books.google.it/books?id=1w5buwEACAAJ.

[126] Nikolai Bogduk, Garth Johnson, and Deborah Spalding. "The morphology and biomechanics of latissimus dorsi". In: *Clinical Biomechanics* 13.6 (1998), pp. 377–385. ISSN: 0268-0033. DOI: https://doi.org/10.1016/S0268-0033(98)00102-8. URL: https://www.sciencedirect.com/science/article/pii/S0268003398001028.

[127] Dong Hyun et al. "A light-weight passive upper arm assistive exoskeleton based on multi-linkage spring-energy dissipation mechanism for overhead tasks". In: *Robotics and Autonomous Systems* 122 (Oct. 2019), p. 103309. DOI: 10.1016/j.robot.2019.103309.

[128] Ilaria Pacifico et al. "Experimental evaluation of the proto-MATE: A novel ergonomic upper-limb exoskeleton for reducing the workers physical strain". In: *IEEE Robotics & Automation Magazine* PP (Jan. 2020). DOI: 10.1109/MRA.2019.2954105.

[129] Jean Theurel et al. "Physiological consequences of using an upper limb exoskeleton during manual handling tasks". In: *Applied Ergonomics* 67 (Feb. 2018), pp. 211–217. DOI: 10.1016/j.apergo.2017.10.008.

[130] Stefania Spada et al. "Investigation into the applicability of a passive upper-limb exoskeleton in automotive industry". In: *Procedia Manufacturing* 11 (2017), pp. 1255–1262.

[131] Stefania Spada et al. "Passive Upper Limb Exoskeletons: An Experimental Campaign with Workers". In: *Proceedings of the 20th Congress of the International Ergonomics Association (IEA 2018)*. Ed. by Sebastiano Bagnara et al. Cham: Springer International Publishing, 2019, pp. 230–239.

[132] Silvia Gilotta et al. "Acceptability Beyond Usability: A Manufacturing Case Study". In: *Advances in Intelligent Systems and Computing* (2018). URL: https://api.semanticscholar.org/CorpusID:115748521.

[133] Sunwook Kim et al. "Potential of Exoskeleton Technologies to Enhance Safety, Health, and Performance in Construction: Industry Perspectives and Future Research Directions". In: *IISE Transactions on Occupational Ergonomics and Human Factors* 7.3-4 (2019), pp. 185–191. DOI: 10.1080/24725838.2018.1561557. URL: https://doi.org/10.1080/24725838.2018.1561557.

[134] K. Desbrosses, M. Schwartz, and J. Theurel. "Evaluation of Two Upper-Limb Exoskeletons during Overhead Work: Influence of Exoskeleton Design and Load on Muscular Adaptations and Balance Regulation". In: *European Journal of Applied Physiology* 121.10 (Oct. 2021), pp. 2811–2823. ISSN: 1439-6319, 1439-6327. DOI: 10.1007/s00421-021-04747-9. (Visited on 02/26/2023).

[135] Pauline Maurice et al. "Objective and Subjective Effects of a Passive Exoskeleton on Overhead Work". In: *IEEE Transactions on Neural Systems and Rehabilitation Engineering* PP (Oct. 2019), pp. 1–1. DOI: 10.1109/TNSRE.2019.2945368.

[136] Sunwook Kim et al. "Assessing the influence of a passive, upper extremity exoskeletal vest for tasks requiring arm elevation: Part II – "Unexpected" effects on shoulder motion, balance, and spine loading". In: *Applied Ergonomics* 70 (Mar. 2018). DOI: 10.1016/j.apergo.2018.02.024.

[137] Francisco Anaya Reyes, Ding Shuo, and Haoyong Yu. "Shoulder-Support Exoskeletons for Overhead Work: Current State, Challenges and Future Directions". In: *IEEE Transactions on Medical Robotics and Bionics* (2023), pp. 1–1. DOI: 10.1109/TMRB.2023.3275761.

[138] Nahema Sylla et al. "Ergonomic contribution of ABLE exoskeleton in automotive industry". In: *International Journal of Industrial Ergonomics* 44 (July 2014), pp. 475–481. DOI: 10.1016/j.ergon.2014.03.008.

[139] Amir Ebrahimi et al. "Control parameter optimization of the actively powered upper body exoskeleton using subjective feedbacks". In: Apr. 2017, pp. 432–437. DOI: 10.1109/ICCAR.2017.7942733.

[140] Muhammad Gull, Shaoping Bai, and Thomas Bak. "A Review on Design of Upper Limb Exoskeletons". In: *Robotics* 9 (Mar. 2020), p. 16. DOI: 10.3390/robotics9010016.

[141] Valentina Di Pasquale, Salvatore Miranda, and W. Patrick Neumann. "Ageing and human-system errors in manufacturing: a scoping review". In: *International Journal of Production Research* 58.15 (2020), pp. 4716–4740. DOI: 10.1080/00207543.2020.1773561. URL: https://doi.org/10.1080/00207543.2020.1773561.

[142] Sander De Bock et al. "Passive Shoulder Exoskeletons: More Effective in the Lab Than in the Field?" In: *IEEE Transactions on Neural Systems and Rehabilitation Engineering* PP (Mar. 2021). DOI: 10.1109/TNSRE.2020.3041906.

[143] Bernward Otten, Robert Weidner, and Andreas Argubi-Wollesen. "Evaluation of a Novel Active Exoskeleton for Tasks at or Above Head Level". In: *IEEE Robotics and Automation Letters* PP (Mar. 2018), pp. 1–1. DOI: 10.1109/LRA.2018.2812905.

[144] Andrea Calanca, Eldison Dimo, and Francesco Pascucci. "Sistema semi-attivo per la compensazione auto-riconfigurabile della gravità e la generazione di profili di coppia in robot, esoscheletri o altre macchine". 102025000005030 (Grezzana (VR), Italia). Depositante: Riccardo Berti. Presentato il 12/03/2025. 2025.

[145] Basilio Lenzo et al. "New Gravity Balancing Technique and Hybrid Actuation for Spatial Serial Manipulators". In: *Advances in Robot Kinematics*. Ed. by Jadran Lenarčič and Oussama Khatib. Cham: Springer International Publishing, 2014, pp. 419–427. ISBN: 978-3-319-06698-1. DOI: 10.1007/978-3-319-06698-1_43. URL: https://doi.org/10.1007/978-3-319-06698-1_43.

[146] Oliver MizeraAnnedore KURZWEGLüder MOSLERJonas BORNMANNSamantha FoxBenjamin Schirrmeister. "Device for supporting at least one arm of a user". European Patent EP3504033B1. Ottobock SE and Co KGaA. Mar. 2023.

[147] Michael Watterworth et al. "Equations for estimating the static supportive torque provided by upper-limb exoskeletons". In: *Applied ergonomics* 113 (July 2023), p. 104092. DOI: 10.1016/j.apergo.2023.104092.

[148] Marek Sierotowicz et al. "Unobtrusive, natural support control of an adaptive industrial exoskeleton using force myography". In: *Frontiers in Robotics and AI* 9 (Sept. 2022). DOI: 10.3389/frobt.2022.919370.

[149] Andrea Calanca et al. "Sistema adattivo di compensazione della gravità per robot assistivi con uno o più gradi di libertà basato su attivazione di bicipite e tricipite". 102025000005058 (Grezzana (VR), Italia). Depositante: Riccardo Berti. Presentato il 12/03/2025. 2025.

[150] *Leaderdrive, Jiangsu, China*. https://www.leaderdrive.com/. Accessed: 2023-12-11.